THE UNIVERSITY OF ALBERTA

DEUTERON INDUCED REACTIONS ON ^{28}Si

by

David Preston Gurd

A THESIS

SUBMITTED TO THE FACULTY OF GRADUATE STUDIES

IN PARTIAL FULFILLMENT OF THE REQUIREMENTS FOR THE DEGREE

OF DOCTOR OF PHILOSOPHY

DEPARTMENT OF PHYSICS

EDMONTON, ALBERTA

April, 1968

UNIVERSITY OF ALBERTA

FACULTY OF GRADUATE STUDIES

The undersigned certify that they have read, and recommend to the Faculty of Graduate Studies for acceptance, a thesis entitled DEUTERON INDUCED REACTIONS ON ^{28}Si, submitted by David Preston Gurd in partial fulfillment of the requirements for the degree of Doctor of Philosophy.

ABSTRACT

Absolute cross-sections for the elastic scattering reaction $^{28}Si(d,d)^{28}Si$ have been measured from 25^{o} to 140^{o} at seven energies in the range E_d = 4.74 MeV to E_d = 5.26 MeV. The distribution of protons from the $\ell n = 0$ reaction $^{28}Si(d,p)^{29}Si_{gs}$ and the $\ell n = 2$ reactions $^{28}Si(d,p)^{29}Si^{*}$ 1.28 and 2.03 has been obtained at E_d = 5.0 MeV, as well as the polarization of the ground state proton group. This data has been compared with predictions of D. W. B. A. theory using several deuteron optical model parameter sets obtained by fitting the elastic distributions. The theory is unable to explain the polarization data, but some of the deuteron potentials provide fair agreement with the measured stripping distributions. Spectroscopic Factors have been extracted, and compared with predictions of the Nilsson Model for ^{29}Si.

ACKNOWLEDGEMENTS

I wish to express my gratitude to Dr. G. Roy, who not only suggested the projects described in this thesis, but participated actively in carrying them out. His unfailing optimism and encouragement has helped me over many a bad moment.

I am particularly thankful to those who sacrificed so many nights of sleep and weekends of play to see these experiments completed: Bob Humphries, Jan Bogaards, and especially Henry Leighton, who has been involved with this project since its inception, has shared fully in every step of its development, and with whom credit for whatever may be of value in this work is fully shared. More cooperative, sympathetic, or good-spirited colleagues could surely not be found.

I am deeply grateful to Mr. Jock Elliot, both for his selfless help in the two years of these experiments, and for his painstaking execution of each drawing in this thesis according to my every wish. It typified the cooperative and friendly attitude of the entire technical staff of the Nuclear Research Center, to whom I also express my thanks.

I am also indebted to Mrs. Marjorie Lybacki for her careful typing from totally undecipherable manuscript.

To my wife, Margrit, and the girls, for their patience and understanding: Thank you.

Finally, I wish to acknowledge gratefully the financial support of the National Research Council and of the University of Alberta.

TABLE OF CONTENTS

LIST OF ILLUSTRATIONS

Illustrations Continued

LIST OF TABLES

INTRODUCTION

The experiments described in this thesis were undertaken as a part of a larger project initiated at the Nuclear Research Center at the University of Alberta. Using the available 5 MeV Van der Graaff accelerator and neutron time-of-flight system, the reactions $^{40}Ca(d,n)^{41}Sc$ and $^{28}Si(d,n)^{29}P$ had been studied in the energy region 4-6 MeV with a view to testing the validity of the Distorted Wave Born Approximation (DWBA) in describing the mechanism of these reactions. Moreover, experiments to measure the polarization of several of the outgoing neutron groups in these reactions were planned. The analysis of this work, however, was hindered by the unavailability of suitable experimentally determined deuteron optical model parameters to describe the distortion of the incoming waves.

The installation and calibration of a 50 cm. Broad Range Magnetic Spectrograph - Spectrometer, as described earlier, made possible measurements of the elastic scattering cross sections for deuterons incident on ^{28}Si and ^{40}Ca at appropriate energies from which suitable optical model potentials might be obtained. It was felt that a rather stringent test on these optical model parameters might be made by requiring that, when used in a DWBA calculation, they fit both (d,n) and (d,p) angular distributions and polarizations. Moreover, such a rigid requirement might allow some of the familiar ambiguities in the deuteron optical model potential to be eliminated. Consequently, the first experiments planned for the magnetic spectrometer were measurements of:

(i) The elastic scattering cross-sections of deuterons on ^{28}Si and ^{40}Ca in the vicinity of 5 MeV;

(ii) Angular distributions of the first few proton groups from the $^{28}Si(d,p)^{29}Si$ and $^{40}Ca(d,p)^{41}Ca$ reactions in this region; and

(iii) The polarization of the protons of the ground state group from the above two reactions.

The overall project is illustrated in figure 1, and the results of this work has been described in references (Davies 66, Lam 67, Gedke 67, Grandy 67, Leighton 68, 68a). It was hoped that with the accumulation of all this data several objectives might be realized:

(i) That some of the deuteron optical model potential ambiguities might be removed;

(ii) That the validity of the DWBA theory might be tested in this region of low energy and light nuclei, and in particular that some measure might be obtained of the extent to which these reactions proceed by a "Direct" mechanism;

(iii) That the polarization data might allow the selection of an appropriate spin-orbit interaction in the deuteron optical model potential; and

(iv) That absolute cross-sections obtained from the stripping reactions might be compared with the predictions of different nuclear models.

As suggested by figure 1, the reactions $^{28}Si(d,d)^{28}Si$, $^{28}Si(d,p)^{29}Si$ and $^{28}Si(d,p)^{29}Sigs$ polarization constitute the

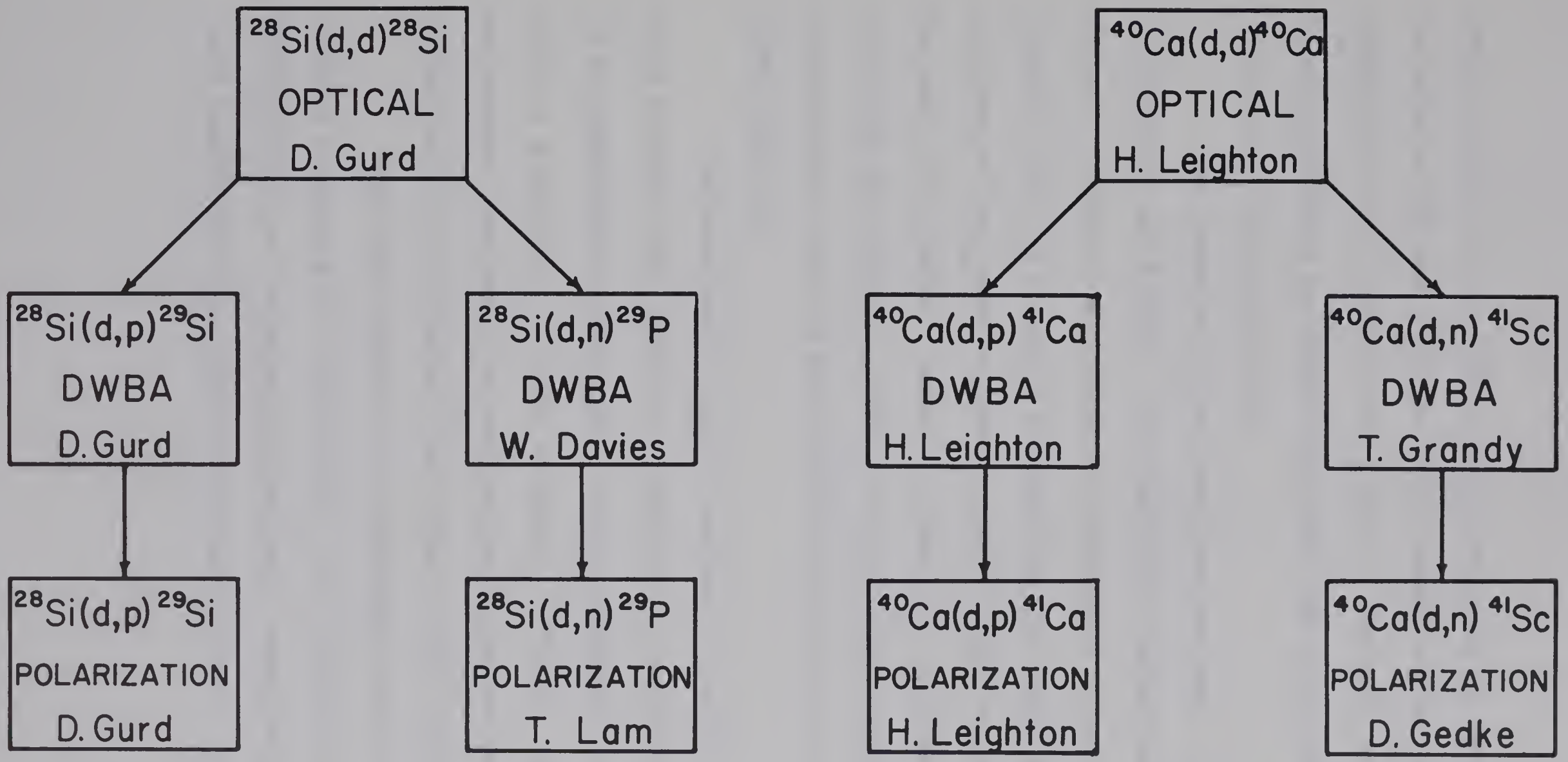

FIG. I – 1 SCHEMATIC DIAGRAM OF EXPERIMENTAL PROGRAM

subject matter of this thesis. Since virtually no elastic scattering data on ^{28}Si was available in this energy region, considerable emphasis has been placed on this aspect of the work, and the optical potentials so obtained have been used in the DWBA analysis of the (d,n) reactions as well.

The thesis is divided into three sections: Theoretical, Experimental, and Results. The theoretical chapters make no attempt to present the mathematical development of the subjects covered, which can be easily obtained from the numerous review articles and text books referred to, and to which no contribution was made by the author. Rather an attempt has been made to put into words the principle concepts, with particular emphasis on the approximations which are made and their validity in the special case under study here.

The experimental section consists of a single chapter which describes very briefly the apparatus and techniques used in the experimental measurements. This is augmented by an appendix which is a preprint of a paper to appear in "Nuclear Instruments and Methods" describing the construction and calibration of the charged particle polarimeter used in some of these experiments.

Part Three describes the experimental results in three chapters concerning the $^{28}Si(d,d)^{28}Si$; the $^{28}Si(d,p)^{29}Si$ and the $^{28}Si(d,p)^{29}Si$ g.s. polarization experiments respectively. Some of these results have been reported previously (Gurd 67, Roy 67).

PART I: THEORETICAL

CHAPTER 1: THE NILSSON MODEL AND ^{29}Si

The target nucleus ^{28}Si used in the experiments described in the following chapters consists of 14 neutrons and 14 protons which may be thought of as completing the 1d 5/2 orbital in the simple shell model picture. A 15^{th} nucleon stripped from a deuteron in a nuclear reaction might then be thought of as belonging the 2 s 1/2 orbital, accounting for the 1/2 + ground state spins of ^{29}Si and ^{29}P. The remaining spectroscopic information on ^{29}Si contained in figure 1-1 might then also be explained on the basis of the shell model. An extreme single particle model, however, would certainly not be expected to be adequate, and a complete shell model calculation would have to include for each state contributions from all the orbitals in the 2s - 1d shell and would be extremely complex and difficult.

Such complete calculations performed for nuclei in the middle of shells are known in many cases to give spectra characteristic of rotations, suggesting collective rotational motion. Rather than performing complete shell model calculations, then, models in which such motions are assumed a priori have frequently been applied to nuclei which are not located near closed shells, including many such examples in the 2s - 1d shell.

D. A. Bromley, H. E. Gove and A. E. Litherland (Bromley 57) had considerable success in applying a strong coupling (Nilsson) model to ^{29}Si, and this model has been used in most subsequent discussions of this nucleus. The Nilsson Model is simply a

$\frac{6{\cdot}253}{^{28}Si + d - p}$

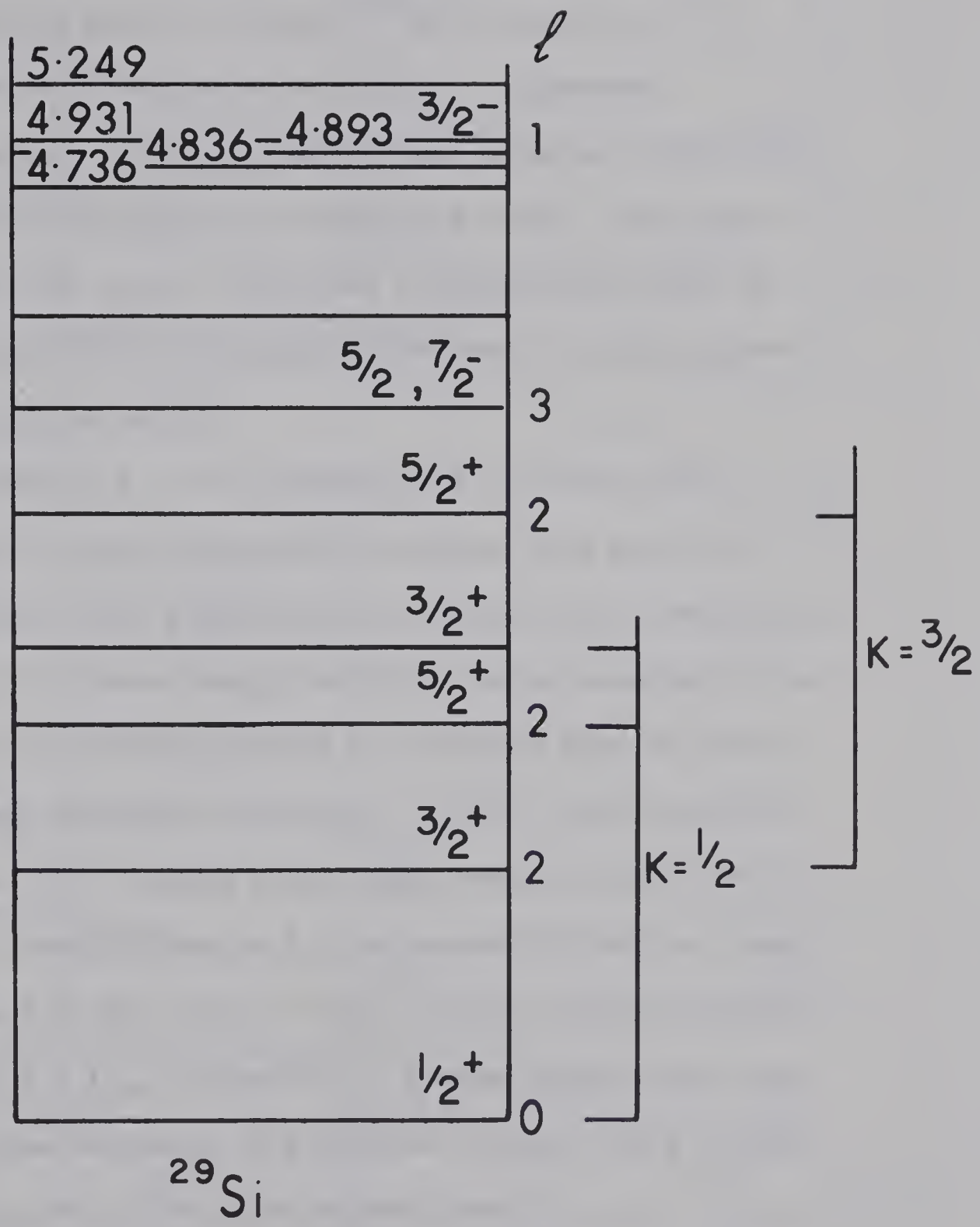

FIGURE 1 - 1: ENERGY LEVELS OF SILICON 29

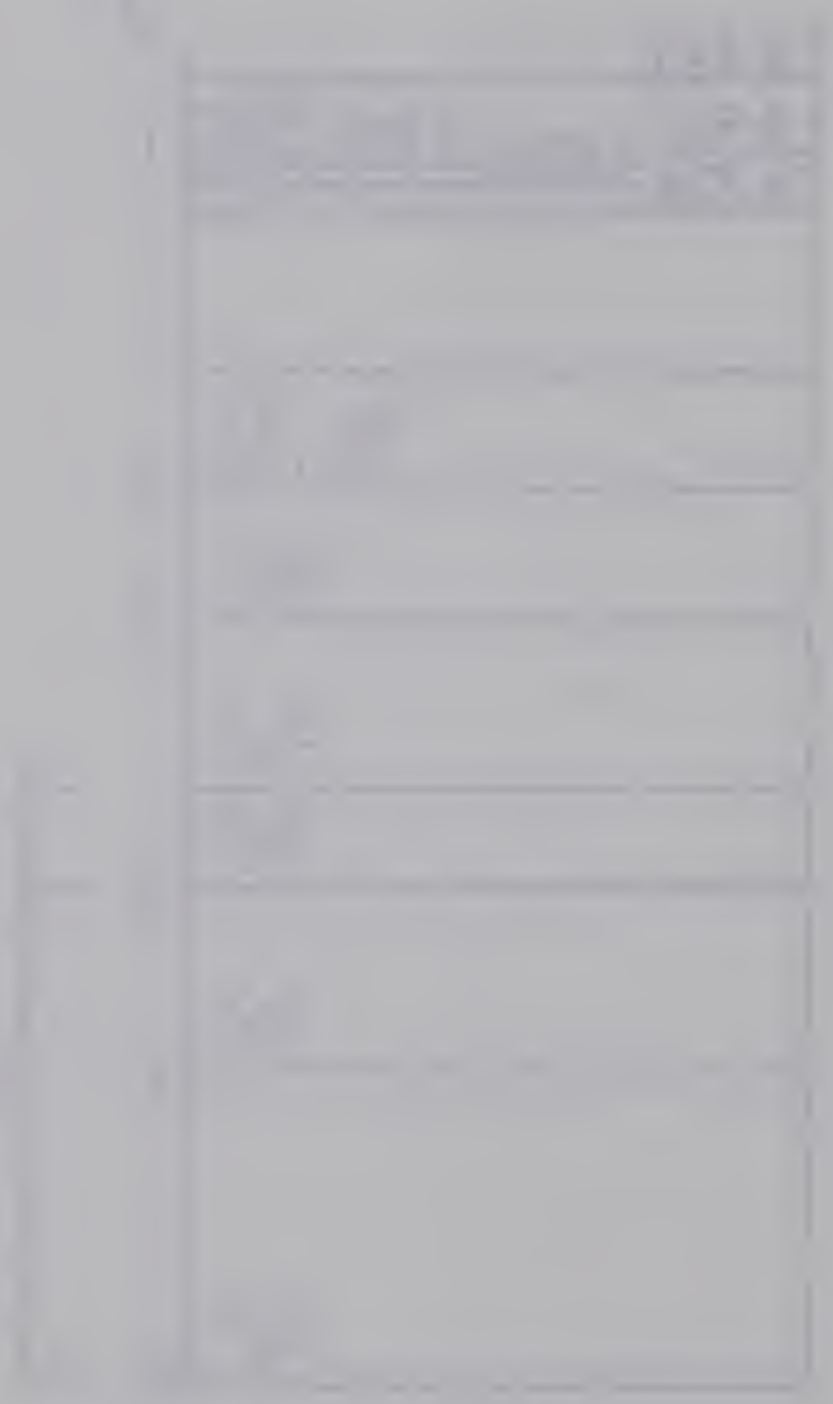

generalized single particle model in which a single nucleon is considered to move in the field of a permanently deformed core, rather than the spherical core of the simple shell model. The relative levels of these single particle states in the vicinity of the 2s - 1d shell is shown in figure 1-2 as a function of the core deformation δ. The notation at the $\delta = 0$ intercept identifies the single particle state corresponding to a spherical potential on which the particular orbits are based. The number and sign on the orbit curves themselves represent the values of K, the projection of the total angular momentum I on the nuclear symmetry axis, and the parity.

The value of $\delta = -0.15$ established by Bromley for ^{29}Si is indicated on the Nilsson Model diagram, from which the relative positions of the single particle states can be determined.

On each of these single particle levels, rotation of the deformed nucleus as a whole produces a rotational band of levels each with the same intrinsic structure. In ^{29}Si, the rotational band based on the 1/2 + ground state could comprise either the level sequence at excitations of 0.0, 1.28 and 2.03 MeV, or that at 0.0, 2.03 and 2.43 MeV, both of which contain levels of total angular momentum I = 1/2, 3/2 and 5/2. Bromley demonstrated that the second of these sequences is preferred, leaving the 1.28 MeV level as the base for a K = 3/2 rotational band.

Coupling between rotational and particle angular momenta (RPC) has the effect of mixing together states with differing K. Generally, for nuclei with well-developed asymmetry, the rotational spacing is small compared with the particle excitation energies, and

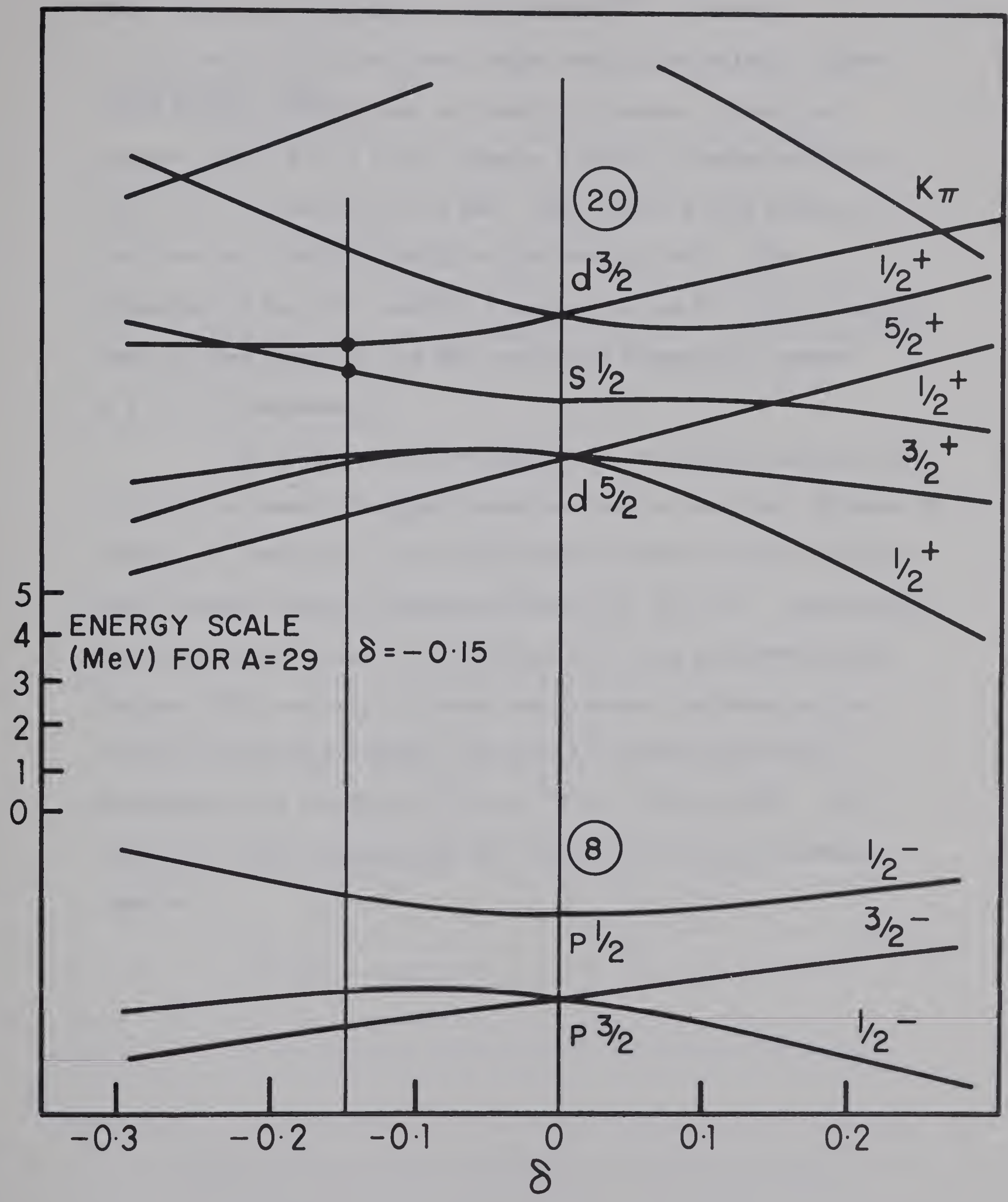

FIGURE 1 - 2: NILSSON MODEL DIAGRAM

this effect can be ignored. However for ^{29}Si, where the K = 1/2 and K = 3/2 rotational bands overlap appreciably, these "band mixing" effects must be taken into account. Thus, for example, the 3/2 +, K = 3/2 state at 1.28 MeV is mixed with the 3/2 +, K = 1/2 state at 2.43 MeV. The effect of this mixing is to alter the relative spacing of the energy levels. The inversion of the 3/2 + and 5/2 + members of the K = 1/2 rotational band is also caused by the RPC term which essentially removes a K = $\pm$ 1/2 degeneracy.

The mathematical development of the strong coupling model is given in several original papers and review articles, (Nilsson 55, Davydov 58, Newton 60) and is discussed in detail in most graduate level nuclear physics textbooks (Preston 63, Roy 67). Calculations, including the effects of band mixing, have been performed on the nucleus ^{29}Si, not only to obtain spectroscopic information concerning its level structure, but also to predict the cross-sections in the reactions $^{28}Si(d,n)^{29}P$ and $^{28}Si(d,p)^{29}Si$. The results of these calculations are referred to in the following chapter.

CHAPTER 2: REACTION THEORY

1. The Optical Model

The approximation that the many-body problem arising from interactions between an incident particle and the many nucleons of a target nucleus may be replaced by a two-body problem is known as the "Optical Model". As in the Nuclear Shell Model, the effect of the many nucleons in the target is approximated by a potential, U(r), and the motion of the incident particle is assumed to be described by the Schrodinger equation:

$$\nabla^2 \psi + \frac{2\mu}{\hbar^2} (E - U(r)) \psi = 0$$

where μ is the reduced mass

and $U(r)$ is the "Optical Potential".

The optical potential used in the following discussion has the form:

$$U(r) = V_c(r) - Vf_{ws}(r,r_o,a) + 4ia_I W \frac{d}{dr} f_{ws}(r,r_{oI},a_I) + \left(\frac{\hbar}{m_\pi c^2}\right)^2 V_s \frac{d}{rdr} f_{ws}(r,r_o,a) \vec{\ell}\cdot\vec{\sigma} \qquad 2\text{-}1$$

where r is the relative separation of the interacting nuclei,

and

$V_c(r)$ is the Coulomb potential of a sphere of radius $R_c = r_{oc} A^{1/3}$, namely:

$$V_c(r) = \frac{Ze^2}{2R_c}\left\{3 - \frac{r^2}{R_c^2}\right\} \qquad r < R_c$$

$$V_c(r) = \frac{Ze^2}{r} \qquad r > R_c \qquad 2\text{-}1(a)$$

f_{ws} is the Wood-Saxon form factor:

$$f_{ws}(r,r_o,a) = \frac{1}{1 - \exp((r-r_o A^{1/3})/a)} \qquad 2\text{-}1(b)$$

where r_o and a are the radius and diffuseness parameters respectively. To properly account for deformed nuclei such as ^{29}Si, it would probably be better to use a non-spherical potential, however this has only been attempted in a few isolated cases (Shey 59).

V is the strength of the refracting part of the potential; and the imaginary part, with strength W, accounts for attenuation of the incident beam through inelastic processes. At low energies, where the Pauli principle prevents collisions, particularly in the dense nuclear interior, most absorption is likely to take place on the surface. Strong surface absorption, of course, is also required to take into account the easy break-up of the loosely bound deuteron. Consequently, a derivative form of absorptive potential has been used. It should be pointed out that to replace all absorption processes with a smoothly varying imaginary potential can obviously not account for the effects of resonances typical of compound nucleus formation, but only for an energy average of the cross-section.

V_s is the strength of a spin-orbit interaction of the Thomas type, which is also peaked at the surface,

m_π is the pion mass

$\vec{\ell}$ is the orbital angular momentum; and

$\vec{\sigma}$ is the spin operator.

Both V and W are found to depend upon the incident deuteron energy. This energy dependence is probably due at least in part to the fact that the potential is almost certainly non-local. That is, the energy of a particle at point $\vec{r}$ depends not only on $\vec{r}$ but also on the wave function at $\vec{r}' \neq \vec{r}$. Such a non-local potential may be described (Perey 62) by:

$$V\psi(r) = \int V(r,r')\psi(r')dr'$$

where $$V(r,r') = U(1/2|r+r'|)H(|r-r'|)$$

and $$H(|r-r'|) = \frac{\exp(-((r-r')/\beta)^2)}{\pi^{3/2}\,\beta^3}$$

where the length β is known as the non-locality range. Solving the Schrodinger Equation with such a non-local potential is generally very difficult, and some approximation must be made. In the "local energy approximation" the distorted wave given by this potential can be obtained from that given by the equivalent local potential $U_L(r)$ (which gives the same scattering) by multiplying it by:

$$f(r) = 1/\sqrt{1 - 1/2\ U_L(r)(m\beta^2/h^2)}$$

where m is the mass of the particle. This has no effect outside the nucleus where $U_L(r) \to 0$, but damps the wave function in the interior where $U_L(r) < 0$.

2. Compound Nucleus

Elastic Scattering, to which the optical model is applied, is only the special case $a = b$, $A = B$ of the general nuclear reaction

$$A(a,b)B$$

where A is the target nucleus,

a is the incident particle,

b is the outgoing particle, and

B is the residual nucleus, which may be left in an excited state, designated B^*.

Such reactions may proceed through "Compound Nucleus" formation, in which the incident particle is completely absorbed by the target nucleus into a compound state, sharing its energy at least partially with some or all of the target nucleons before one particle acquires sufficient energy to escape the compound system. Such a process may take approximately 10^{-16} seconds. Alternatively, the reaction could proceed via a "direct" mode, in which the incident nucleon interacts with only one or a few of the surface nucleons of the target in the time it takes to pass by the nuclear diameter - typically 10^{-22} - 10^{-23} seconds.

Any reaction observed in the laboratory may be proceeding by both of these mechanisms simultaneously, and its analysis may be further complicated by interference between these two amplitudes. An attempt has been made to analyse the direct part of the reactions studied in this thesis using the Distorted Wave Born Approximation (DWBA), and the compound nucleus amplitude with a statistical, or

Hauser-Feshbach calculation. The interference effects cannot easily be treated theoretically, and so nothing has been done beyond commenting on their magnitude and probable effect on the experimental results.

The compound nucleus may be thought of as a system whose configuration is constantly changing, periodically separating into two or more parts which may either escape from each other or redissolve into another configuration. The ratio of the number of times the escape occurs to the number of times the particular configuration arises is known as the "transmission coefficient" for that channel.

The cross-section for the compound nucleus contribution to a given reaction is then simply the probability of formation of a compound nucleus at a certain energy multiplied by the probability of its decay through a certain channel. The latter probability is simply the ratio of the transmission coefficient for the channel in question to the total transmission coefficient for all possible decays. The probability for formation of the compound nucleus is clearly closely related to the absorption of particles from the incident beam, and hence to the imaginary part of the optical potential discussed in the previous section. For the reactions under study in this thesis, namely ^{28}Si + d, the calculation assumed the values of the deuteron optical potential 1B obtained in Chapter 4, although the results are found to be rather insensitive to this potential.

The compound nucleus ^{30}P was formed at an excitation of ~ 16.5 MeV, and proton decays to levels up to 11.25 MeV in ^{29}Si were possible. This includes well over 100 levels, about which very little spectroscopic information is available. Consequently it was necessary

to assume a statistical distribution of states in ^{29}Si based on a level density calculation incorporated into the Hauser-Feshbach program of W. R. Smith (Smith 67) by N. E. Davison (Davison 68). The level density was assumed to increase exponentially, and values for higher excitations were extrapolated from figure 2-1 which was plotted for the first 70 levels.

3. Direct Reactions:

(a) DWBA: Having subtracted the compound nucleus contribution as computed by the Hauser-Feshbach calculations from the experimental cross-sections, predictions of the direct reaction amplitude were compared with the remaining angular distributions.

The calculation of the transition amplitude between the initial state (A,a) and the final state (b,B) is performed to first order only in the interaction potential between the incident particle and the target nucleus. That is, the actual initial state wave function is assumed to differ little from the incident wave, and is replaced by the latter in the calculation of the transition amplitude. This is known as the Born Approximation. The Born Approximation, by equating the initial wave function with the elastic scattering wave function, assumes that contributions from other channels are small, that is, that elastic scattering predominates. The validity of this assumption is somewhat in doubt in the case of a deformed nucleus where rotational levels built on the ground state might cause inelastic scattering channels to be strongly coupled to the incident channel. In such a case the Born Approximation is no longer valid, and contributions from the strongly coupled channels should

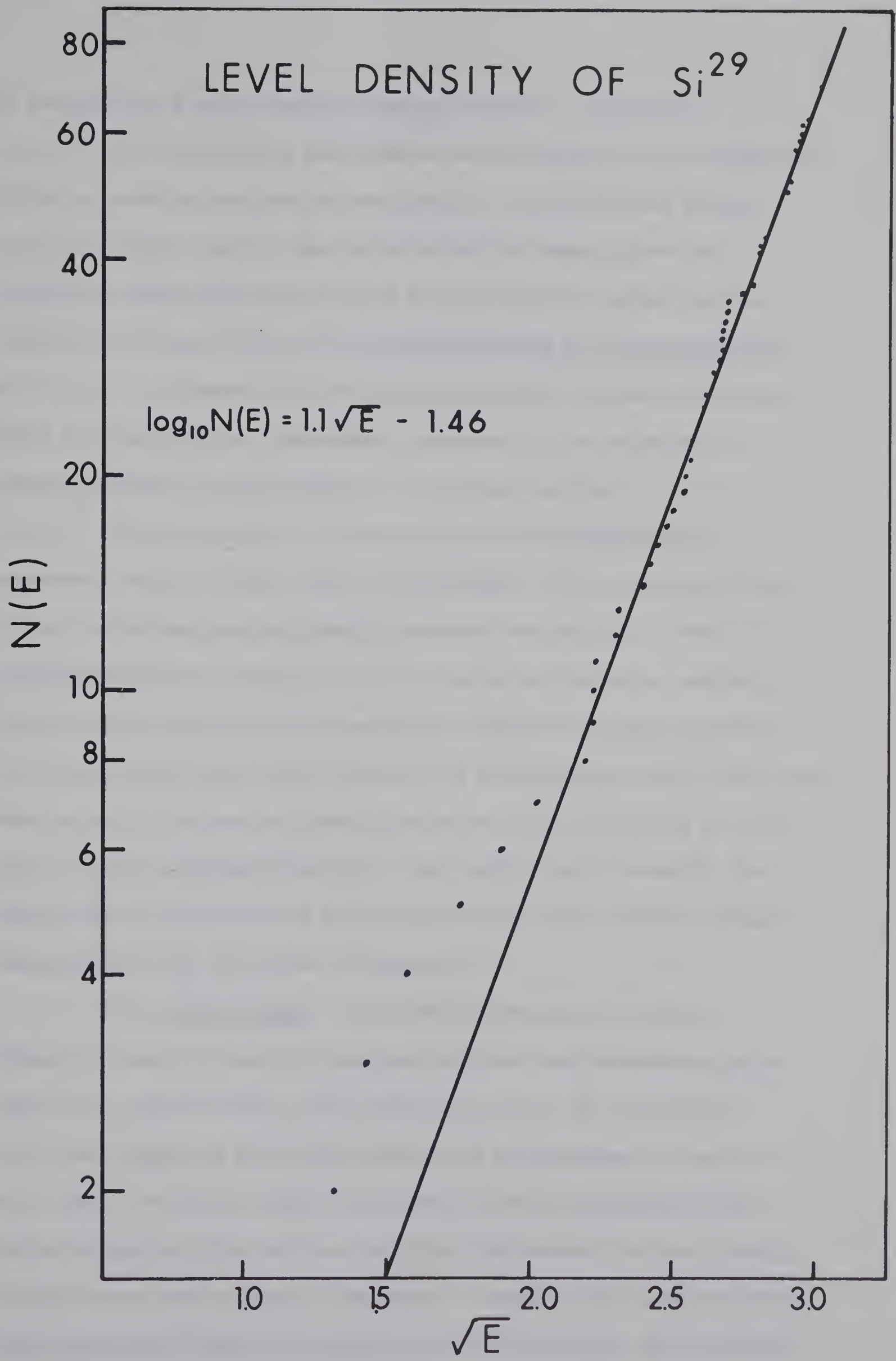

FIGURE 2 - 1: LEVEL DENSITY OF SILICON 29

be included in a more complex "Coupled Channel" calculation.

If the incident and final waves are allowed to be distorted by the scattering and partial absorption of the deuterons before actual stripping, and of the proton after the event, then the transition amplitude is calculated using distorted waves, and the calculation is said to be in the Distorted Wave Born Approximation, or D. W. B. A. These distorted waves are simply the wave functions found from solving the Schrodinger Equation for the appropriate optical potential as described in a previous section.

It is important to observe that elastic scattering determines only the phase shifts at infinity, and consequently many optical potentials may be found to account for the data. The corresponding wave functions will be similar at infinity, but will differ in the vicinity of the nucleus. Reactions, being sensitive to the wave functions in the vicinity of the nucleus, impose additional constraints on the optical model parameters, and it was one of the hopes of this experiment that this fact might clarify some of the ambiguities in the deuteron optical potentials obtained from elastic scattering on ^{28}Si described in Chapter 4.

(b) Finite Range: A further approximation which is frequently made in these calculations is that the interaction which causes the transition has "zero-range", that is, the transition occurs only when the interacting particles are extremely close to each other. A "finite range" calculation, which accounts for the finite projectile size and the fact that the interaction must surely act over some finite range, is extremely complex; but, like the non-local potential, can be estimated in the "local energy approximation"

by multiplying the bound state wave function by a factor which is a function of the various optical potentials involved, and a "range parameter", R. It was discovered early in the history of the DWBA theory that fits to experimental data could be much improved by cutting off the radial integration at some arbitrary point in the nuclear interior. Both non-local and finite range calculations have the effect of decreasing contributions from the nuclear interior, and consequently the same effect as a radial cut-off. These approximations are far preferable to a radial cut-off as they have some physical basis and affect the wave function smoothly. They are now frequently included in DWBA calculations.

(c) Spectroscopic Factors: Because only a few nucleons actively participate in a direct reaction, the transition amplitude contains an overlap integral involving the passive nucleons. This overlap measures the degree to which the passive nucleons occupy the same configuration in the initial and final states, and is called the spectroscopic factor. If in a stripping reaction, for example, a particle is stripped into a pure single particle state leaving an assumed core unaffected, the spectroscopic factor, S, would be unity. If, on the other hand, the final state of the residual nucleus is a rotational level, the core configuration will have changed a great deal and the spectroscopic factor would be expected to be small.

In evaluating the final state wave function from a stripping reaction, most DWBA calculations simply couple the stripped nucleon to the inert core, producing a single particle wave function, and therefore a spectroscopic factor of 1. If the corresponding experiment determines an absolute cross-section, then the ratio

$$\frac{(d\sigma / d\Omega)exp}{(d\sigma / d\Omega)DWBA}$$

is the experimental spectroscopic factor.

By overlapping the wave function predicted by a nuclear model for a given residual state, predictions of spectroscopic factors may be obtained. W. G. Davies (Davies 66) has done such a calculation by applying the Nilsson Model discussed earlier to ^{29}P and the results should be the same for ^{29}Si. Expressed relative to the ground state spectroscopic factor, they are:

$$S_{rel}\ gs = 1.0$$

$$S_{rel}\ 1.28 = 2.1$$

and $$S_{rel}\ 2.03 = 0.45$$

These predictions are compared in Chapter 5 with the experimental results.

(d) Polarization: One consequence of the different absorption for deuterons and protons by the nucleus is that protons emitted from reactions for which $\ell n \geq 1$ may be polarized, that is, be spinning in a preferred direction relative to the reaction plane. For $\ell = 0$ transfer, however, no such effect is possible, and the polarization, if any, of outgoing protons must be a direct result of the influence of spin-dependent forces in the optical potential. Such forces are known to have a small effect on both the elastic and stripping cross-sections, and so the measurement of the proton polarization can be expected to be the most sensitive probe of this part of the optical potentials causing the distortion. This fact has

been referred to in Chapter 6, where the proton polarization for the $\ell n = 0$ angular momentum transfer reaction $^{28}Si(d,p)^{29}Si$ gs is discussed.

(e) Improvements: Although it has had notable successes, the DWBA theory is far from being entirely satisfactory. It fails to predict the proper shape for angular distributions at angles farther back than 90^{o}, particularly for reactions with high angular momentum transfer. Moreover, it has had only occasional success in predicting the polarization in stripping reactions. Several efforts are being made to improve the theory by including the effect of the deuteron d wave (Johnson 67) and polarizability, or by the use of deuteron optical potentials constructed from nucleon potentials (Perey 67). Including the effects of other strong channels by solving coupled channel equations is another promising approach. Others are meeting with considerable success by using entirely new stripping theories (Pearson 66, 66a, 66b, Butler 67). In any case it is clear that a great deal of work, both experimental and theoretical, is required in the study of nuclear reaction mechanisms.

PART II: EXPERIMENTAL

1. Instrumentation:

(a) General Design: Most of the apparatus used in these experiments has been described in some detail elsewhere (Gurd 66, Gurd 68, Leighton 68). This chapter, therefore, is restricted to a very brief outline of the equipment, with emphasis on those components which are new or improved from the description of reference Gurd 66.

Figure 3-1 shows the overall layout of the experiment. After 90^{o} magnetic analysis, the beam from the University of Alberta 5.5 MeV CN Van der Graaff* enters the target chamber (A) through a pair of tantalum collimating slits (D). Scattered particles then enter a 50 cm. magnetic spectrometer**(G) where they are momentum analysed before impinging on the detection system (J).

For the very low yield double scattering (polarization) experiments, a single quadrupole lens (B) is inserted between the spectromagnet and the target chamber. This allows focussing of particles in the direction normal to the reaction plane (Enge 58) thereby increasing the solid angle from $\sim 4 \times 10^{-4}$ steradians without the lens to $\sim 2 \times 10^{-3}$ steradians with it. The lens is not used for cross-section measurements because of the difficulty then present of maintaining a constant solid angle (Gurd 66).

(b) Target Chamber: An 8" diameter stainless steel target chamber of the sliding seal type has been used in all of these experiments. The sliding seal, of 0.010" stainless steel, allows the magnet to be rotated from -20^{o} to $+140^{o}$, or -20^{o} to $+115^{o}$ with the quadrupole lens in position. The target chamber contains facilities for mounting three targets, which may be inserted into the beam line without affecting the

*High Voltage Engineering Corp., Burlington, Massechusettes
**Spectromagnetic Industries, Inc., Hayward, California

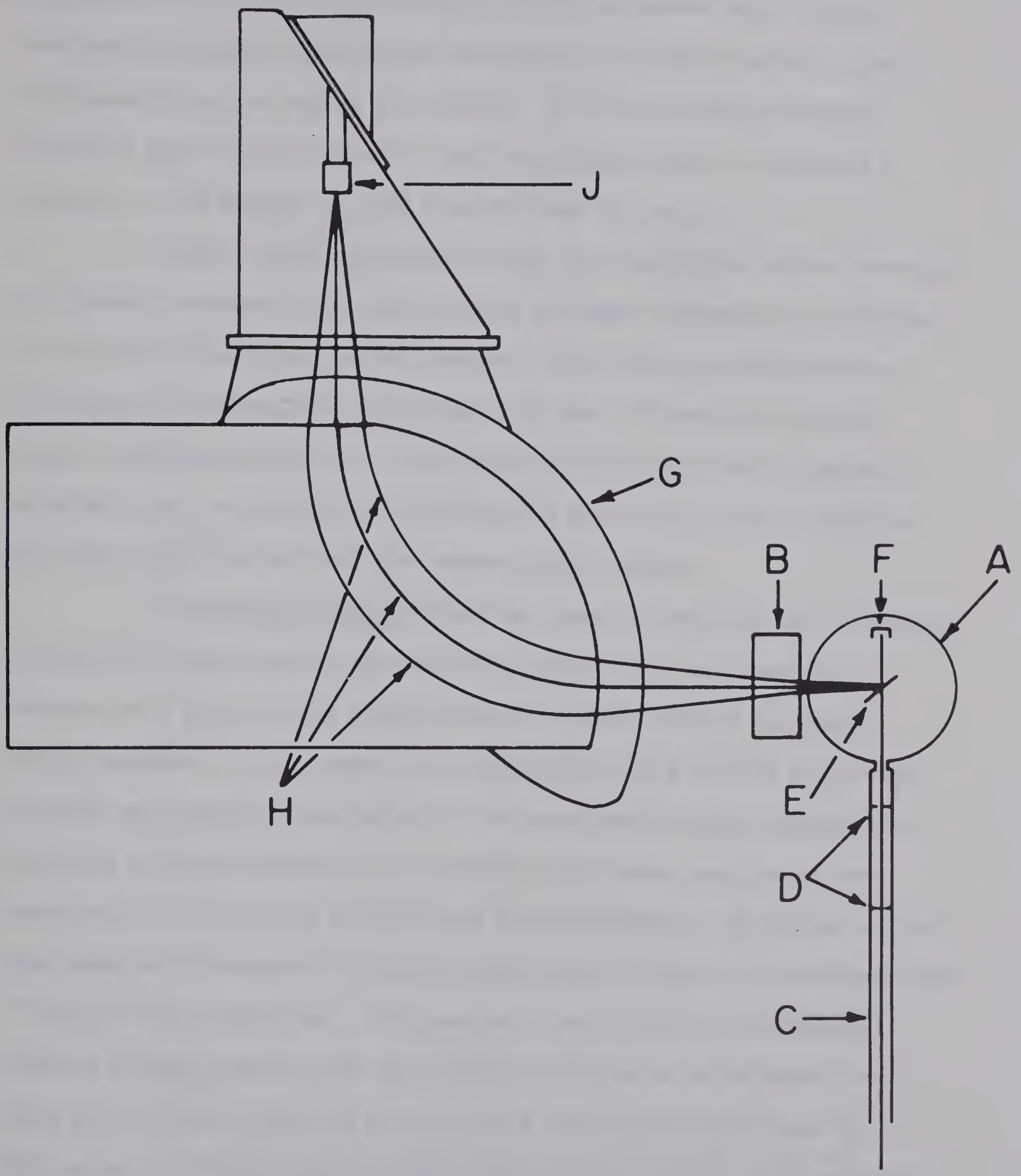

FIGURE 3 - 1: SCHEMATIC DIAGRAM OF APPARATUS

vacuum. An air-cooled Faraday Cup stops the beam at the back of the chamber for purposes of current integration, and allows for electron suppression. Facility is provided for mounting several solid state detectors at angular intervals of 20 degrees, and these can be rotated independently of the magnet and chamber. A two inch Edwards Mercury Diffusion Pump* coupled directly into the chamber helps to maintain a pressure in the chamber of less than 10^{-5} mm. Mercury.

The slit telescope through which the beam passes before entering the chamber, consists of an outer sleeve of brass into which slit systems with different apertures may be inserted. Each system consists of two rectangular tantalum slits separated by 20 cms, followed by a slightly larger anti-scattering slit. The position of the slits may be adjusted externally both vertically and horizontally within the sleeve, allowing the beam to be directed into the center of the chamber.

(c) Detection System: For the elastic scattering and stripping cross-section measurements the detection system ((J) in figure 3-1) consists of a single solid state detector mounted behind a four-step energy degrader, or step wedge. As described in Gurd 66, the step wedge provides some position resolution in the spectrometer mode, allowing the scattered particles always to be focussed at the same position on the detector, and the quality of the focus to be estimated. The effect of the step wedge is illustrated in the test spectrum of figure 3-2 (obtained from $^{197}Au(p,p)^{197}Au$ scattering). In practice, the particles were generally focussed between steps #2 and #3, the criterion for a satisfactory focus being that not more than 20% of the counts fall into steps #1 and #4. This criterion insured that not more than 1% of the counts could be lost off the side of the detector.

---

*Edwards, 430 South Service Road, West, Oakville, Ontario

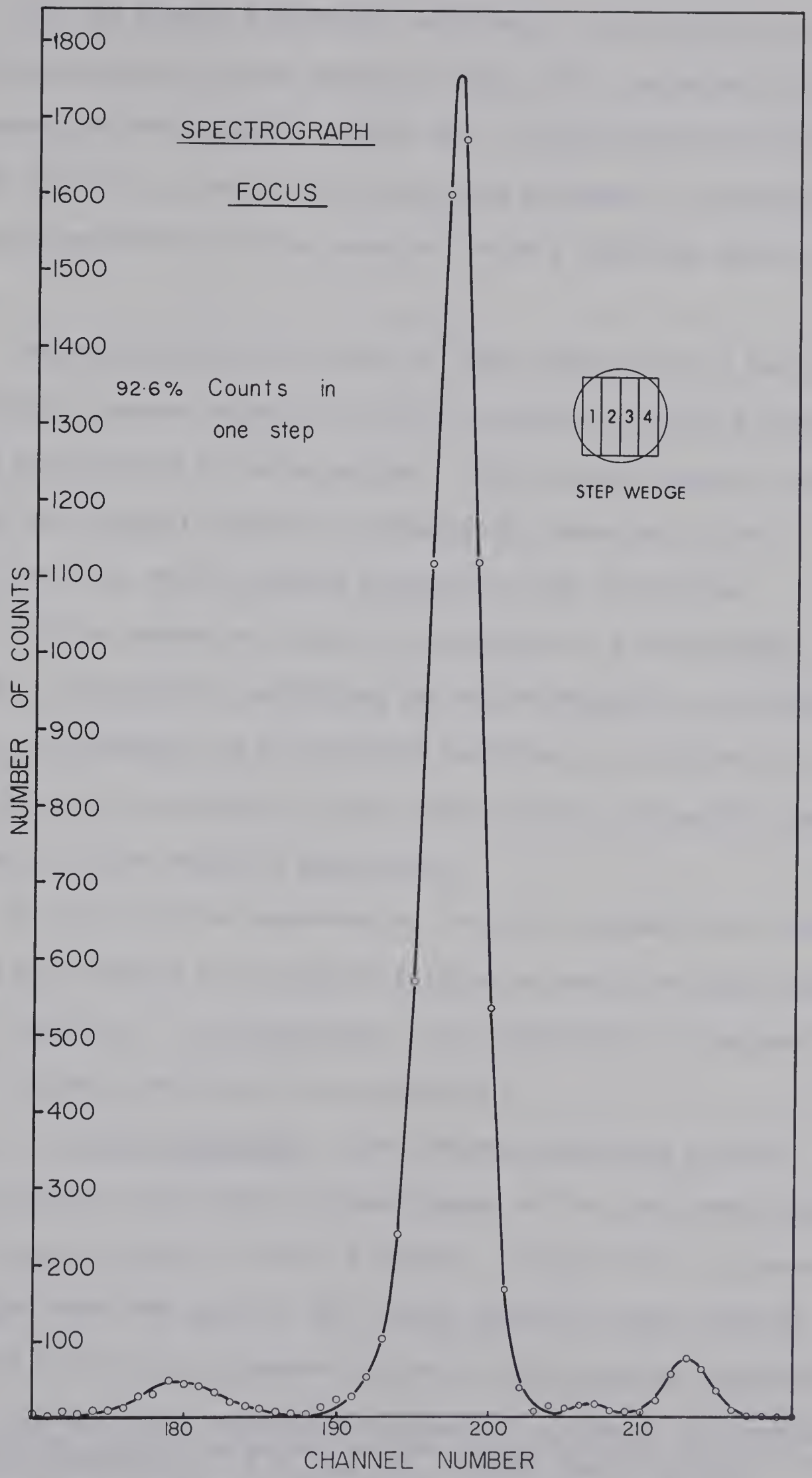

FIG. 3-2
EFFECT OF STEP WEDGE

For the elastic scattering experiments, the detector was a 78 mm^2 Silicon surface barrier detector with a 400 μ depletion depth.* This detector was not adequate to stop the ~ 11 MeV protons from the stripping reaction, so the detector mount was designed to accomodate a 100 mm^2 Lithium drifted Silicon detector** with a depletion depth of 1 mm as well.

Negative pulses from either of these detectors were fed into a preamplifier† located directly outside the magnet box before being amplified and analyzed for pulse height. The live-time display system on the SDS 920 computer greatly facilitates the focussing of the scattered particles at the desired positions on the step wedge.

The step wedge and detector are mounted on a plate which connects to a threaded rod permitting the entire assembly to be moved parallel to the central ray of scattered particles. In this way it can be located at the position of best focus, which is dependent upon the kinematics of the reaction under study.

For polarization measurements, the entire assembly can easily be removed and replaced by the carbon Polarimeter which has been described elsewhere (Gurd 68). For completeness, this description is included in an only slightly modified form as Appendix A.

(d) Field Measurement: The frequency modulated nuclear magnetic resonance system used for measurement of the spectrometer magnetic field has been described in detail elsewhere. (Olsen 62). Two important changes which have been made in this system should be noted, however. Firstly, all the circuits intended for use in field control have been eliminated, as they were considered unnecessary in view of the satisfactory

---

* Nuclear Diodes Inc., P.O. Box 135, Prairie View, Illinois
** Simtec Ltd., 3400 Metropolitan Blvd. East, Montreal 38
† Ortec #108, Oak Ridge Technical Enterprises Corp., Oak Ridge.

field stability achieved without them. This made possible the second alteration; the modulating frequency was changed from 200 cps. to 60 cps. and synchronized with the line voltage. These changes have not only greatly simplified, but also much improved the performance characteristics of the NMR system.

(e) Targets and Target Preparation: Several different targets were used during the course of this work, some prepared in this laboratory and others purchased. The majority of the elastic scattering data was taken with a natural silicon target of 450 $\mu gm/cm^2$ provided by the Oak Ridge Target Preparation Center.* The first elastic distributions, however, were taken with a self-supporting target of silicon prepared by the evaporation with an electron gun of natural silicon onto a well cleaned glass slide which had previously been coated with an evaporated layer of salt (NaCl). When the slide is placed in a bath of warm water, the dissolving salt leaves a layer of silicon floating on the surface which can then be picked up on a target holder. In this way, targets of thickness 200-500 $\mu gms/cm^2$ were prepared.

Using a similar technique, targets of SiO_2 of varying thicknesses were also prepared, and targets of SiO were made by evaporation from a resistance heated tantalum boat. The stripping reactions were performed with targets of Si and SiO with thicknesses of 200-300 $\mu gms/cm^2$. Thinner targets of SiO_2 (50-100 $\mu gms/cm^2$) were found to be convenient for the back angle measurements.

Several attempts were made to prepare targets sufficiently thick (~ 5 mg/cm^2) for use in the polarization experiment. Evaporation of silicon for long periods, blowing of quartz (SiO_2) bubbles, and the sawing of a thin wafer (~ 25 microns) from a silicon crystal were all

---

*Oak Ridge Target Preparation Center, Oak Ridge, Tennessee

attempted without success. The experiments were eventually performed using a 25 micron (~ 5.5 mg/cm^2) natural silicon target which had been sawed from a crystal by Nuclear Diodes* and mounted in a ceramic ring. This target proved quite satisfactory from the point of view of thickness and uniformity (less than 10% variation in thickness), however the rather thick (1/8") ceramic mount caused some problems in orienting the target at the optimum angle (Chapter 6). Moreover, the ceramic mount increased problems of heat dispersion, and after long exposure (2-3 days) to deuteron beams of 1-2 microamperes, they tended to crack if not allowed to cool very slowly before being exposed to air.

Because of the method used to measure absolute cross-sections (next section), it was never necessary to measure target thicknesses carefully. Consequently the thicknesses quoted here are only approximate, and have been arrived at by their relative yield in comparison with the thickness of 450 μgms/cm^2 quoted by the manufacturer of the natural silicon used in much of the elastic scattering work.

2. Data Taking:

(a) Relative Cross-Section Measurement: The relative cross-sections for the angular distributions from both elastic scattering and stripping reactions were obtained by normalizing to the integrated beam current collected on the Faraday cup. Normalization to beam current rather than to a stationary monitor counter was found to be necessary when a monitor counter installed in the target chamber gave inconsistant results by comparison with the spectromagnet. It was discovered that the counting rate in the monitor counter was rather sensitive to small changes

---

*Nuclear Diodes Inc., P. O. Box 135, Prairie View, Illinois.

in beam focussing conditions, due primarily to the fact that the small target chamber did not permit the detector to be removed sufficiently far from the target.

Before each series of runs, the current integrater* was calibrated with a resistor and a battery, as well as internally calibrated from scale to scale. At the end of each angular distribution, a point taken early in the distribution was checked to insure against target deterioration. The reproducibility of the data, as well as continuing checks on the current integrator calibration, suggest that errors introduced into the relative cross-section measurements due to current integration are certainly less than 2-3%. It should be reemphasized that the measurement of the total collected charge was not relied upon to give the Absolute cross-section.

Data points every 5^{o} between 20^{o} and 100^{o} for each angular distribution were obtained with the target at 45^{o} to the incident beam and in the transmission mode. The target was then rotated through 90^{o}, and the differential cross-section from 80^{o} to 140^{o} measured in the reflection mode. This provided 5 points between 80^{o} and 100^{o} to obtain a normalizing factor between data taken in the two target orientations. Due to target inhomogeneities and the difficulty of resetting the target angle exactly, this factor was not always unity.

(b) Absolute Cross-section Measurement: Absolute cross-sections were obtained by first scattering low energy protons (2 1/2 - 3 1/2 MeV) at forward angles (25^{o} - 35^{o}) from a silicon target. This scattering was assumed to be entirely coulomb, an assumption later verified by an optical model calculation, and so the cross-sections are

---

*Elcor, 1225 West Broad Street, Falls Church, Virginia.

known to be Rutherford. Plotting the number of counts accumulated for a specified total charge against the known cross-section (figure 3-3) allows one to find, from the slope, the factor which converts any measured number of counts to an absolute cross section.

With the same target, all the reactions studied - (d,d) and (d,p) at each energy - were then performed at 40^{o}, 50^{o} and 60^{o}. Thus the absolute cross-sections had been measured at three points on each of the elastic and stripping angular distributions, and the previously measured relative cross-sections were normalized to these points. It should be pointed out that this method of absolute cross-section measurement eliminates the need to know any of:

(i) the target thickness;

(ii) the solid angle of the detection system; or

(iii) the absolute total collected charge.

A measurement of the absolute cross-section of three points on the 5 MeV elastic scattering distribution which had been performed with a different target nearly one year earlier agreed in all cases to better than 5%, and it is felt that the absolute cross-sections obtained in this way are accurate to within ±5%.

3. Data Reduction

The raw data recorded for each data point included the laboratory angle at which the magnet was situated, the total integrated charge, the live and dead times, and, of course, the total number of counts accumulated. This information, together with normalization factors for conversion to absolute cross-sections, was then submitted in punched card form to the University of Alberta IBM 360 for reduction. The output of the reduction program included the center of mass angle, absolute cross-sections σ, averaged over any number of runs taken at

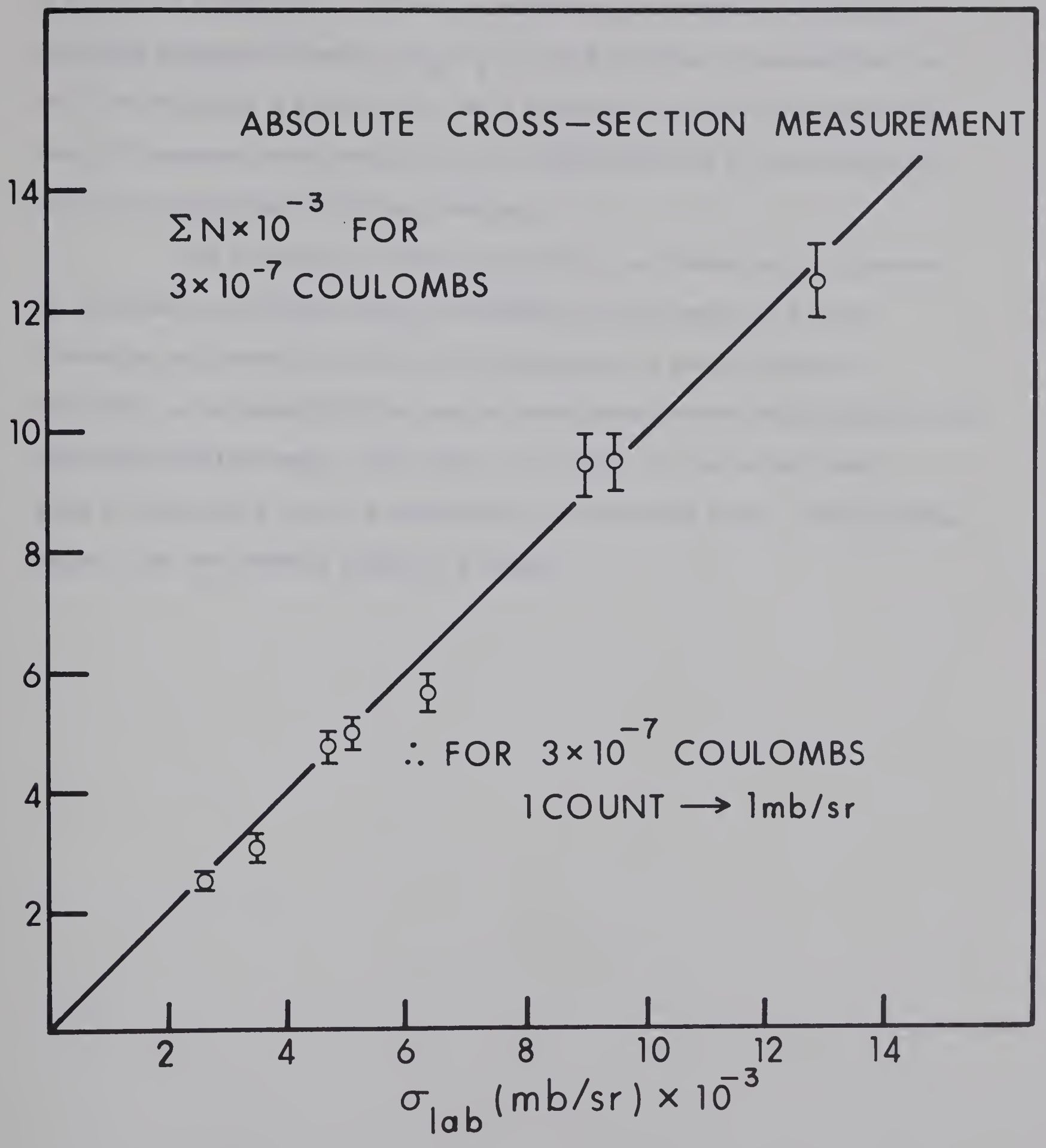

FIGURE 3 - 3: ABSOLUTE CROSS-SECTION MEASUREMENT

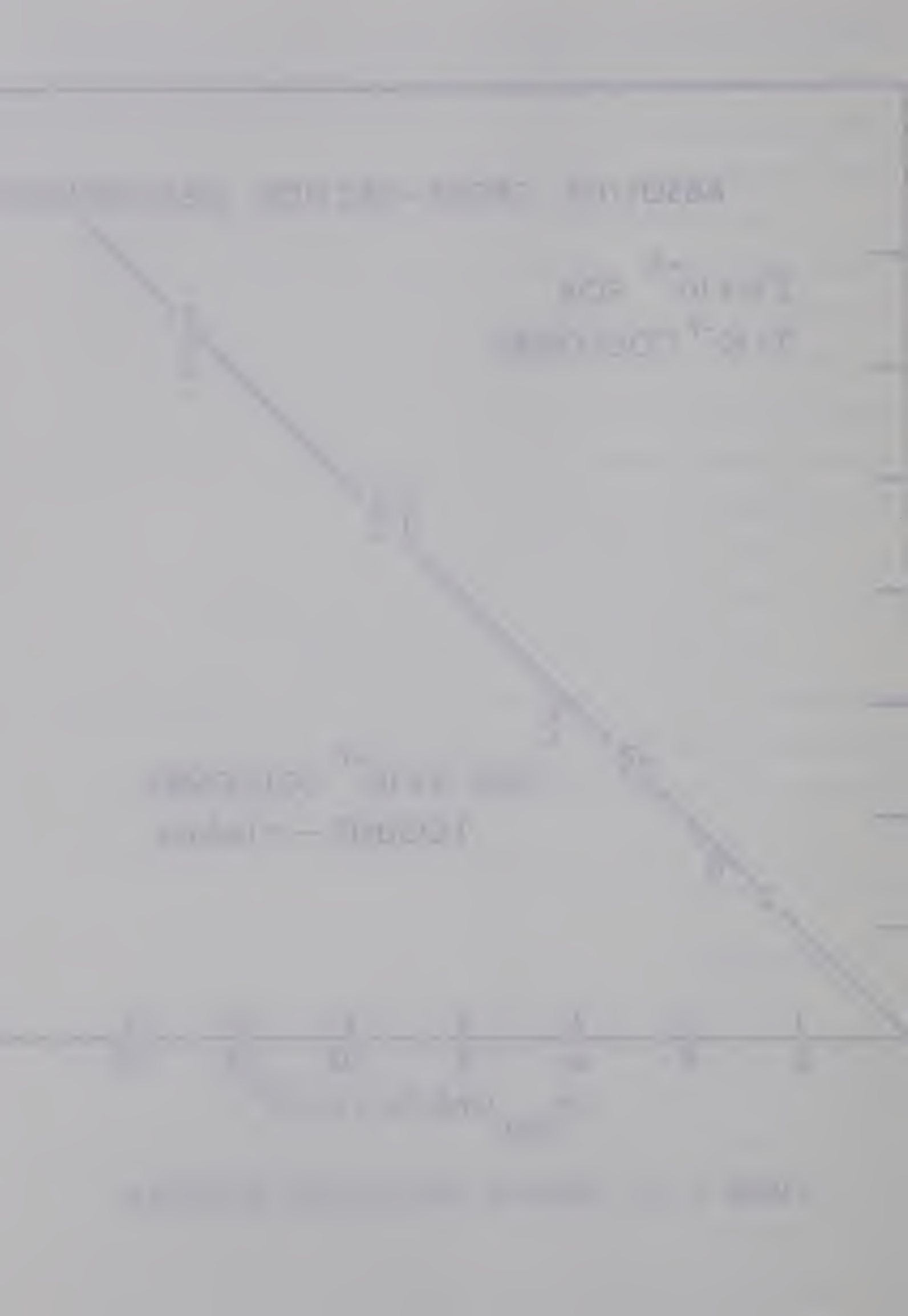

one angle, the statistical errors associated with each data point, and a plot of σ against c.m. angle. In addition, the elastic scattering analysis program evaluated σ/σ_R (σ_R is the Rutherford cross-section), as well as producing a plot of σ/σ_R as a function of c.m. angle, and a new deck of computer cards containing the reduced data in a form compatible with the optical model fitting program.

This simplicity of data reduction is a characteristic feature of experiments performed using the magnetic spectrometer. No time consuming and uncertain background subtraction or peak fitting is required, as is generally the case in experiments where entire spectra are observed simultaneously. The price, of course, is the rather slow rate at which data can be accumulated; one laborious level, one agonizing angle, just one painful point at a time.

PART III: RESULTS

CHAPTER 4: THE $^{28}Si(d,d)^{28}Si$ REACTION

1. Previous Work:

At the time that these experiments were initiated, no deuteron elastic scattering data was available on ^{28}Si in the energy region from 0-10 MeV. As a consequence of this Davies (Davies 66) was obliged to search over possible optical model parameters in order to obtain DWBA fits to the neutron angular distributions from the $^{28}Si(d,n)^{29}P$ reaction, with no assurance that the resulting optical potential would fit the elastic scattering. Lam (Lam 67), in analysing the neutron polarization from the same reaction, made use of the optical potentials given by Perey and Perey (Perey 66) from their analysis of the elastic scattering distributions taken at 11.8 MeV by Lorenz and co-workers (Lorenz 63). There is very little reason to expect that these parameters can be applied with no change at 5 MeV. Although some deuteron elastic scattering data was available for other nuclei in the same mass region and energy range (Maddison 62, Hodgson 60), the need for such an experiment on ^{28}Si was apparent.

2. Excitation Curves

As a preliminary to measuring angular distributions, excitation functions of the elastically scattered deuterons were taken at 60^{o} and 90^{o} in the energy region of interest. They are reproduced in figure 4-1. The solid line indicates the trend of $1/E^2$, the variation with energy of the Coulomb scattering cross-sections. It is immediately apparent that there are compound nucleus resonant effects present in these excitation functions, with fluctuations of over 15% on the 60^{o} curve, and of over 20% on the 90^{o} yield curve where the smoothly varying Coulomb contribution is much smaller. This resonant structure can be expected to be even

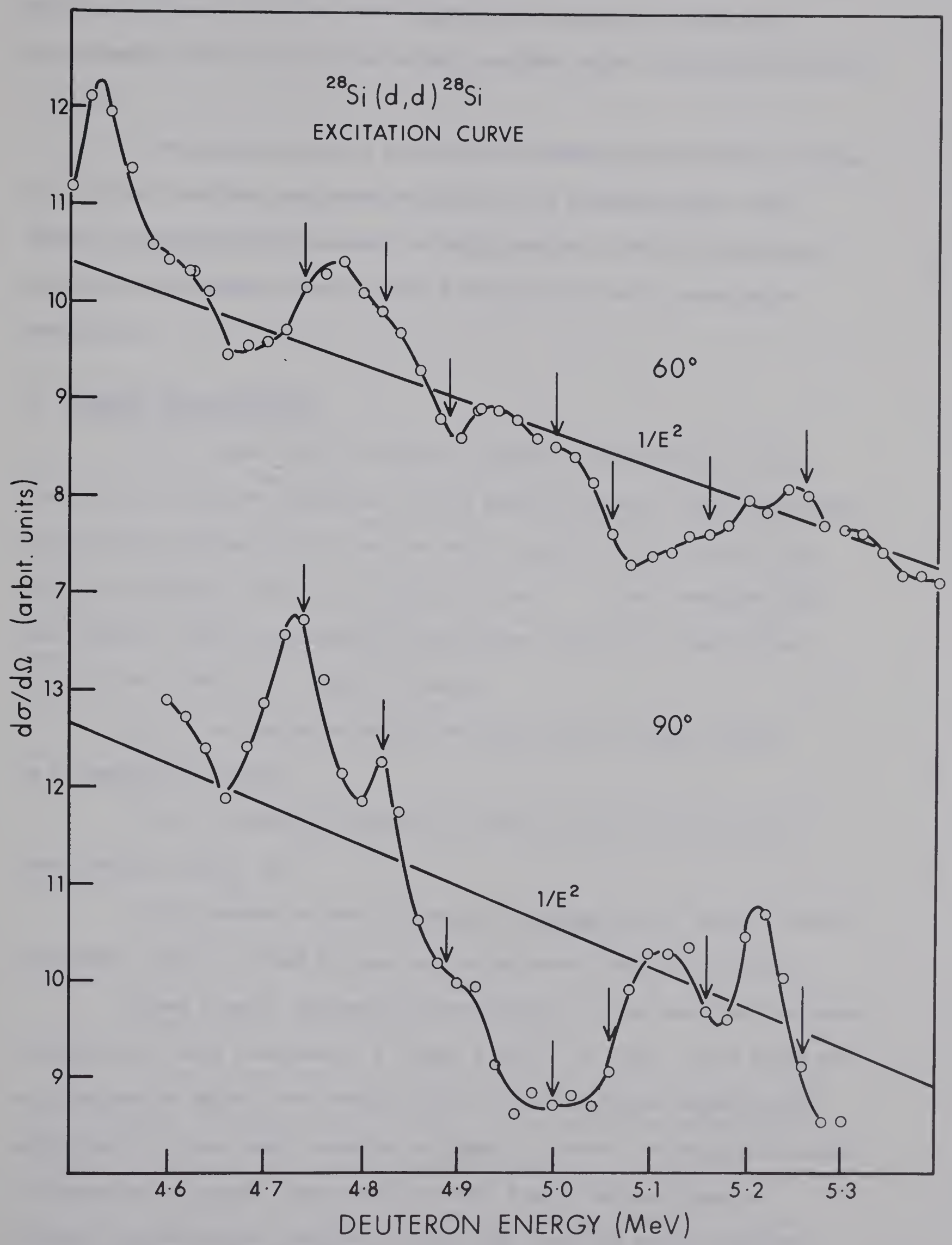

FIG. 4 – 1
ELASTIC EXCITATION CURVES

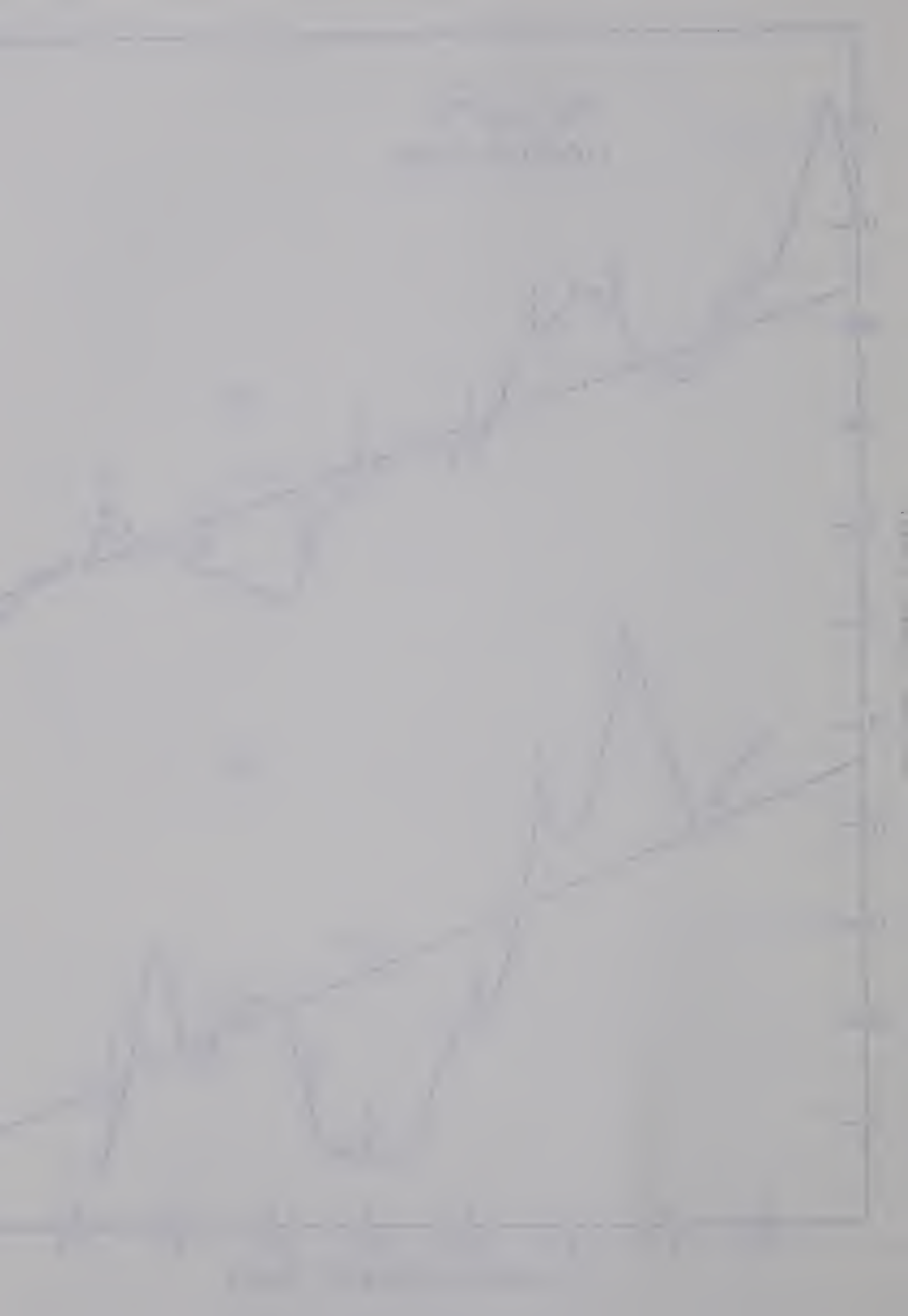

more pronounced at farther back angles. The resonance widths are approximately 100 keV, somewhat wider than the target thickness which was ~ 50 keV.

The apparent lack of correlation between the structure of these two curves, together with other evidence to be presented that shape elastic scattering predominates, strongly suggests that this structure reflects interference between shape and compound elastic scattering amplitudes.

3. Angular Distributions

It is clear that the shape of angular distributions of the elastically scattered deuterons in this highly resonant region could well be distorted substantially from that which would be obtained were the reaction mechanism known to be entirely direct. It was therefore felt that several elastic scattering distributions should be taken in the vicinity of 5 MeV with a view to finding

(i) the extent to which the distribution shapes varied as a function of energy,

(ii) the extent to which the optical potentials which fit these shapes varied, and

(iii) whether or not a reasonable average set of optical model parameters could be found for use in the projected DWBA calculations.

Seven elastic scattering distributions at the energies indicated in figure 4-1 were obtained in 5^{o} steps from 25^{o} to 140^{o}. Data could not be obtained at angles more forward than 25^{o}, as deuterons elastically scattered from even small amounts of Oxygen or Carbon contamination could no longer be resolved. Moreover, the very high cross-sections at extreme forward angles resulted in very high counting rates requiring either large dead time corrections or extremely low beam currents. It was

felt that either of these two alternatives resulted in too large uncertainties in the cross-section measurement.

It must be pointed out that all of the elastic angular distributions were performed with targets of natural Silicon, containing only 92.3% ^{28}Si. Deuterons scattered from the other isotopes (4.7% ^{29}Si and 3.0% ^{30}Si) could not be resolved at forward angles, and hence were included in the measured cross-sections. This does not affect the absolute cross-sections, however, since the same contaminants are included in the absolute measurement from proton scattering. There is an assumption implied here, that the nuclear contribution to the elastic scattering will differ little between these isotopes.

At angles farther back than 90^{o}, contributions from those isotopes cause a broadening of the image, although they do not become completely resolved. It is possible that some deuterons are thereby lost off one end of the step wedge, causing the measured relative cross-sections at back angles to be somewhat low. The maximum possible value for this effect is -8%, but it is not likely to be more than 1% or 2%. Because of the difficulty of estimating this unknown contribution, no correction has been made, and somewhat increased errors have been assumed in the relative cross-sections at angles farther back than 90^{o}.

At least 3000 counts were collected for each data point, insuring statistical errors of less than 2%, and in many cases 10,000 counts (<1% statistical error) were accumulated.

At the completion of each distribution, a recheck of an early angle was made to insure against target deterioration or other possible errors. In all cases but two this check fell within statistics. For the data at 4.89 MeV, which was taken with a different target, there appeared to be a deterioration of ~ 15% during the course of the run.

Further checks at other angles indicated that this deterioration had been linear with time, and a correction increasing by 1/2% per point was made to the data.

The recheck of the data at 5.06 MeV revealed a discrepancy of ~ 20%. The target used gave no indication of any deterioration during distributions taken either before or after this one, and repeating the measurements at several other angles gave no evidence of a linear deterioration here. Moreover this distribution, as is evident in figure 4-2, had a shape distinctly different from the shape of the other distributions. It was therefore felt, particularly in view of the proximity of this data to that at 5.0 MeV, that it would be best not to include it in the subsequent analysis.

The angular distribution at 5 MeV was taken several months before the 6 others. When these remaining distributions were taken, using a different target, a new detector assembly, and after having twice changed the coupling between the target chamber and the magnet, several points on the 5 MeV distribution were rechecked. The largest difference between these completely new absolute measurements and the previous determination of the cross-section was only 5%. The small statistical errors, combined with the generally high reproducibility of the data, has led to an estimated error in the absolute cross-sections of ±5%.

The seven elastic scattering distributions are shown in figure 4-2, plotted logarithmically as the ratio of the measured cross-section to the Rutherford cross-section in order to display better the pattern at back angles. The lines drawn through the experimental points are intended only as a guide to the eye. This presentation illustrates the essential similarity of the different shapes. Each has a minimum in the region of 50^{o}-60^{o}, and another, deeper minimum, between 100^{o} and 120^{o}.

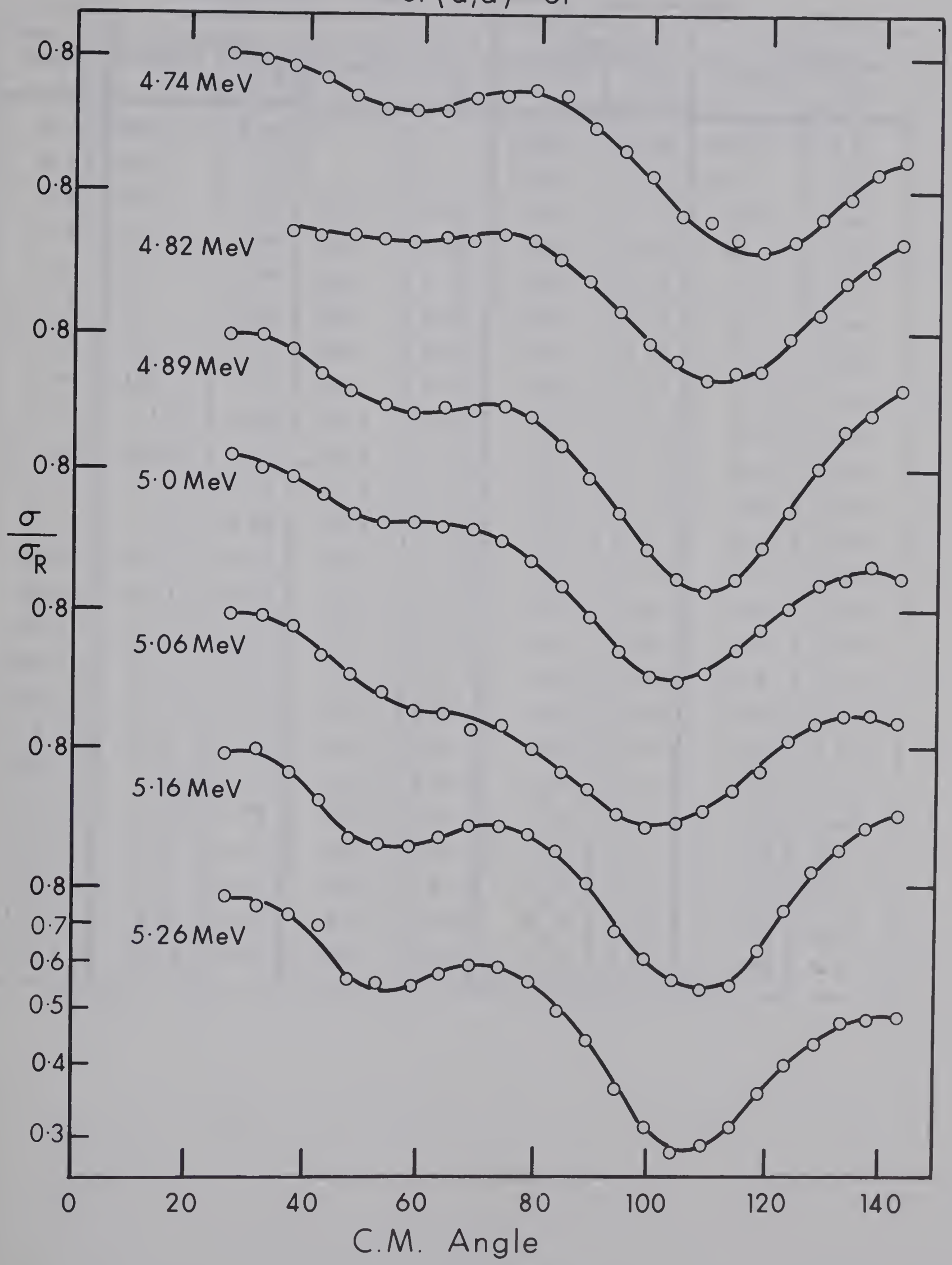

FIGURE 4 - 2: ELASTIC SCATTERING ANGULAR DISTRIBUTIONS

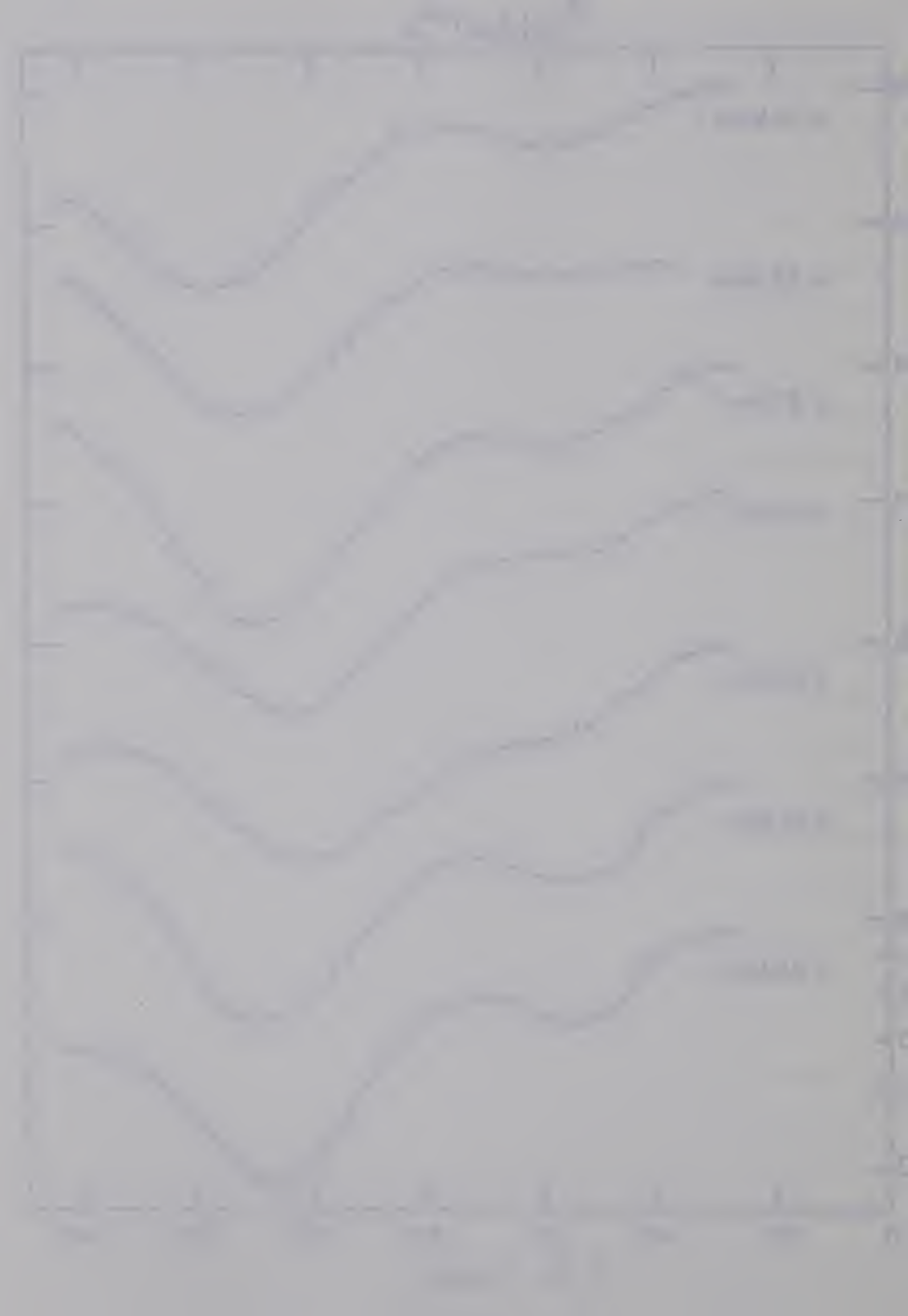

TABLE 4-1

$^{28}Si(d,d)^{29}Si$ - Elastic Scattering Cross-Sections

cm. Angle	4.74 MeV		4.82 MeV		4.89 MeV		5.0 MeV	
	σ mb/sr	σ/σ_R x 10	σ mb/sr	σ/σ_R x 10	σ mb/sr	σ/σ_R x 10	σ mb/sr	σ/σ_R x 10
26.75	3670	8.08			3394	7.95	3430	8.41
32.07	1766	7.91			1648	7.86	1622	8.08
37.4	962	7.80	831.1	6.97	870	7.51	866	7.81
42.7	548	7.38	489	6.80	477	6.94	483	7.23
47.9	329	6.89	314	6.79	284	6.34	290	6.76
53.2	211	6.51	208	6.65	185	6.07	189	6.49
58.4	150	6.53	146	6.59	126	5.85	134	6.51
63.6	110	6.53	110	6.74	94.4	5.95	97.7	6.45
68.8	87.3	6.83	82.6	6.68	71.6	5.96	72.7	6.33
73.9	69.0	6.93	65.8	6.83	56.4	6.03	54.4	6.07
79.0	56.1	7.07	50.8	6.61	43.0	5.76	40.5	5.67
84.1	45.1	6.98	39.0	6.24	31.3	5.15	29.5	5.07
89.1	32.3	6.02	30.0	5.70	23.1	4.59	21.7	4.51
94.1	25.1	5.55	22.2	5.07	16.7	3.92	16.0	3.93
99.1	19.7	5.08	16.7	4.45	12.5	3.43	12.4	3.56
104.1	14.5	4.31	13.6	4.17	9.47	3.00	10.6	3.50
109.0	12.4	4.20	11.0	3.86	8.07	2.90	9.59	3.61
113.9	10.4	3.95	10.1	3.97	7.47	3.02	9.37	3.96
118.8	8.97	3.78	9.14	3.99	7.59	3.41	9.20	4.32
123.6	8.35	3.88	9.45	4.53	7.91	3.91	9.07	4.68
128.4	8.41	4.25	9.61	5.02	8.75	4.71	9.08	5.11
133.2	8.47	4.62	9.96	5.62	9.33	5.42	8.72	5.29
137.9	8.79	5.13	9.91	5.98	9.39	5.83	8.45	5.49
142.7	8.63	5.35	10.4	6.64	9.77	6.44	7.64	5.27

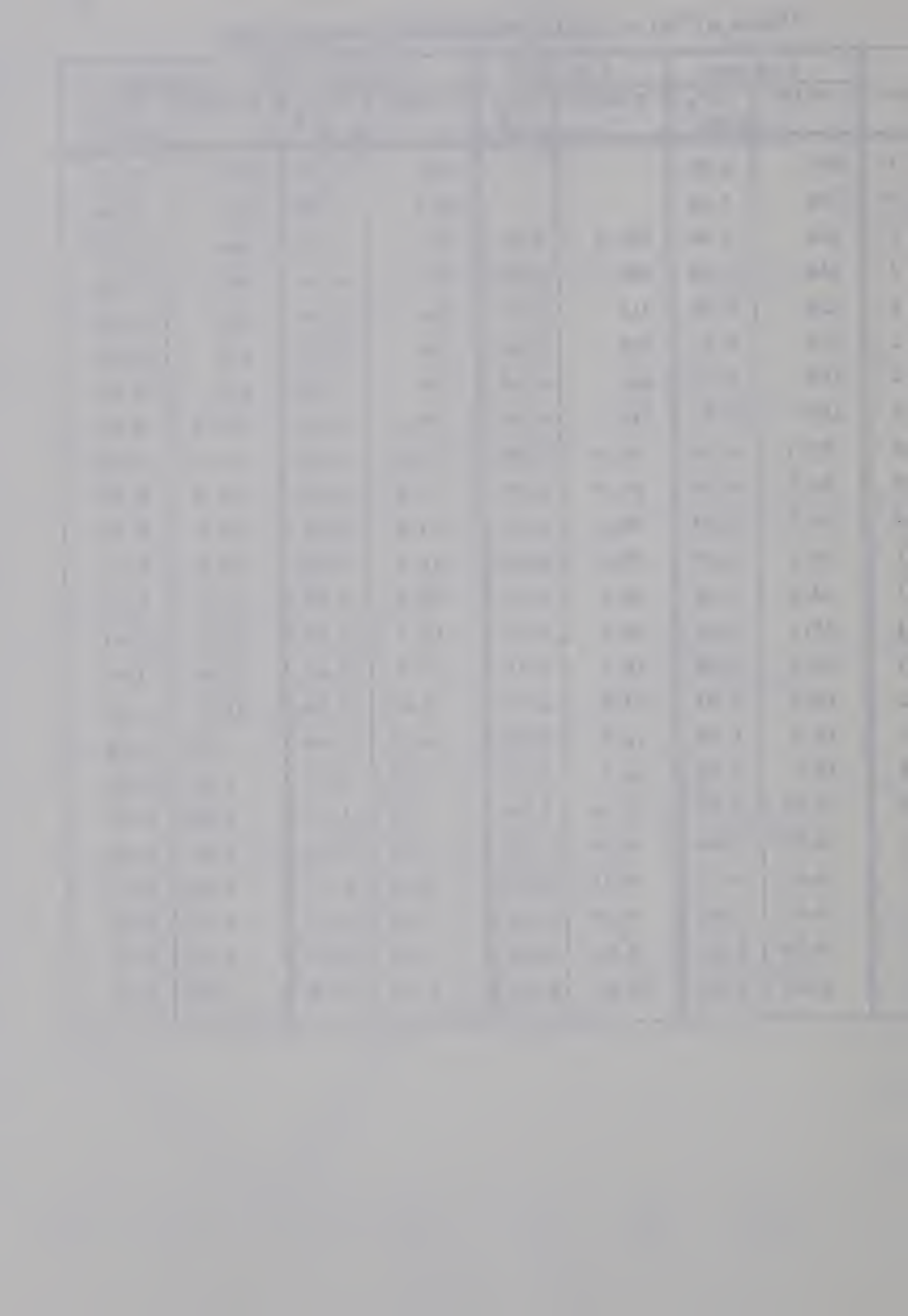

TABLE 4-1 (Continued)

$^{28}Si(d,d)^{28}Si$ - Elastic Scattering Cross-Sections

cm. Angle	5.06 MeV		5.16 MeV		5.26 MeV	
	σ mb/sr	σ/σ_R x 10^R	σ mb/sr	σ/σ_R x 10^R	σ mb/sr	σ/σ_R x 10^R
26.8	3140	7.88	2984	7.79	2825	7.66
32.1	1524	7.78	1484	7.87	1338	7.38
37.4	815	7.53	756	7.26	712	7.11
42.7	436	6.69	407	6.49	407	6.75
47.9	261	6.23	224	5.54	212	5.48
53.2	164	5.76	150	5.48	143	5.44
58.4	109	5.40	104	5.38	99.5	5.34
63.6	79.2	5.35	79.7	5.60	77.6	5.66
68.8	56.4	5.02	62.1	5.75	60.3	5.80
73.9	44.5	5.10	48.9	5.82	46.4	5.74
79.0	32.7	4.69	37.9	5.66	35.1	5.44
84.1	24.3	4.28	28.6	5.24	25.6	4.87
89.1	18.7	3.97	20.9	4.63	18.7	4.30
94.1	14.2	3.59	14.8	3.89	13.1	3.57
99.1	11.6	3.42	11.2	3.44	9.55	3.04
104.1	10.3	3.48	8.97	3.16	7.56	2.77
109.0	9.46	3.64	7.57	3.03	6.82	2.84
113.9	9.20	3.98	6.89	3.10	6.61	3.09
118.8	8.81	4.24	7.09	3.54	6.71	3.49
123.6	9.14	4.83	7.48	4.11	6.89	3.94
128.4	9.01	5.19	8.16	4.89	6.90	4.29
133.2	8.54	5.31	8.23	5.32	6.87	4.62
137.9	8.10	5.39	8.34	5.77	6.51	4.68
142.7	7.29	5.15	8.23	6.04	6.20	4.73

The differences in shape, due mainly to the interference resonant structure revealed by the excitation curves, is more apparent in figure 4-3. The main minimum of the 5.0 MeV distribution occurs at 100^{o}, that of the 4.74 MeV distribution at 120^{o}. The depth of this minimum for the 4.82 MeV distribution is $\sigma/\sigma_R = 0.39$; of the 5.26 MeV distribution is 0.28. Clearly, any deuteron optical potential which fits the elastic data at one energy will not fit any of the other distributions well. The need for caution in the optical model analysis is obvious.

4. Optical Model Analysis

The elastic scattering distributions were fit using the optical model code of Perey. The potential is of the usual Wood-Saxon form with surface absorption given in Chapter 2, equation 2-1. The Coulomb radius parameter, r_{oc}, was fixed at 1.30 fm.

The program does not allow for the inclusion of a spin-orbit potential for particles of spin one. Consequently, in these fits, $V_s = 0$. Perey, however, has shown that the inclusion of such a term does not improve the fit substantially, nor does it affect very greatly the values of the other parameters. The approach adopted, then, was to fit the elastic data without a spin-orbit potential, which could later be included when fitting stripping and polarization data without seriously affecting the quality of the elastic fits.

Without a spin-orbit term, there are 6 free parameters in potential 2-1 which may be independently adjusted to obtain a good fit. The quality of a fit is measured by the familiar χ^2 function:

$$\chi^2 = \sum_i \left(\frac{\sigma_i(\text{exp}) - \sigma_i(\text{theory})}{\Delta\sigma_i(\text{exp})} \right)^2$$

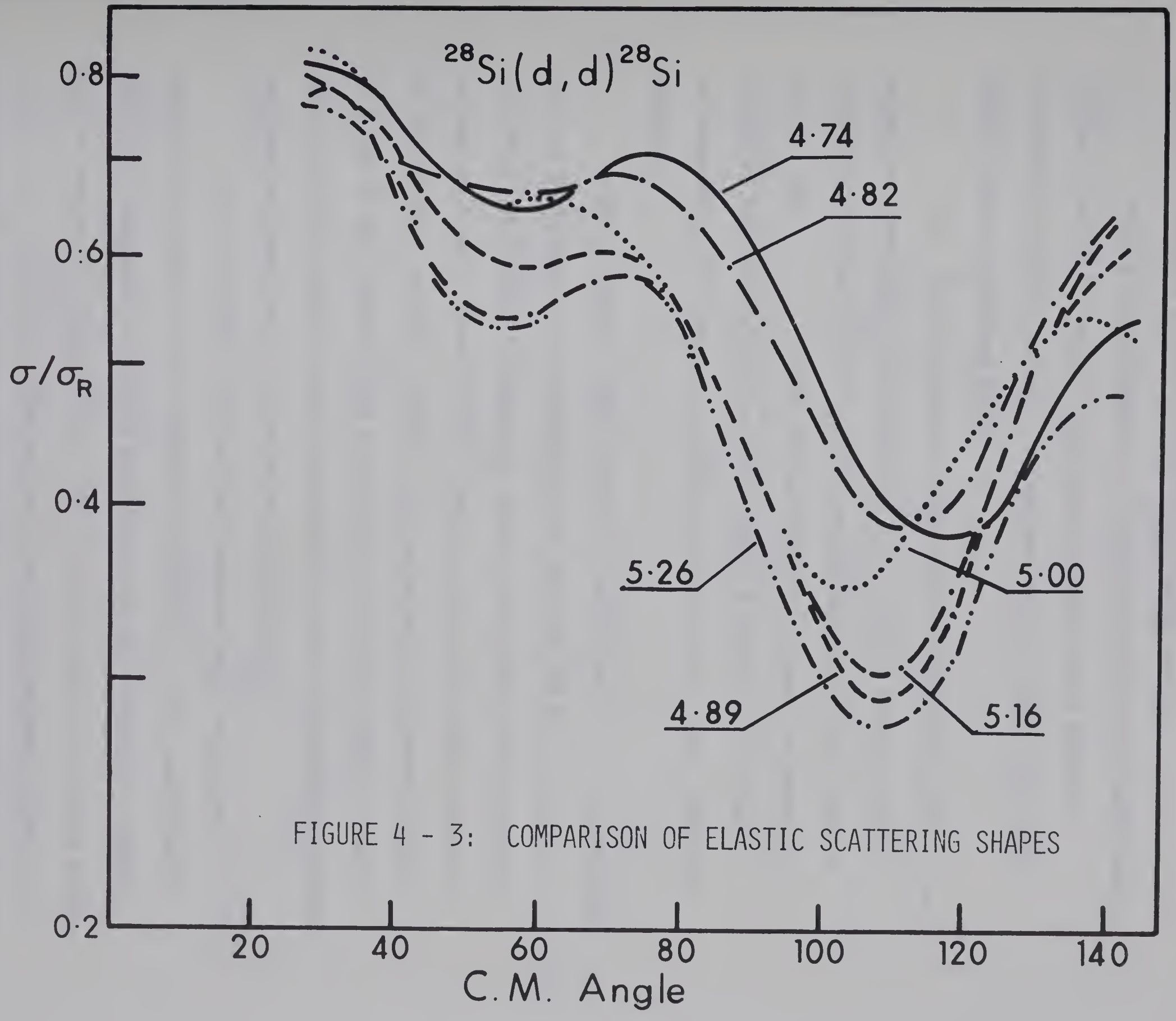

FIGURE 4 - 3: COMPARISON OF ELASTIC SCATTERING SHAPES

summed over all the points in the distribution. This is the function which is minimized by the optical model search routine.

With 6 free parameters, χ^2 space is filled with small local minima in which the search routine may become trapped unless a systematic approach is used. The method used to obtain the results which follow is outlined below.

(i) With the shapes of the real and imaginary parts of the potential constrained to be equal (i.e. $r_o = r_{oI}$, $a = a_I$), three parameter searches over W, r_o and a were carried out for V fixed at 30, 40, 50.....180, 190 and 200 MeV. Figure 4-4 shows the resulting best values for the fit to the 5.0 MeV data, with their corresponding χ^2. Several features to which we will later refer are evident.

(a) Firstly, there are three deep minima in χ^2 corresponding to real well depths of approximately 50, 100 and 150 MeV. In the following, potentials belonging to these three groups are referred to as sets A, B and C respectively. This is a very well known ambiguity in the deuteron optical potential, corresponding to different numbers of nodes of the deuteron wave function in the nuclear interior, and it was one of the objects of these experiments to see if any evidence could be found to favour one of these three potential sets.

(b) Secondly, the saw-tooth pattern which can be seen in the best fit values of the radius is a reflection of the equally well known Vr_o^2 ambiguity in optical potentials for all particles. Indeed, Vr_o^2 is constant to within better than 5% within each of the three groups.

(c) Thirdly, there is also a saw-tooth pattern in the diffuseness, a, which did not always show up on these diagrams, but which, in connection with the series of plateaus which always appears in the plot of the imaginary well depth, W, and is very evident in this example, may

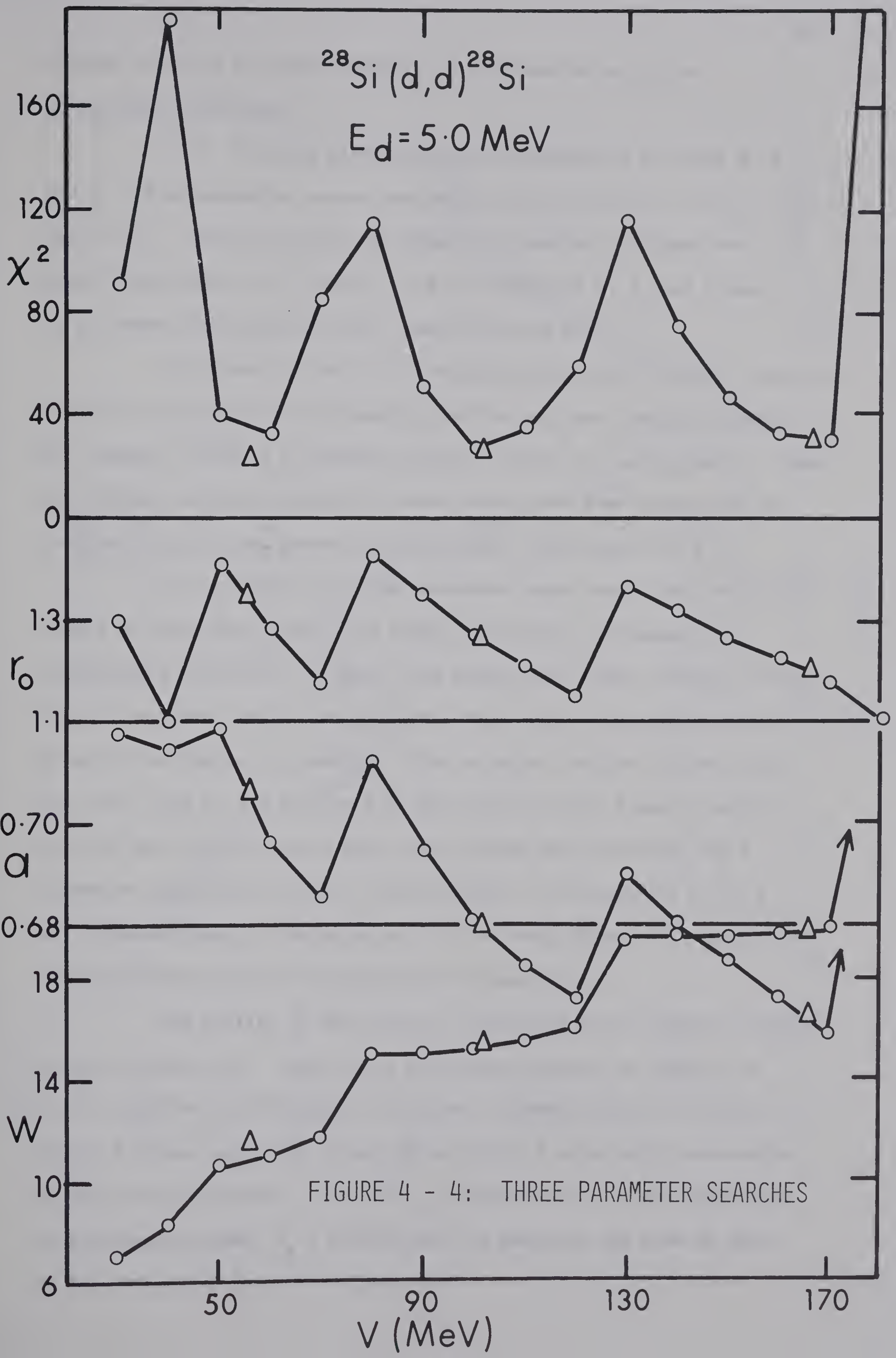

FIGURE 4 - 4: THREE PARAMETER SEARCHES

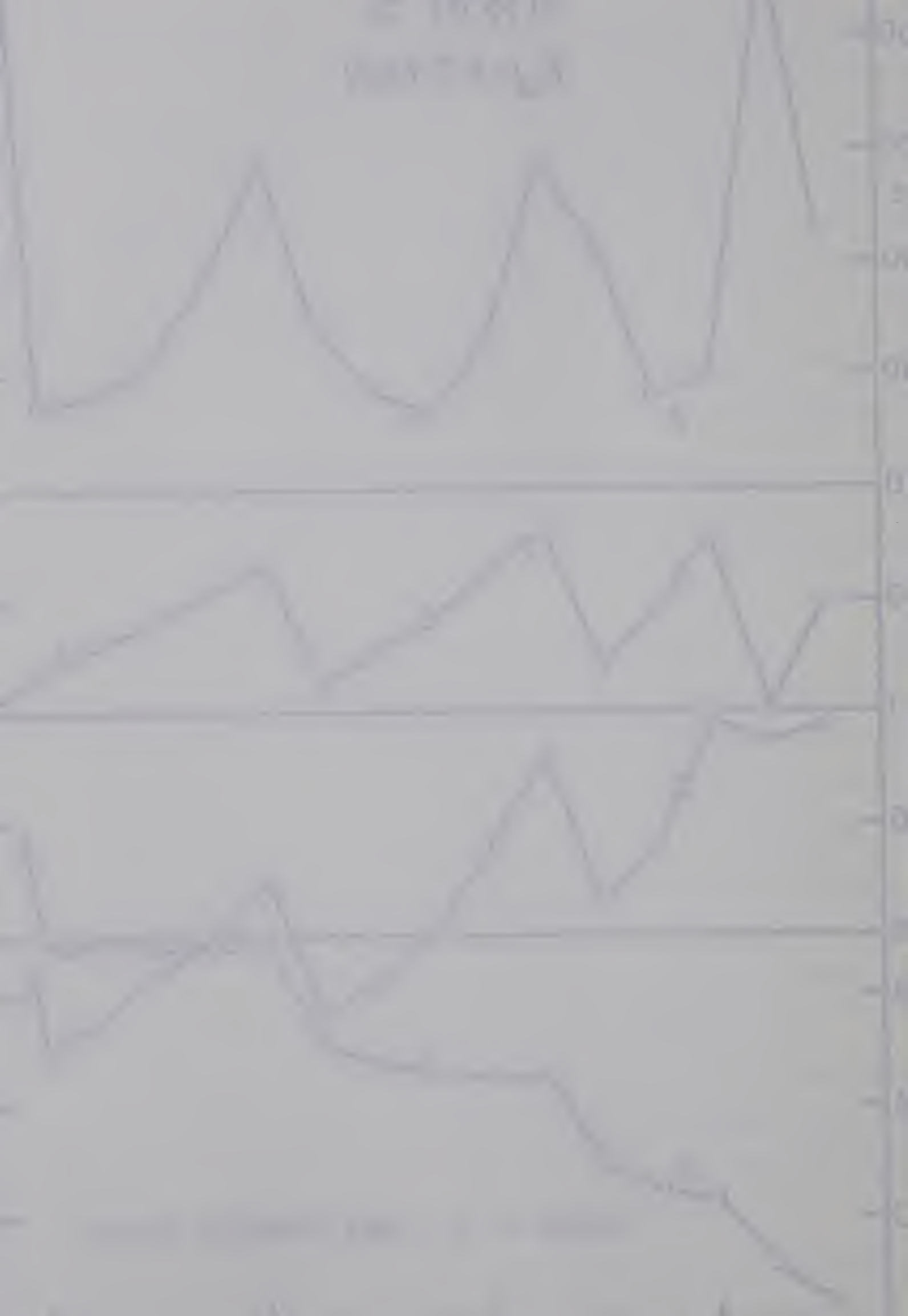

provide evidence for some ambiguity of the form Wa^n which is occasionally discussed.

(ii) Starting with the best fit parameters for sets A, B and C, a four parameter search was next carried out over V, W, $r_o = r_{oI}$ and $a = a_I$. The best values are shown as triangles in figure 4-4. No great improvement in χ^2 results, and the values of W, r_o and a tend to go toward the middle of their range for each set.

(iii) Next, V was held constant at its best value for each set while the constraint on the equality of the real and imaginary shapes was removed, giving a 5 parameter search over W, r_o, a, r_{oI} and a_I. Here the effects varied, although the usual result was some changes in the imaginary part of the potential and a slight improvement in χ^2.

(iv) Finally, all six parameters were freed from their best values as determined above. In almost all cases, no changes or improvements resulted. In one or two exceptional cases, however, allowing a 6 parameter search revealed that there was no true minimum in χ^2 space in the region in question. This occurred for the 5.16 MeV data for sets A and C, and for the 5.26 MeV data for sets B and C, and for the 4.89 MeV data for set C only, even though the fits after the 5 parameter search was in every case excellent. The analysis of 11.8 MeV deuteron elastic scattering on ^{28}Si by Perey (Perey 66) suggested a similar problem which is discussed in an appendix.

The quality of the fits is illustrated by the typical results shown in figure 4-5. There is no difference between the quality of fits to all the distributions, or between parameter sets A, B and C. Figure 4-5 also shows the effect of including a spin-orbit interaction in the optical potential, that is V_s in equation 2-1 is no longer zero. In the example shown, V_s = 10 MeV, and the shape is the same as that of the refracting part of the potential.

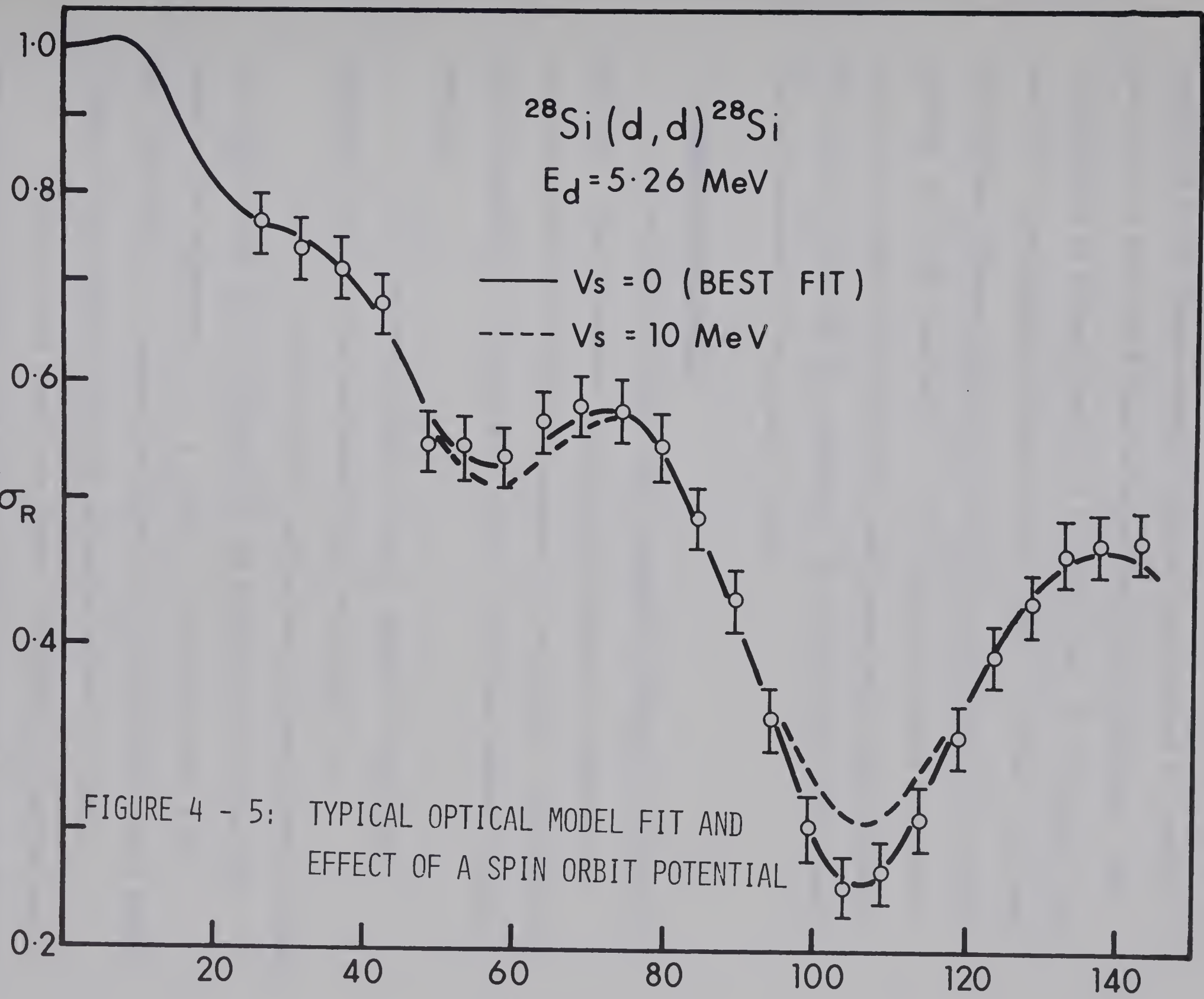

FIGURE 4 - 5: TYPICAL OPTICAL MODEL FIT AND EFFECT OF A SPIN ORBIT POTENTIAL

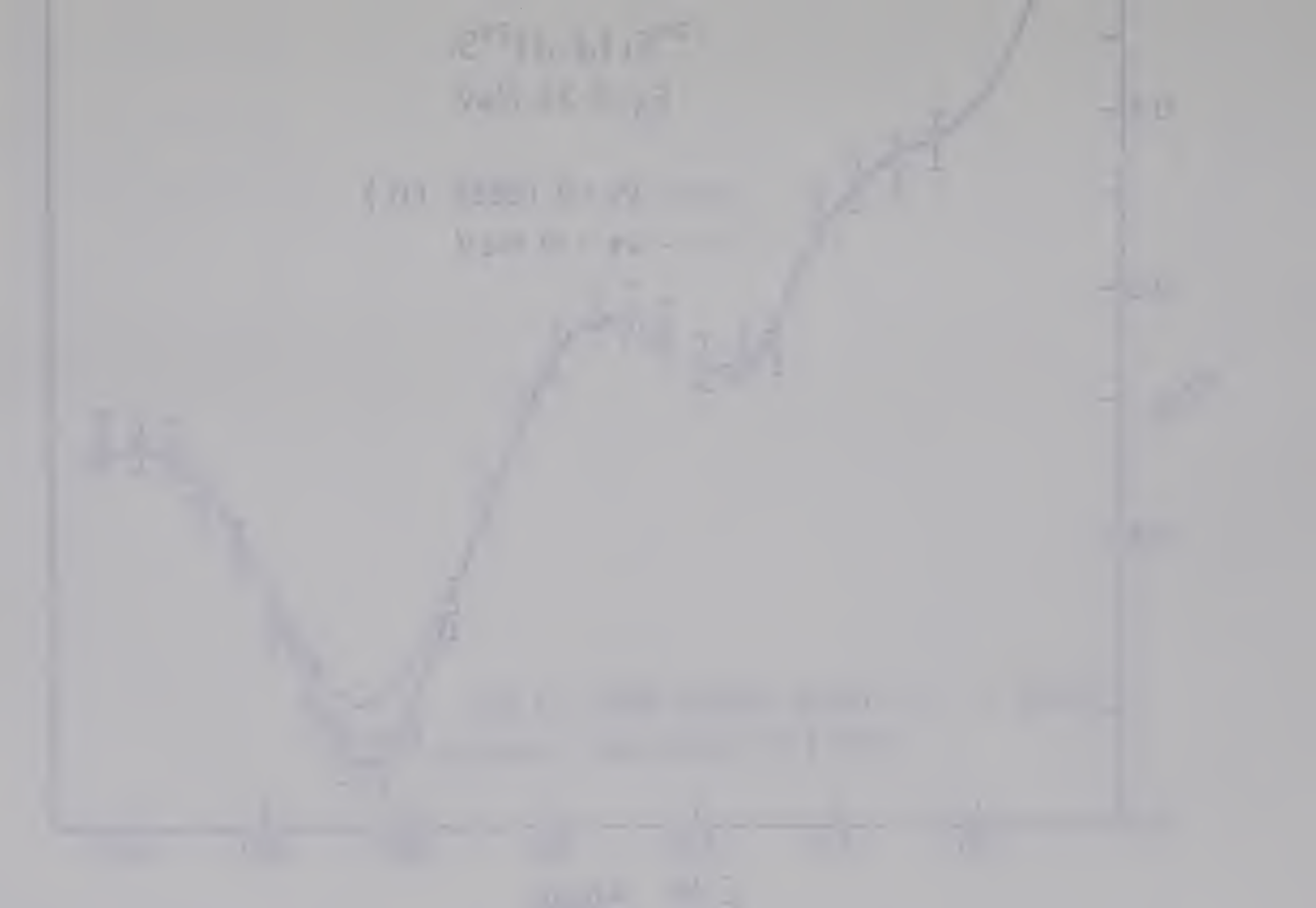

It should be added that the compound elastic contribution as evaluated by the Hauser-Feshbach calculation discussed in Chapter 2 has not been subtracted from the experimental distributions. This contribution is always less than 1 millibarn and, at its largest, is only 10% of the measured cross-section at 140^{o}. In view of the large interference effects, the wide variations in the shape of the distributions, the large uncertainty in the best optical model parameters, and the fact that such a correction would have only a small effect on the values of the best fit parameters, it was felt that this correction was not necessary in the elastic channel.

5. Optical Model Results

The results of the 5 and 6 parameter searches are shown in Table 4-2. The 5 parameter results are included to illustrate the cases where no corresponding 6 parameter fit was found. The results are shown graphically in figures 4-6, and 4-7, which have several striking features.

(i) With some scatter, V and r_o appear to vary nearly linearly, and lines have been drawn which satisfy $Vr_o^2 = k$.

(ii) It is only with the application of liberal doses of imagination that trends can be discerned in the pattern of variation with energy of the parameters a, W, r_{oI} and a_I. Lines have been drawn, quite arbitrarily, to suggest the direction of these trends, which appear at least to have similar shapes for parameter groups A, B and C.

(iii) If such trends are indeed the result of more than mere fancy, then the parameter sets obtained from fitting the 5.0 MeV data are completely anomalous in all cases. No parameter sets fitting in with the trends could be found to give reasonable agreement with the data, even

TABLE 4-2

SET B PARAMETER SEARCHES

			4.74	4.82	4.89	5.00	5.16	5.26
5 Parameter Searches	V	(MeV)	103.4	103.4	103.4	103.4	103.4	103.4
	r_o	(fm.)	1.23	1.21	1.17	1.29	1.15	1.18
	a	(fm.)	0.54	0.68	0.85	0.56	0.88	0.81
	W	(MeV)	9.58	11.28	17.4	11.28	18.63	15.6
	r_{aI}	(fm.)	1.03	1.35	1.67	0.75	1.66	1.47
	a_I	(fm.)	1.03	0.75	0.41	1.16	0.45	0.62
	χ^2		8.6	16.2	8.6	13.9	14.9	11.1
	Vr_o^2		156.5	151.3	141.3	172.0	136.7	144.0
6 Parameter Searches	V	(MeV)	101.3	100.7	106.6	111.7	RAN up to SET C	114.5
	r_o	(fm.)	1.25	1.23	1.14	1.21		1.08
	a	(fm.)	0.53	0.68	0.86	0.60		0.85
	W	(MeV)	9.56	11.76	17.0	10.0		14.5
	r_{aI}	(fm.)	1.01	1.35	1.67	0.99		1.49
	a_I	(fm.)	1.04	0.72	0.45	1.05		0.64
	χ^2		10.4	20.9	11.4	14.7		11.4
	Vr_o^2		158.5	152.5	138.5	162.5		133.5

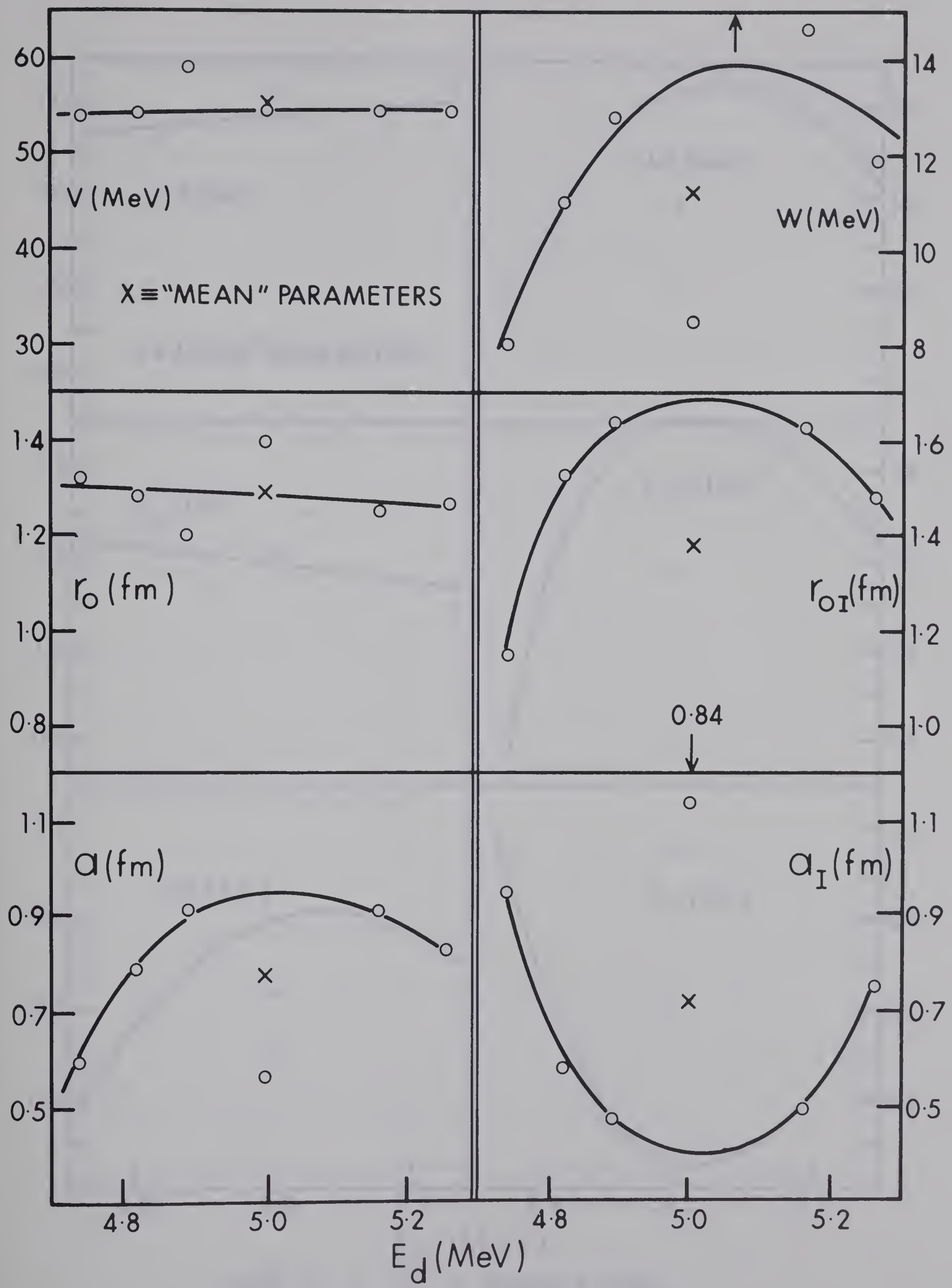

FIGURE 4 - 6: SET A PARAMETER TRENDS

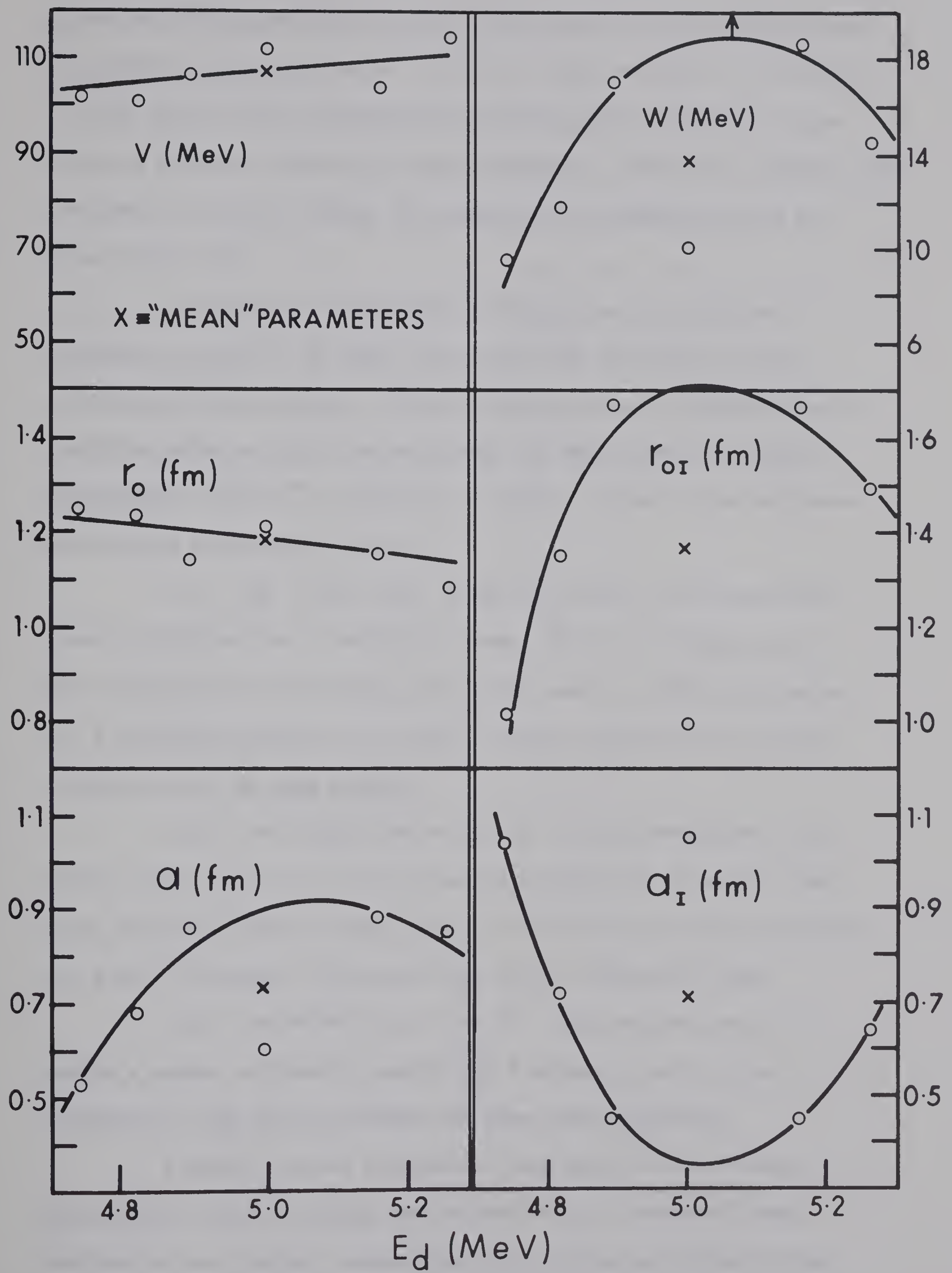

FIGURE 4 - 7: SET B PARAMETER TRENDS

by holding some parameters constant. The shape of this potential has the unusual feature of having $a_I > r_{oI}$ which one might be inclined to rule out as quite unreasonable if paying strict attention to the supposed physical meaning of these parameters. There are, however, some precedents for such a shape, for example in the extensive fits by Perey (Perey 66).

The problem of selecting a suitable deuteron optical potential for use in the DWBA calculation has certainly not been clarified by these results. Three different sets of parameters were therefore selected, with the hope that the DWBA calculation might discriminate against one approach or another. These three sets have been chosen as described below:

(i) The "5 MeV" set, or set #1, which is the potential given by fitting the 5.0 MeV data alone. This is in keeping with the philosophy that the optical potential used in a DWBA calculation for a stripping reaction at a certain energy should fit the elastic scattering data at that energy.

(ii) The "TREND" set or set #2. This corresponds to the points where the trend lines in figures 4-6 and 4-7 cross the 5 MeV axis, following the philosophy that the 5 MeV set is clearly anomolous, and a more "realistic" potential must surely follow the trend.

(iii) The "MEAN" set or set #3. This was arrived at by taking a simple arithmetic mean of all 6 values of each of the 6 parameters. This must correspond to some other philosophy.

A fourth set was considered, that which fit an average distribution found by taking the average of all 6 measured cross-sections at each angle. However the distribution generated by the optical potential of set 3 was quite close to such an average shape,

and the addition of a fourth set so similar to the third appeared to be only an encumberance.

Thus a total of nine parameter sets are available for use in the subsequent DWBA calculation, and these are listed in Table 4-3. It should be added that the rather exhaustive search carried out for optical potentials fitting this data revealed many other potentials and even sets of potentials which gave equally satisfactory fits but which have not been discussed here. A rather subjective process is of course always at work, eliminating parameter sets on the basis of their being "unrealistic", or perhaps more honestly, not pleasing to ones taste.

TABLE 4-3

DEUTERON OPTICAL POTENTIALS

		SET A	SET B	SET C
"5MEV" SET I	V (MeV)	54.6	103.4	166.3
	r_o (fm.)	1.40	1.29	1.25
	a (fm.)	0.56	0.56	0.54
	W (MeV)	8.49	11.28	15.73
	r_{oI} (fm.)	0.84	0.75	0.50
	a_I (fm.)	1.14	1.16	1.24
"MEAN" SET 2	V (MeV)	55.1	106.4	158.3
	r_o (fm.)	1.29	1.18	1.22
	a (fm.)	0.77	0.73	0.66
	W (MeV)	11.2	13.8	19.3
	r_{oI} (fm.)	1.38	1.36	1.30
	a_I (fm.)	0.71	0.72	0.79
"TREND" SET 3	V (MeV)	54.5	107.0	
	r_o (fm.)	1.28	1.18	
	a (fm.)	0.95	0.90	
	W (MeV	14.0	18.5	
	r_{oI} (fm.	1.68	1.70	
	a_I (fm.)	0.42	0.40	

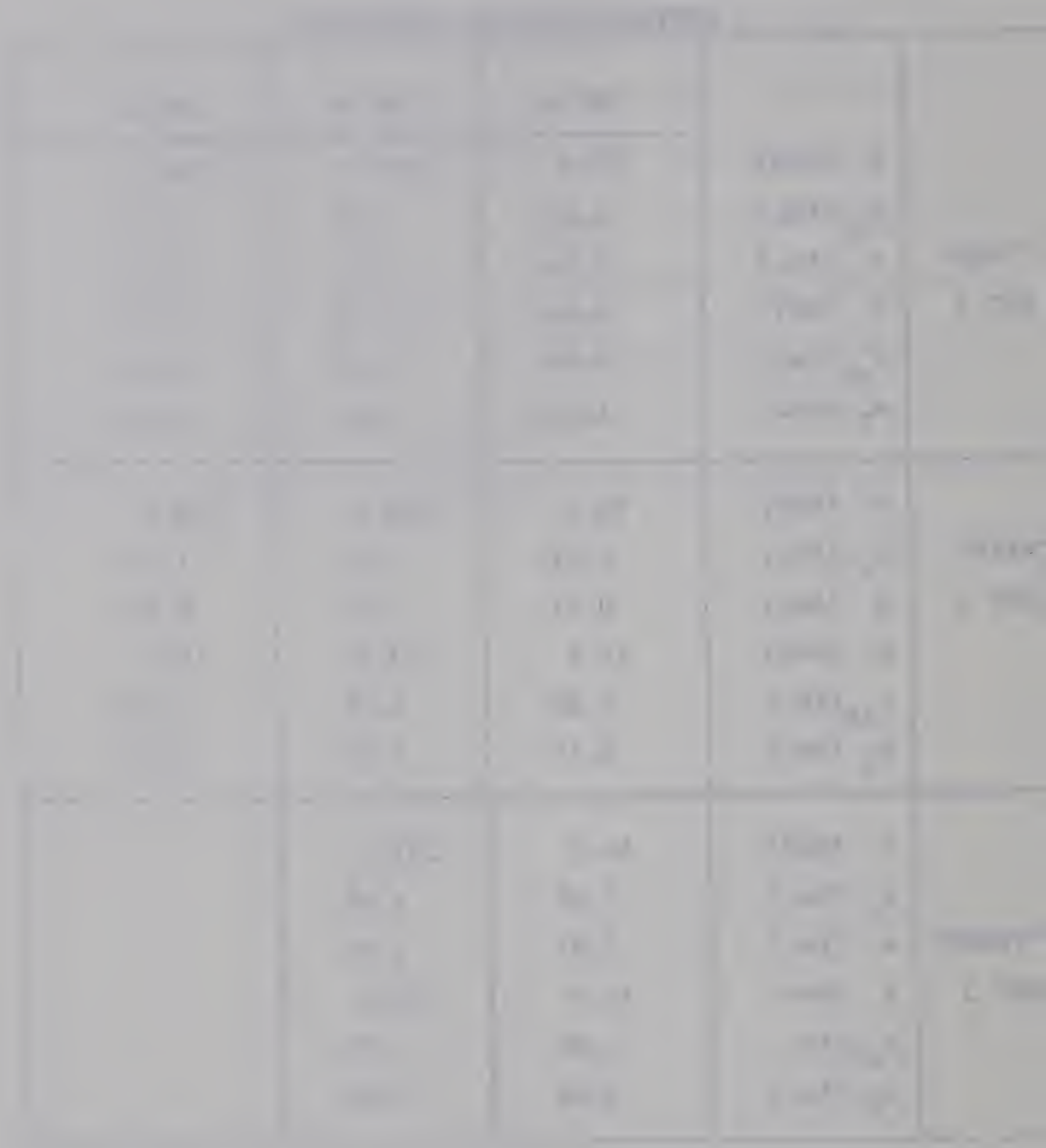

CHAPTER 5: THE $^{28}Si(d,p)^{29}Si$ REACTION

1. Previous Work

The $^{28}Si(d,p)^{29}Si$ reaction has been studied in some detail in earlier work, in particular by Holt and Marsham (Holt 53) at 8 MeV and very extensively by Kuehner et al (Kuehner 60, 60a) at 10 energies between 6.2 and 9.0 MeV. More recently, the reaction has been studied at energies less than 3 MeV by Wildenthal (Wildenthal 64) with special emphasis on compound contributions, and the $^{28}Si(d,p\gamma)^{29}Si$ was studied by H. J. Hausman et al (Hausman 66) at 4-6 MeV. Some of the arguments favouring the Nilsson model for ^{29}Si were also based on this latter reaction as reported by Bromley et al (Bromley 57).

Due to the fact that deuteron elastic scattering cross-sections were not available, distorted wave analysis of the stripping angular distributions were not performed. Moreover, absolute cross-sections, though evidently measured in some instances, were not reported and spectroscopic factors were not obtained.

As mentioned earlier, the mirror reaction $^{28}Si(d,n)^{29}P$ had been performed in this laboratory by W. G. Davies et al (Davies 66) at 5.0 MeV, and it was felt that a comparison between these two reactions might assist to some extent in clarifying the ambiguities and uncertainties in the deuteron optical model potential already described in the previous chapter.

2. Excitation Functions

Kuehner et al (Kuehner 60, 60a) have shown excitation functions for the first three proton groups from the reaction $^{28}Si(d,p)^{29}Si$ taken at 35^{o} and 90^{o} between 6.0 and 10.5 MeV. The 90^{o} curves show very large fluctuations in the differential cross-

section over the entire region, whereas the 35^{o} excitation curves for the first two excited levels are much smoother, showing an approximately constant envelope with 10-20% fluctuations from resonant effects. This is because 35^{o} is close to the maximum of the $\ell_n = 2$ stripping patterns where the relative contributions from non-stripping amplitudes is minimized. On the other hand, 35^{o} is close to the minimum in the $\ell_n = 0$ (ground state) stripping pattern.

Kuehner has also demonstrated that the large fluctuations apparent in the differential cross-section are <u>not</u> observed in the total cross-section for each group, where fluctuations, if present, are certainly less than 10%. His conclusions from this evidence are entirely relevant to the present work and are therefore quoted directly.

"The fact that the fluctuations are observed to be much stronger in the differential excitation functions than in the total cross-sections, and that there is no apparent correlation relating the structure at different angles of observation (nor of different residual states), suggest that they result largely from interference. Other data, namely the angular distributions, which do not change their characteristic diffraction shape over the range of energies studied, imply a dominant direct interaction amplitude. Thus it is strongly suggested that the interference effects observed reflect interference between direct interaction and compound nucleus amplitudes; it is clear that whenever the intrinsic beam energy spread together with the energy spread introduced by the target thickness is small compared to the widths of the local compound states, residual interference effects are expected." It should be pointed out here that a deuteron bombarding energy of 5 MeV corresponds to an excitation of

16.5 MeV in the compound nucleus ^{30}P, where the states are rather dense and broad.

The extensive excitation functions given by Kuehner, together with their clear trend toward more severe fluctuations in the lower energy region, strongly suggests that the results of further yield curve measurements will be similar. For completeness, however, and to assist in estimating the magnitude of possible resonant effects on the angular distributions, excitation functions at 60^{o} and 90^{o} were taken on the ground state group in the vicinity of 5 MeV. The results are shown in figure 5-1. The resonances, as observed by Kuehner, are ~ 100 keV in width. This data, however, was taken with a target ~ 50 keV thick, whereas the earlier data was taken with a 100 keV target, and therefore did not eliminate the possibility that the actual resonances responsible were significantly less than this.

3. Angular Distributions

As in the case of elastic scattering, it is clear that the large resonant structure of the excitation curves could cause substantial distortion of the (d,p) angular distributions as a function of energy. That this is indeed so has been demonstrated clearly by Kuehner who has displayed several angular distributions on one plot to show the rapid variation in their shapes.

Although a large number of angular distributions were not taken, the serious energy dependence of their shapes is evident in figure 5-2, where the angular distribution of the ground state proton group is shown at three different energies. The 5.0 MeV distribution was taken to coincide with the 5.0 MeV $^{28}Si(d,n)^{29}P$ distribution referred to earlier. 4.84 MeV was selected for another distribution as it coincides with a minimum in the 90^{o} excitation function. Finally,

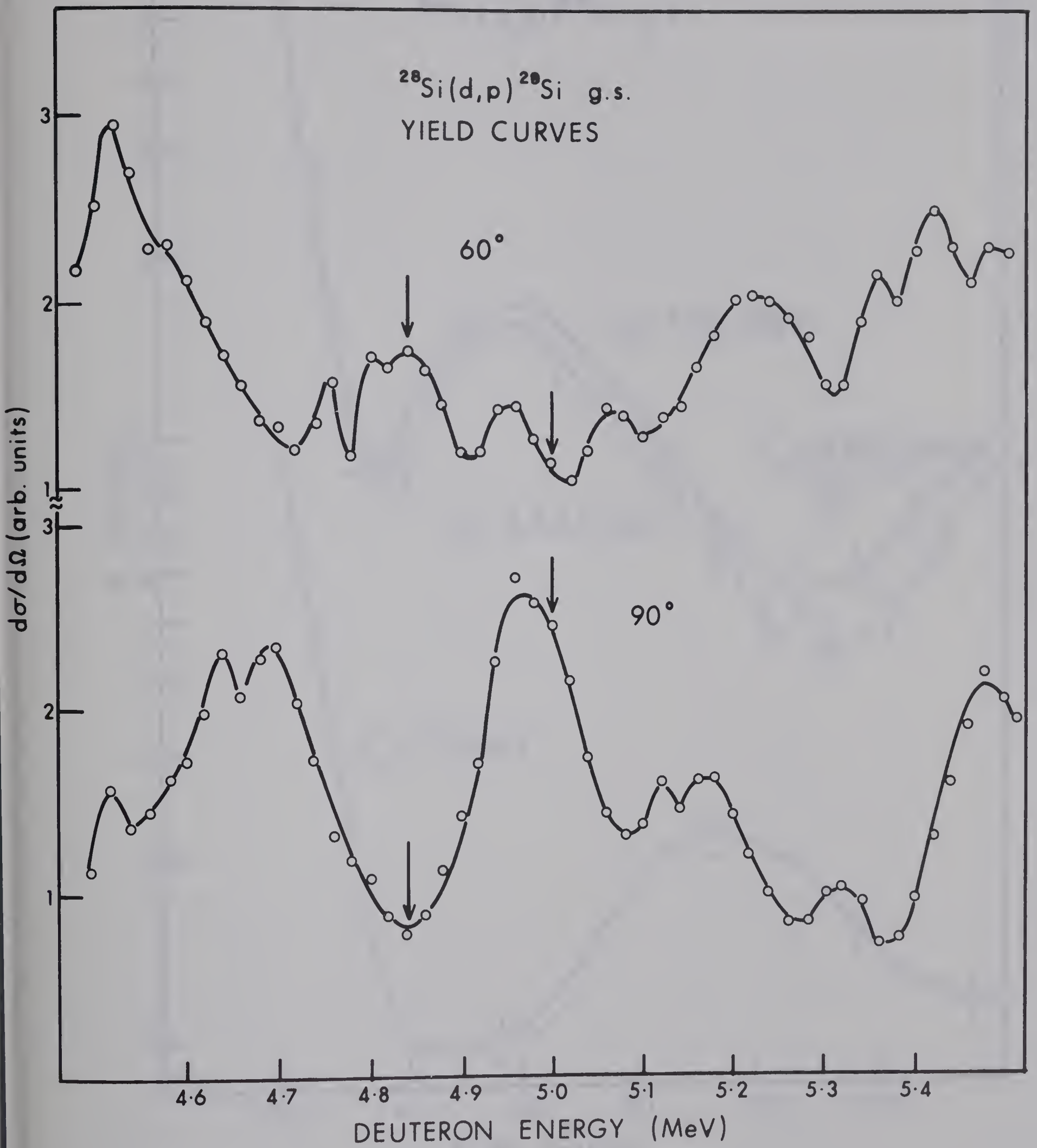

FIG. 5–1
STRIPPING EXCITATION FUNCTIONS

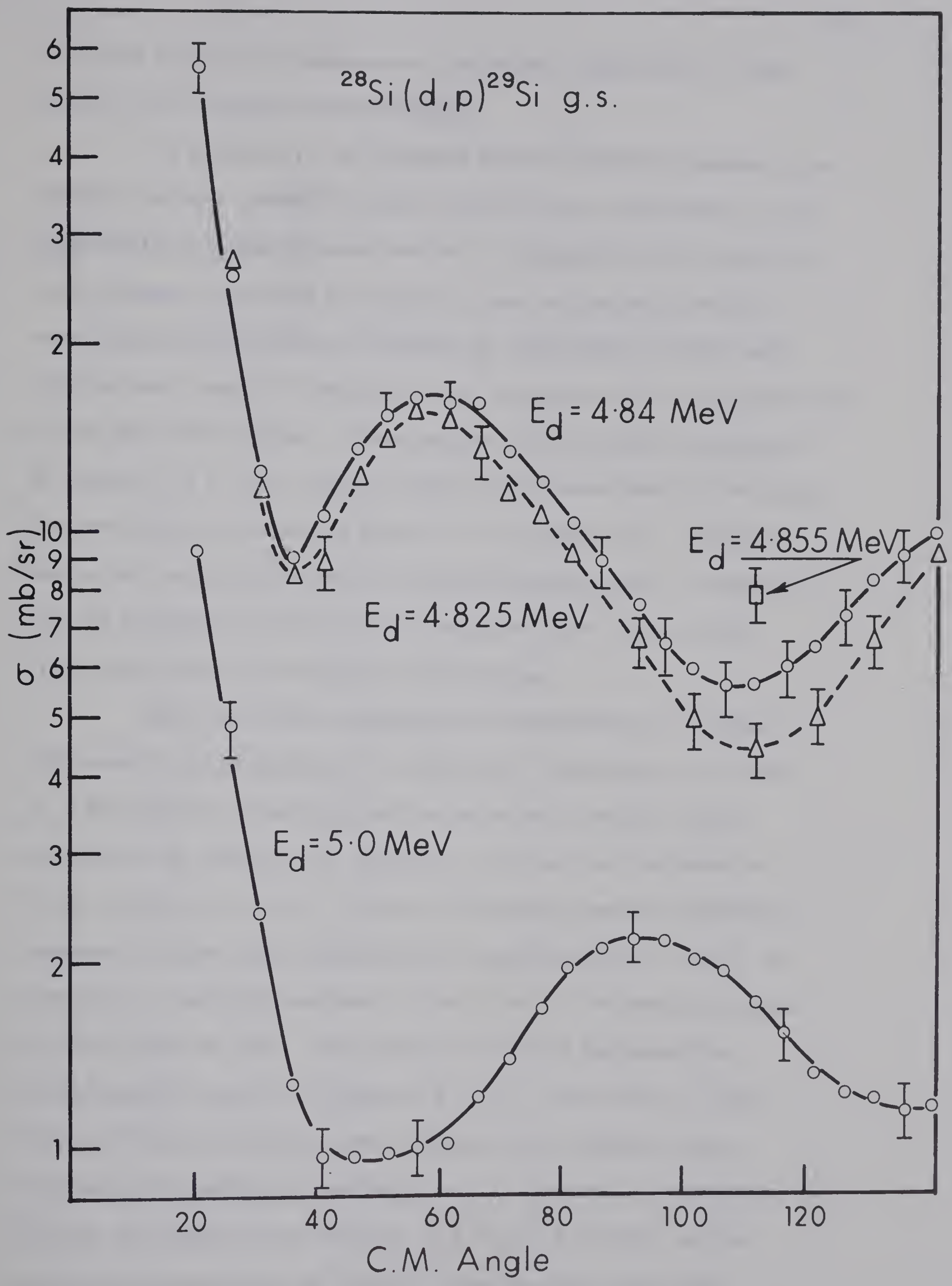

FIGURE 5 - 2: GROUND STATE ANGULAR DISTRIBUTIONS

4.825 was selected to demonstrate the extreme sensitivity of the shape to the incident deuteron energy.

In addition to the resonant effects already discussed, the smoothly varying compound nucleus amplitude also contributes to the experimentally measured cross-section. Consequently this contribution, already calculated in Chapter 2, was subtracted from each experimental distribution to provide an "experimental Direct and Interference" angular distribution for comparison with the predictions of the DWBA calculations. These angular distributions are plotted in figures 5-3 to 5-6, and the values of the experimentally measured cross-sections are shown in Table 5-1. Of course, the conversion factor for obtaining absolute cross-sections described in Chapter 3 must be increased by 8% for (d,p) reactions where contributions from other silicon isotopes are not observed.

Each data point represents an accumulation of at least 1000 counts, corresponding to a statistical uncertainty of at most 3%. The method of measuring both relative and absolute cross-sections is as described in Chapter 3, and does not introduce an error of greater than ±5%. However the extreme energy sensitivity appeared to cause some difficulties in reproducibility, and it is felt that a reasonable estimate of the error in the absolute cross-sections would be ±10%. Error bars of ±10% are indicated for representative points on figures 5-3 to 5-6. The entire 5.0 MeV $^{28}Si(d,p)^{29}Si$ distribution, when repeated on a different date, reproduced to within this estimated error. Moreover, cross-checks between the angular distributions at 4.84 and 5.00 MeV, and the excitation functions at 60^{o} and 90^{o} agree to better than 10%

TABLE 5-1

$^{28}Si(d,p)^{29}Si$

CROSS-SECTIONS IN mb/sr.

θ cm.	ground state		1.28 MeV	2.03 MeV
	Ed = 4.84 MeV	Ed = 5.00 MeV	Ed = 5.00 MeV	Ed = 5.00 MeV
20.6	5.55	9.23	3.60	1.97
25.8	2.59	4.78	3.92	2.24
30.9	1.23	2.40	4.38	2.49
36.1	0.89	1.26	4.74	2.77
41.2	1.04	0.96	4.81	2.66
46.3	1.34	0.96	4.52	2.48
51.4	1.52	0.97	4.02	2.32
56.5	1.64	0.99	3.28	1.83
61.6	1.60	1.00	2.58	1.50
66.7	1.61	1.18	2.08	1.31
71.8	1.34	1.37	1.66	1.13
76.8	1.20	1.65	1.32	1.11
81.8	1.02	1.95	1.21	1.21
86.9	0.89	2.10	1.20	1.26
91.9	0.76	2.15	1.27	1.50
96.9	0.65	2.16	1.38	1.59
101.8	0.60	2.00	1.55	1.75
106.8	0.56	1.92	1.74	1.88
111.8	0.56	1.70	1.91	1.93
116.7	0.60	1.52	2.08	2.04
121.6	0.65	1.32	2.25	2.06
126.5	0.73	1.22	2.30	1.97
131.4	0.83	1.18	2.32	1.93
136.3	0.91	1.13	2.35	1.70
141.2	1.00	1.14	2.31	1.72

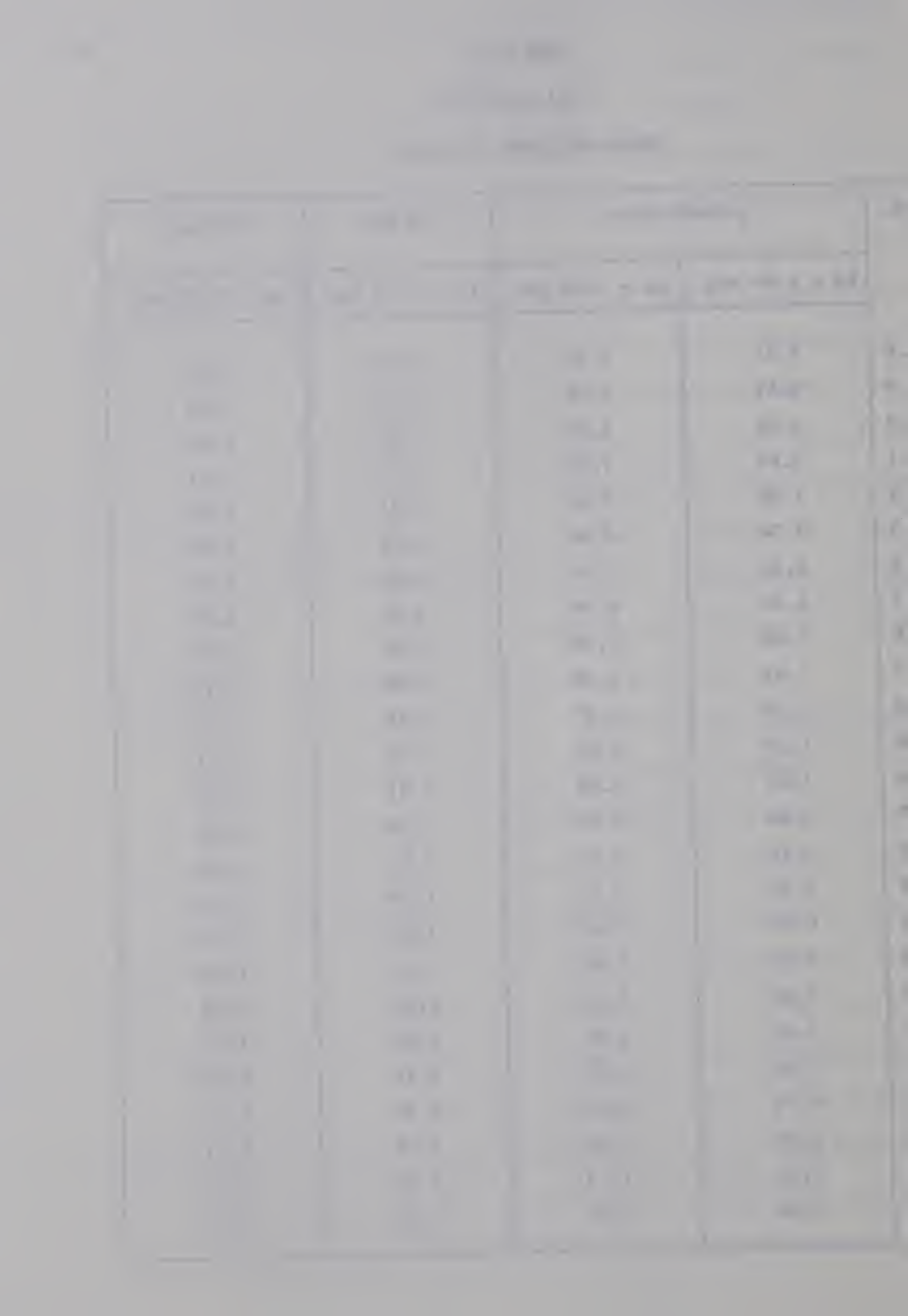

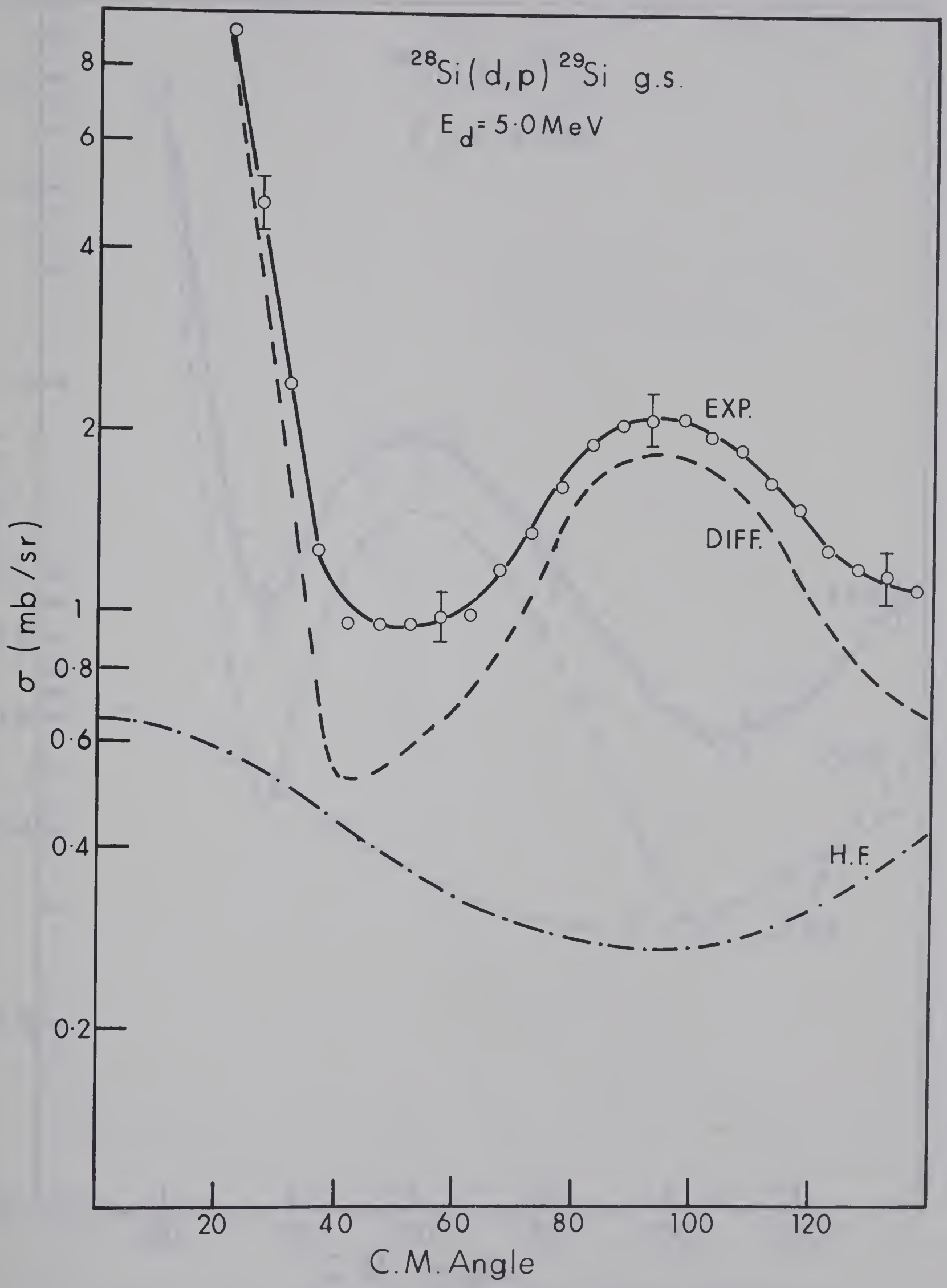

FIGURE 5 - 3: SUBTRACTION OF COMPOUND NUCLEUS CONTRIBUTION FROM GROUND STATE DISTRIBUTION AT 5.0 MEV

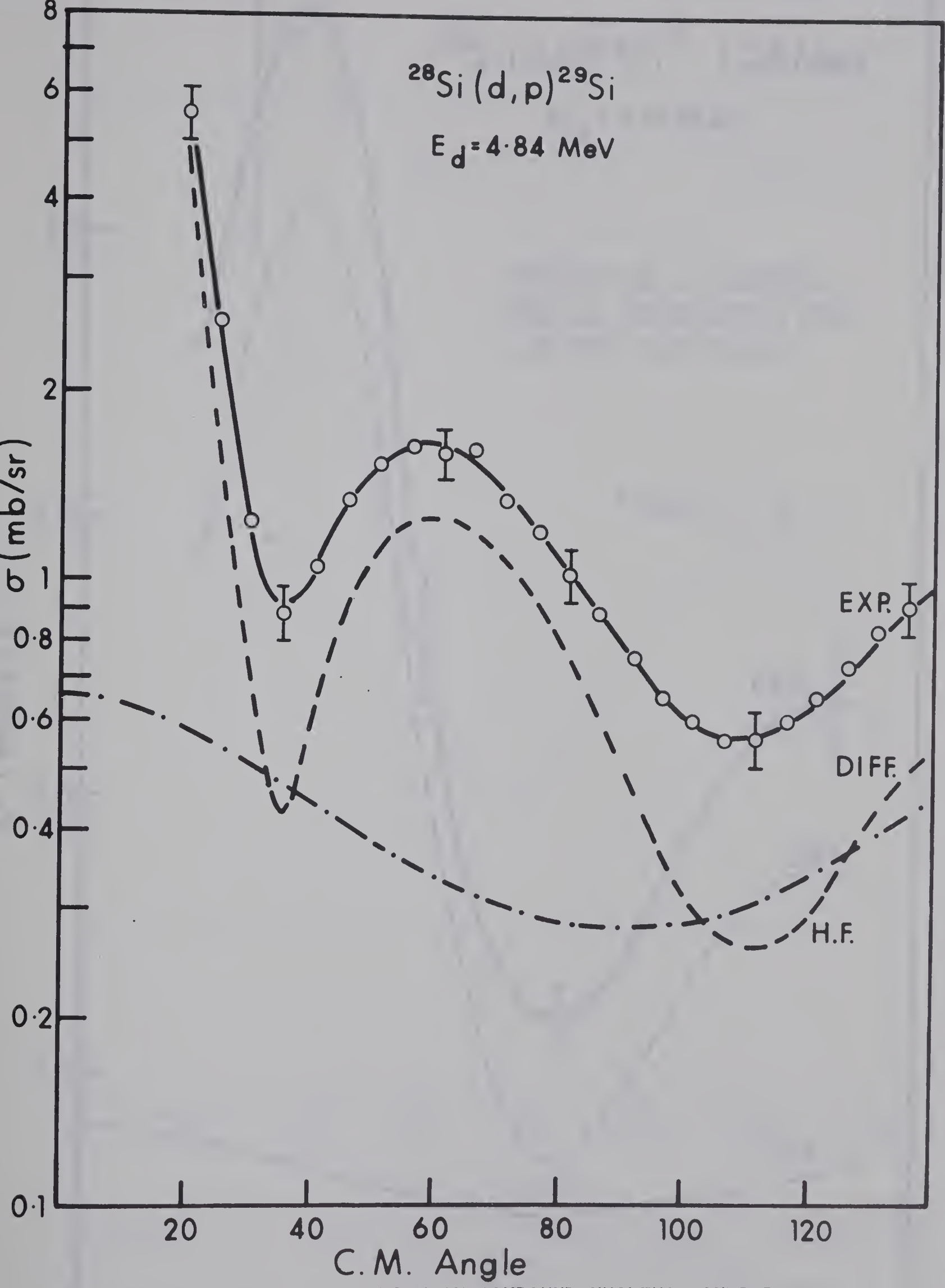

FIGURE 5 - 4: SUBTRACTION OF COMPOUND NUCLEUS CONTRIBUTION FROM GROUND STATE DISTRIBUTION AT 4.84 MEV

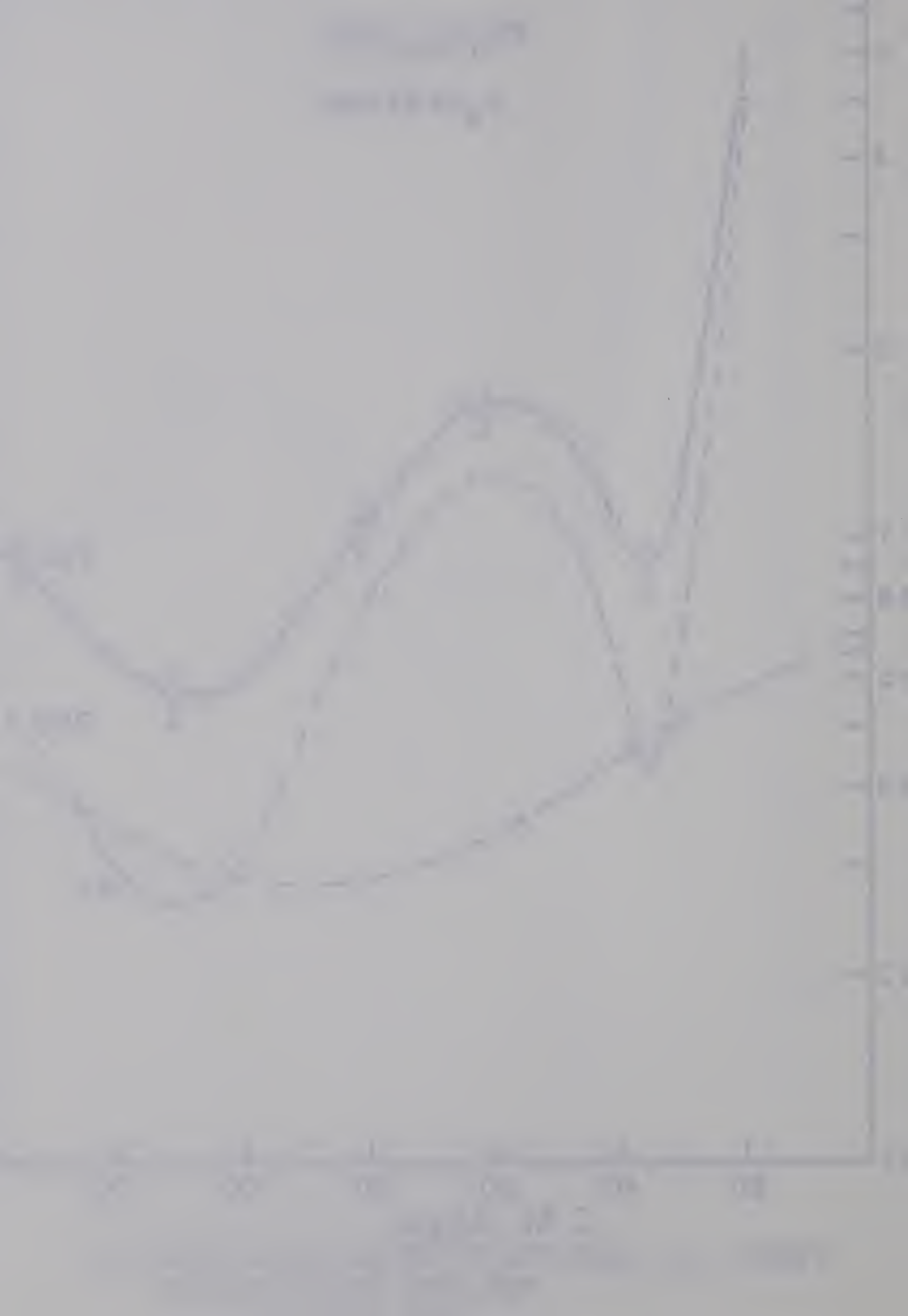

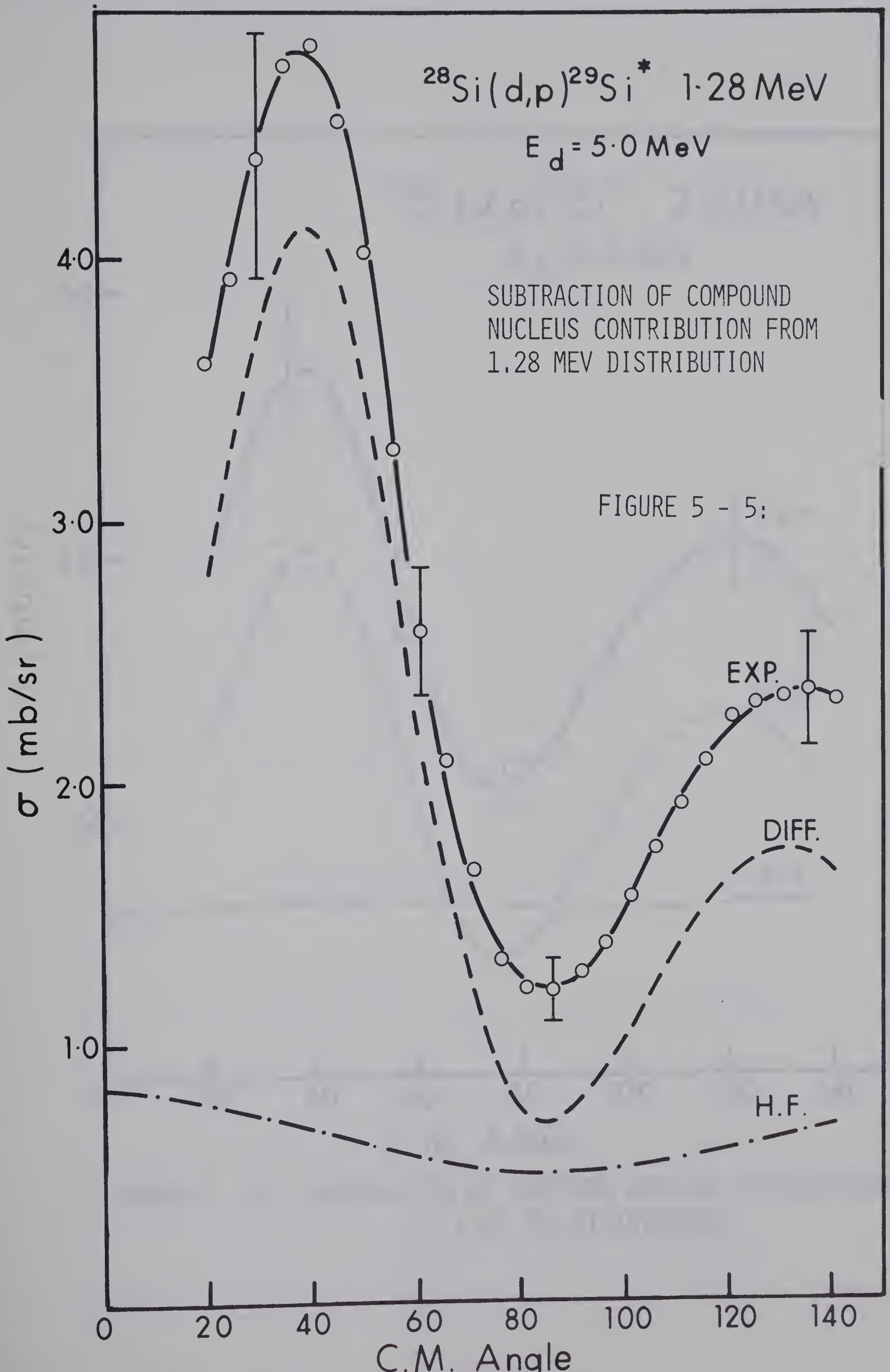
$^{28}Si(d,p)^{29}Si^{*}$ 1·28 MeV
$E_d = 5·0$ MeV
SUBTRACTION OF COMPOUND NUCLEUS CONTRIBUTION FROM 1.28 MEV DISTRIBUTION
EXP.
DIFF.
H.F.
σ (mb/sr)
4·0
3·0
2·0
1·0
0
20
40
60
80
100
120
140
C.M. Angle

FIGURE 5 - 5:

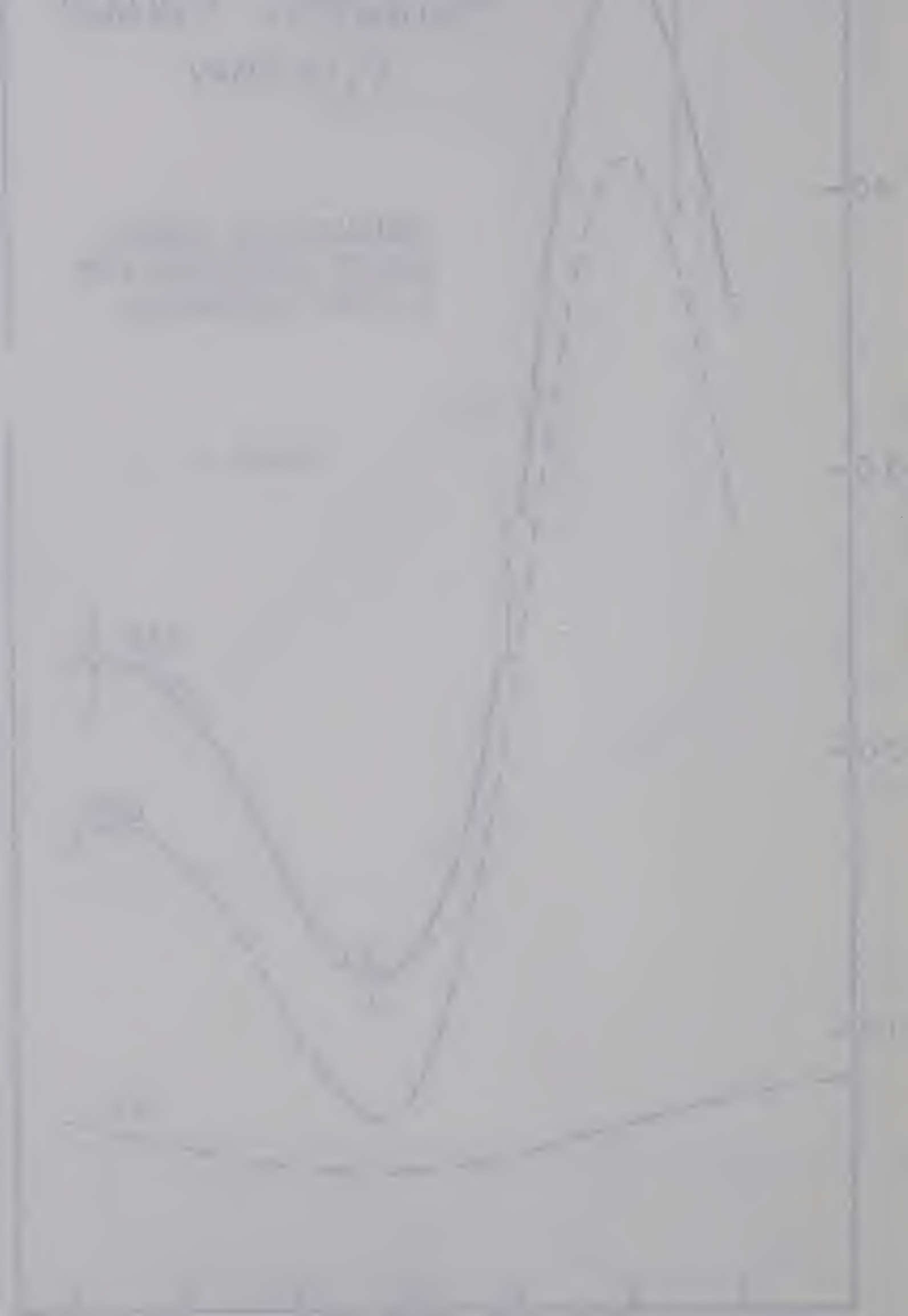

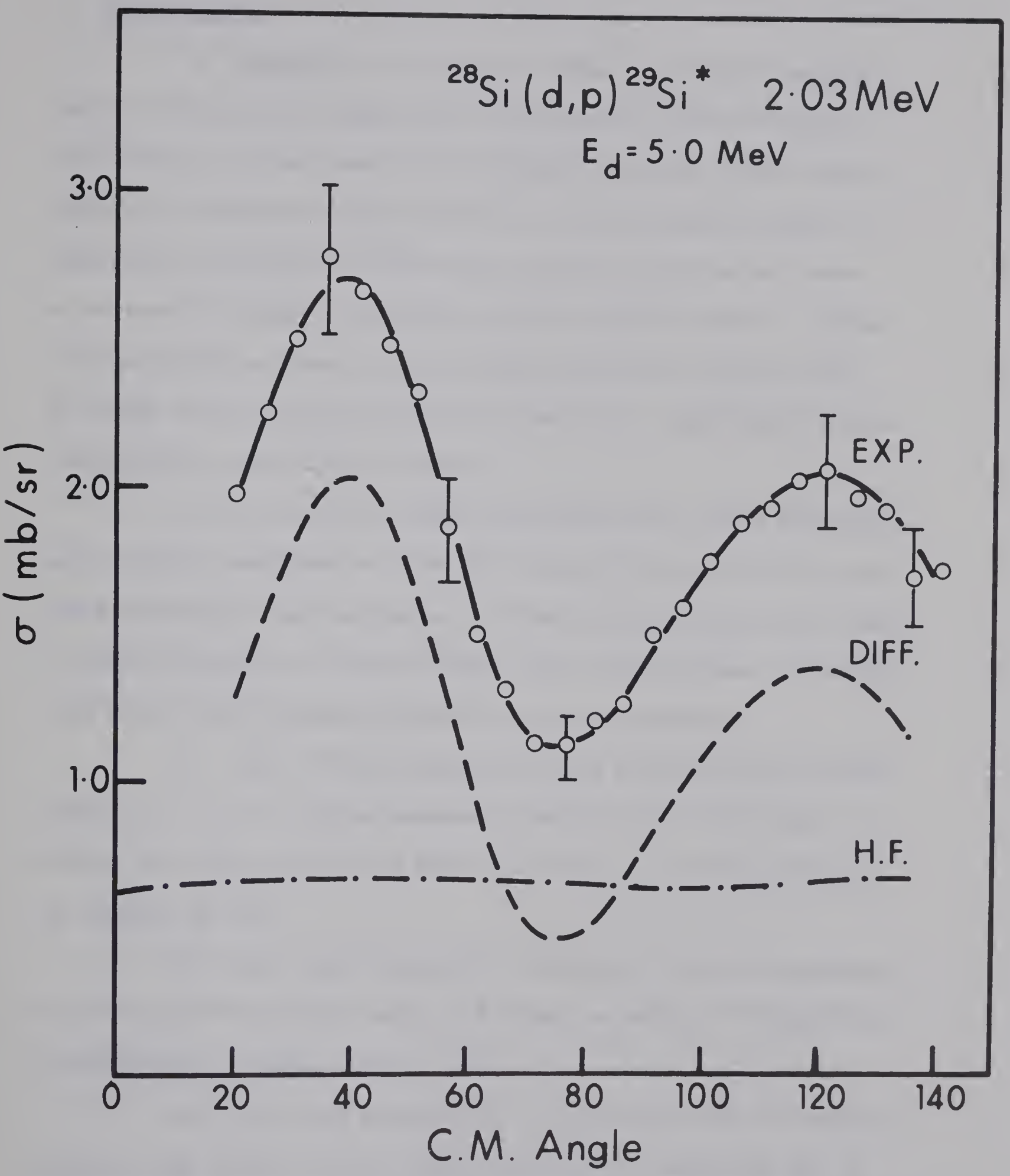

FIGURE 5 - 6: SUBTRACTION OF COMPOUND NUCLEUS CONTRIBUTION TO 2.03 MEV DISTRIBUTION

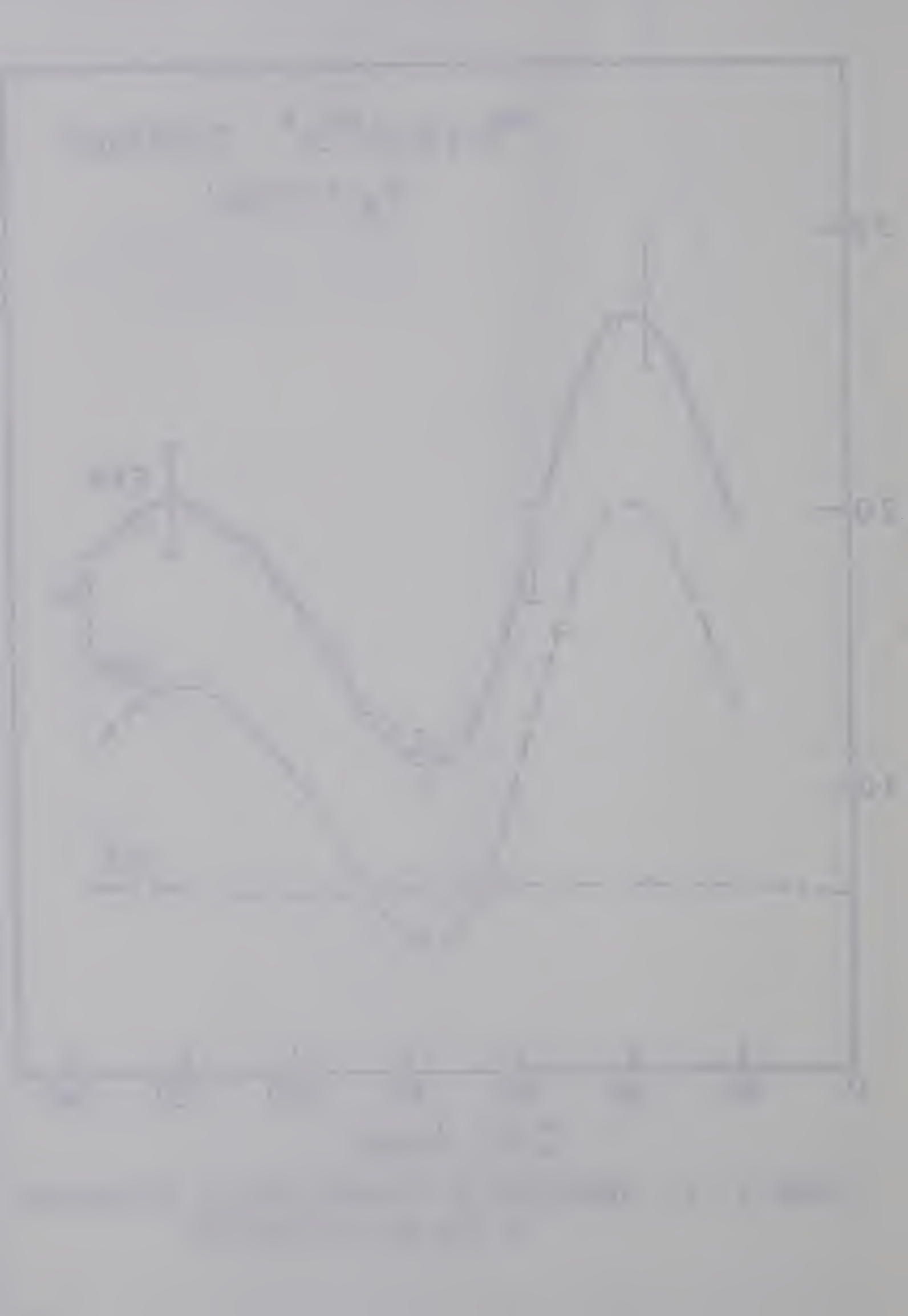

4. DWBA Analysis

(a) General: In theory, the shape of a direct reaction angular distribution changes only very gradually and continuously with energy. In the present work, however, where non-direct amplitudes are contributing significantly to the experimental shapes, a theoretical calculation of the direct reaction distribution cannot be expected to compare favourably with the measured result. Indeed, the temptation is present to do a DWBA calculation, and then find an energy in the vicinity of 5 MeV for which the experimental angular distribution agrees with the shape!

It is clear that a DWBA calculation which agrees moderately well with the experiment at 4.84 MeV, will not compare with the 5.00 MeV distribution, and vise versa. In order to continue at all, then, it seemed necessary to choose between these distributions. In making this choice, the following observations were considered:

(i) the 4.84 MeV distribution has a shape which is quite typical of $\ell_n = 0$ angular momentum transfer direct reactions, whereas the shape of the 5.00 MeV distribution is not characteristic of anything at all;

(ii) that shape agrees very favourably with the corresponding $^{28}Si(d,n)^{29}P$ reaction taken at 5.0 MeV, as well as $^{28}Si(d,p)^{29}Si$ distributions at higher energies; and

(iii) the total experimental cross-section over the measured angular range of the 4.84 MeV distribution is 35% less than that of the 5.00 MeV distribution.

In principle, many distributions might have been taken, and the one with the lowest total cross-section selected. However,

because of the agreement between the shape of the 4.84 MeV distribution and that of corresponding reactions, it was felt that comparison of DWBA calculations with this experimental distribution was justified. It might be added that, quite as anticipated, no set of parameters whatever was able to produce in a DWBA calculation a shape resembling that of the 5.00 MeV experiment.

The original philosophy of this experiment was to obtain deuteron optical potentials from elastic scattering data, and then use those potentials to predict the shape of the stripping angular distribution. No attempt would be made to fit the experimental distribution by adjusting the parameters used in the DWBA calculation. This approach is somewhat defeated by the freedom to select an experimental shape which satisfies ones preconceived ideas, however, having selected the 4.84 MeV distribution on fairly objective grounds the same philosophy may be followed.

(b) DWBA Calculations: The DWBA analysis reported in this section were all performed using the computer code DWUCK (Distorted Wave, University of Colorado, Kunz) written by P. D. Kunz and based on the Oak Ridge DWBA code, Julie. The program was adapted for use on the University of Alberta IBM 360 computer by S. M. Tang, G. N. Stinson, and S. S. M. Wong, and compared extensively with other published DWBA calculations, in particular those of Hjorth et al (Hjorth 65) on the $^{40}Ca(d,p)^{41}Ca$ gs reaction at Ed = 14.3 MeV. In spite of the availability of other DWBA codes (due to W. R. Smith, B. Macefield and L. Hutton) DWUCK was used exclusively because of our greater confidence in the reliability of its calculations, its recent rather widespread use by other groups, and the many options it offers.

The optical potentials used in the DWBA analysis are of the form given in equation 2-1. The Coulomb radius r_{oc} was taken to be 1.25 fermis for protons and 1.30 fermis for deuterons. The proton potentials of Perey, including the spin-orbit potential, were used exclusively. They are discussed in the next section. As explained in section d), no spin-orbit interaction was included in the deuteron potential.

The program allows for both finite-range and non-local calculations in the local energy approximation. All results reported are from finite range, local potential calculations. The finite range calculation gives results which differ very little from a zero-range calculation, affecting the absolute spectroscopic factors by less than 10% and the shapes not noticeably. A finite range parameter $\beta = 0.65$ has been used, but the results are very insensitive to this value within ±20%, with the apparent exception of calculations using deuteron potentials with strengths of $V \geq 150$ MeV.

The effect of using non-local potentials in the calculation is far more pronounced. Using non-locality ranges of $\beta = 0.85$ for the nucleons and $\beta = 0.54$ for the deuterons the absolute spectroscopic factors are reduced by 30%, although the relative spectroscopic factors are not changed by more than 5%. The shapes are also somewhat altered, although in no case by enough to change any conclusions. More specific comments on the effects of non-locality are made in the following discussion where they are relevant.

The effect of reducing contributions from the nuclear interior by cutting off the radial integration at $r = 1.0$ fermis was found, as expected, to be similar to that of doing a non-local

calculation, but is much more arbitrary and difficult to justify, and so has not been pursued.

(c) Proton Parameters: As well as the optical potential for the incident deuteron, the DWBA calculation requires the optical potential which describes the scattering of the outgoing protons, as well as a potential to be used in generating the wave function of the captured neutron. These nucleon optical potentials have been very well established from the work of several authors, and compiled by Rosen (Rosen 66). The proton parameters of Rosen, Perey and Buck are shown in Table 5-2. Their similarity is apparent, the only significant difference being in the imaginary diffuseness parameter a_I used by Rosen. This higher value was obtained by optical model fits to polarization in (p,p) elastic scattering. Perey (Perey 66) has argued that it is preferable to fit the elastic scattering cross-sections only, and then leave the other parameters unchanged while introducing a spin-orbit term to fit the polarization data.

Figure 5-7 shows the effect of using these three different proton potentials with one fixed deuteron potential. The differences are seen to be unimportant, and in the remainder of this discussion the parameters of Perey have been used exclusively.

(d) Spin-Orbit Potential: It is also of interest to point out here the effect of adding a spin-orbit term of various depths to the deuteron potential. This is illustrated in figure 5-8 where a spin-orbit term of the form given in equation 2-1, with $V_s = 0$ and $V_s = 10$ MeV has been added to the deuteron potential 1B. Once again the effect is clearly insignificant, and we may proceed on the assumption of no spin-orbit interaction in the deuteron potential with the knowledge that if such a term must be added in

TABLE 5-2

PROTON OPTICAL PARAMETERS

	ROSEN	PEREY	BUCK
V	$53.8 - 0.33\ E$	$53.3 - 0.55E + 0.42/A^{1/3} + 27(N-Z)/A$	$(52.6 - 0.28E) \pm 7$
W	7.5	13.5 ± 2 Ep < 17 $3A^{1/3} \pm 1.5$ Ep > 17	10.6 ± 1.6
r_o	$1.25A^{1/3}$	$1.25A^{1/3}$	$1.25A^{1/3}$
a	0.65	0.65	0.65
a_I	0.70	0.47	0.47
V_s	5.5	8.5 $17 \leq Ep \leq 22$ 7.5 Ep < 17	8.0

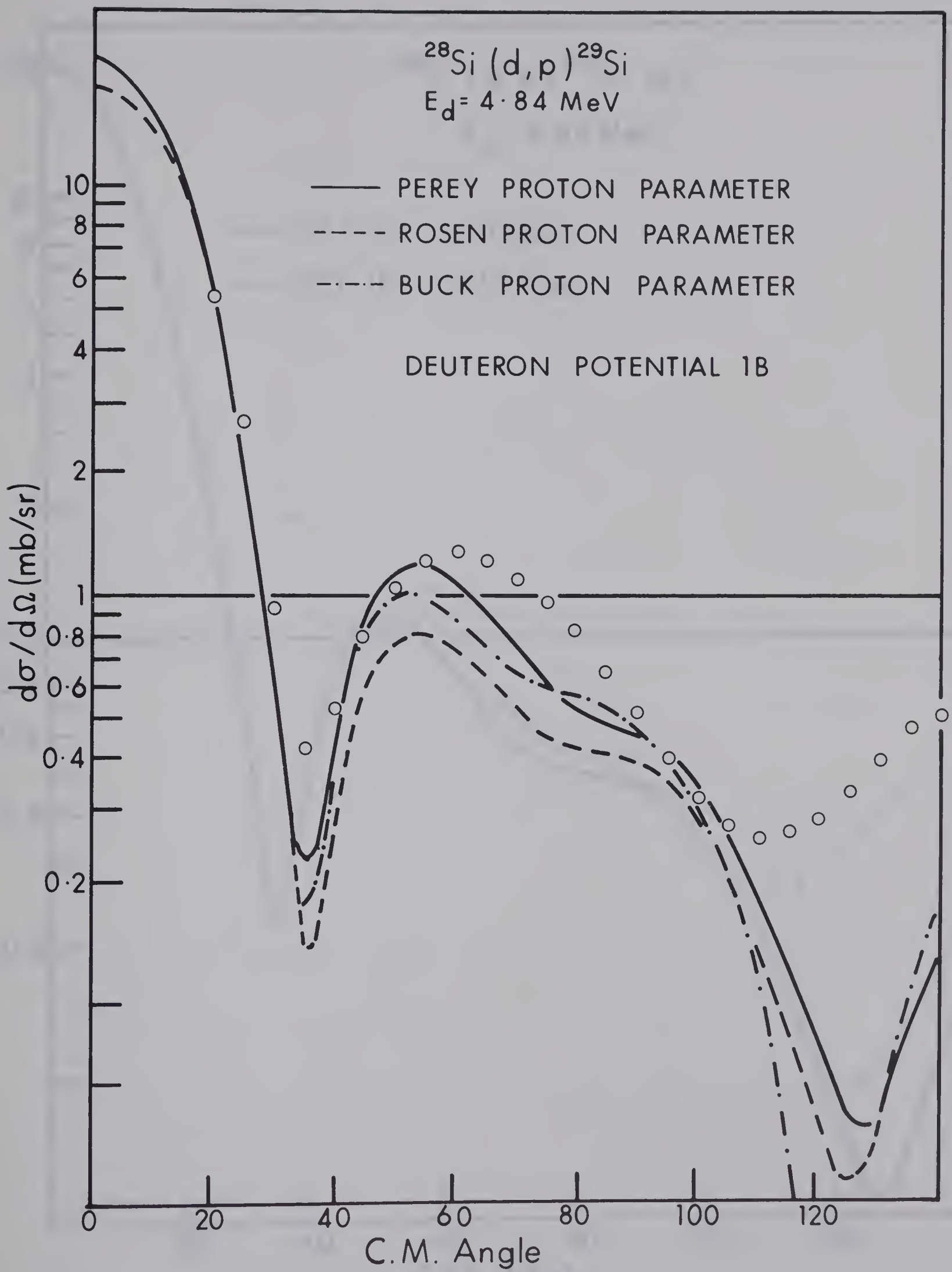

FIGURE 5 - 7: EFFECT OF DIFFERENT PROTON POTENTIALS

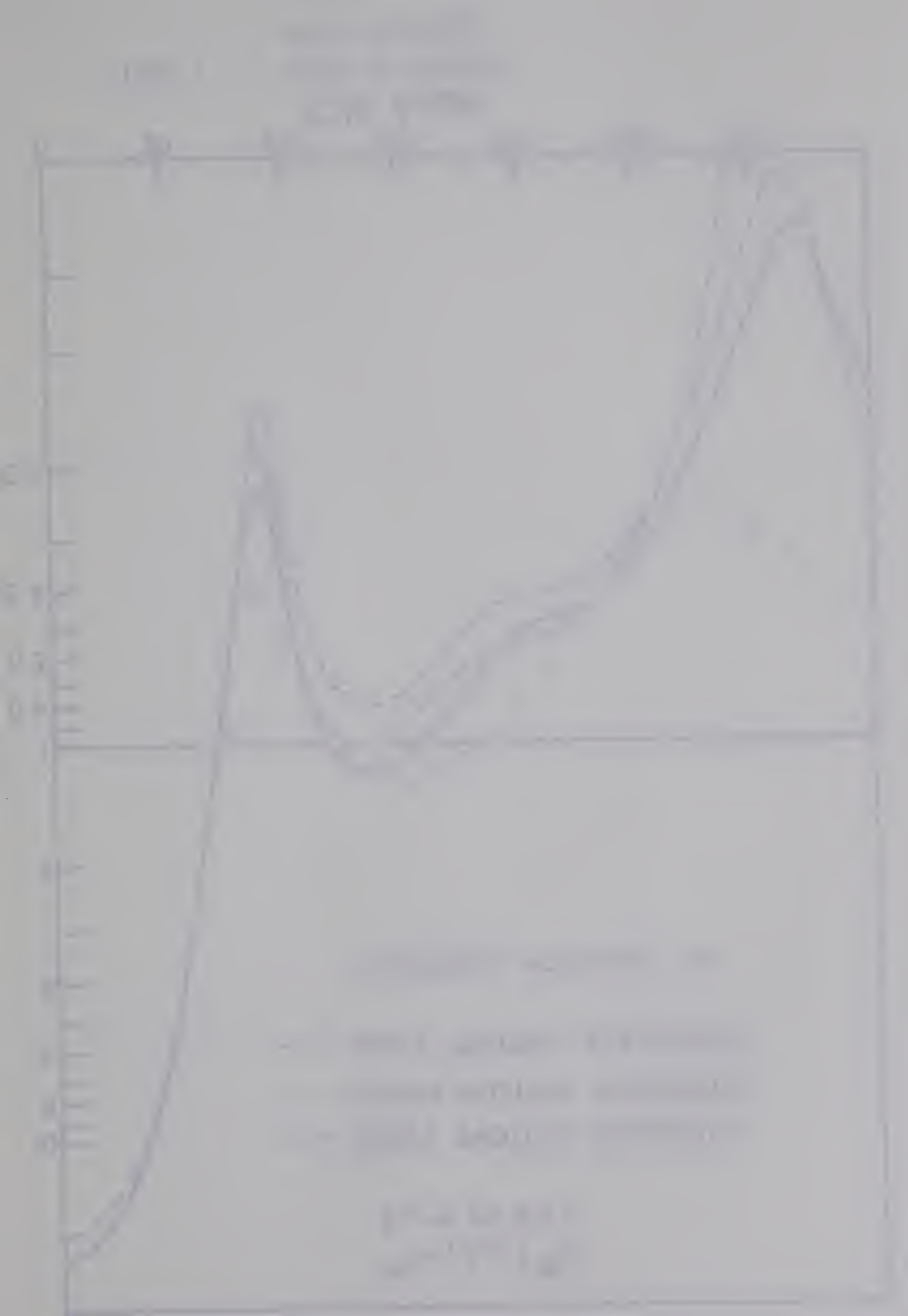

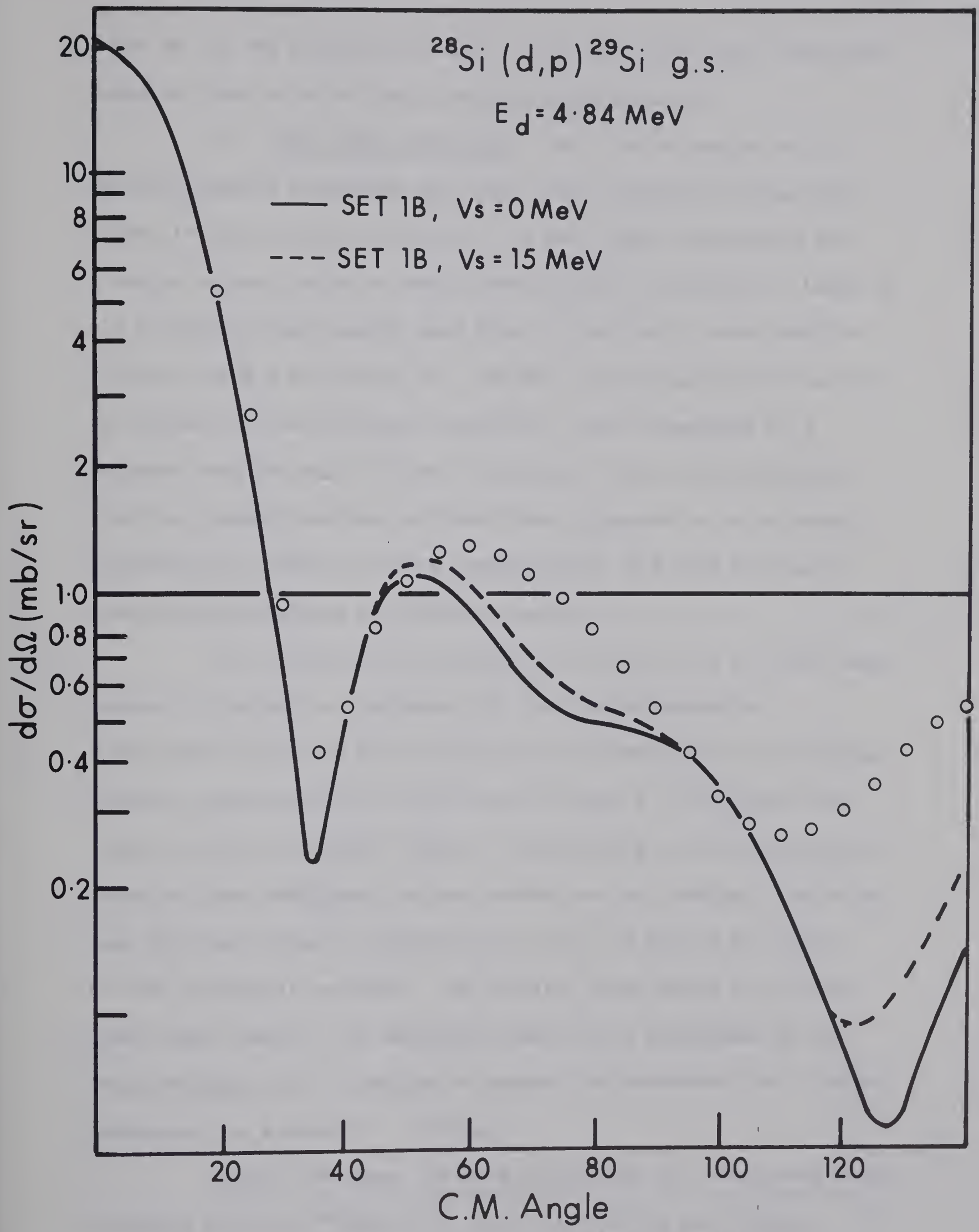

FIGURE 5 - 8: EFFECT OF A SPIN-ORBIT POTENTIAL

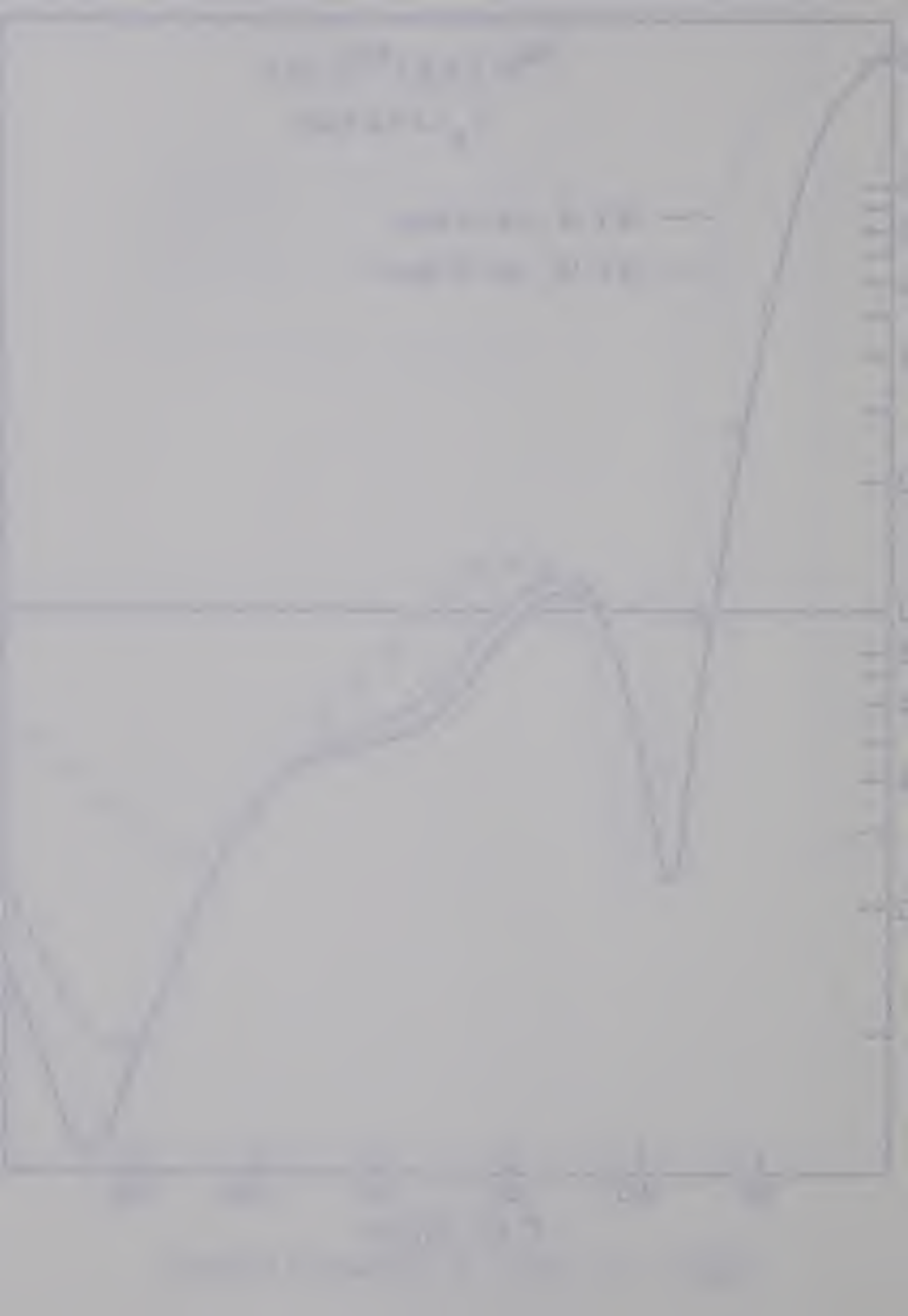

order to fit the polarization data it will not affect any conclusions based on fits to the stripping angular distributions.

(e) Well Depth Ambiguity: The first attempts to fit deuteron elastic scattering data used almost exclusively real well depths in the vicinity of 50 MeV - the well depth appropriate for a single nucleon which is used in shell model calculations. Later it was recognized that equally good fits to the elastic data could be obtained using a well depth of ~ 100 MeV - approximately the sum of the depths for the individual nucleons. This corresponds to a deuteron wave function with one more node in the nuclear interior. When the present work was initiated there appeared to be no strong preference for either of these possibilities, and they were used almost interchangeably by different authors.

An accumulation of evidence in the last two or three years appears to indicate a preference for the 100 MeV potential (Lawergren '67), based on more satisfactory predictions to stripping reaction cross-sections. More recently (Perey 67) has placed this result on some thoeretical basis by constructing a deuteron optical potential from individual nucleon potentials and finding a resulting real well depth equal to somewhat less than the sum of the depths for the individual nucleons. Our results, then, which it had been hoped would clarify this ambiguity, must now be considered in the less ambitious role of seeking to support the moderately well founded preference for a depth of ~ 100 MeV.

Figure 5-9 shows the DWBA predictions for the ground state stripping reaction $^{28}Si(d,p)^{29}Si$ normalized to the most forward experimental point for easier comparison of the shapes. As mentioned

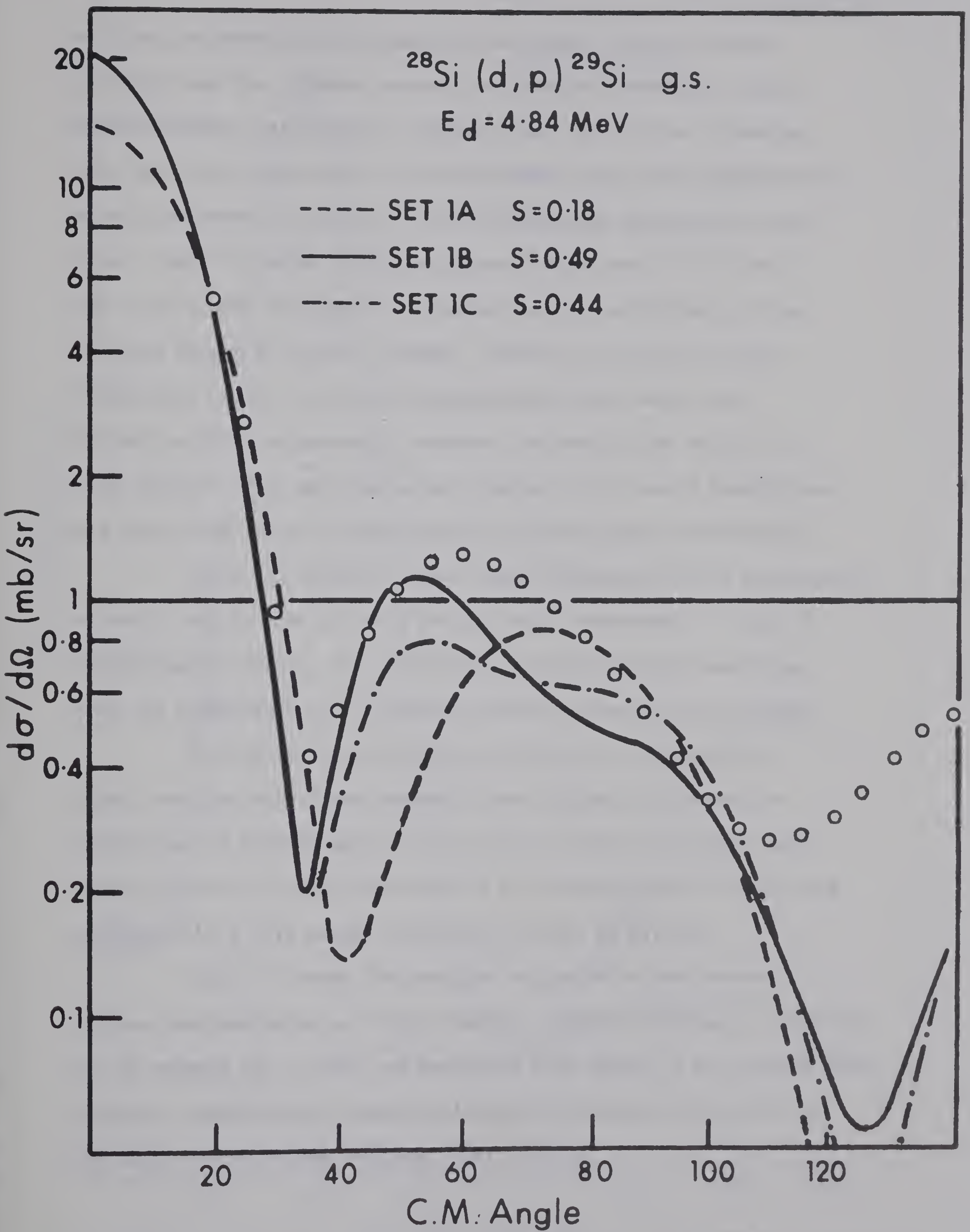

FIGURE 5 - 9: DWBA PREDICTIONS WITH DIFFERENT WELL DEPTHS

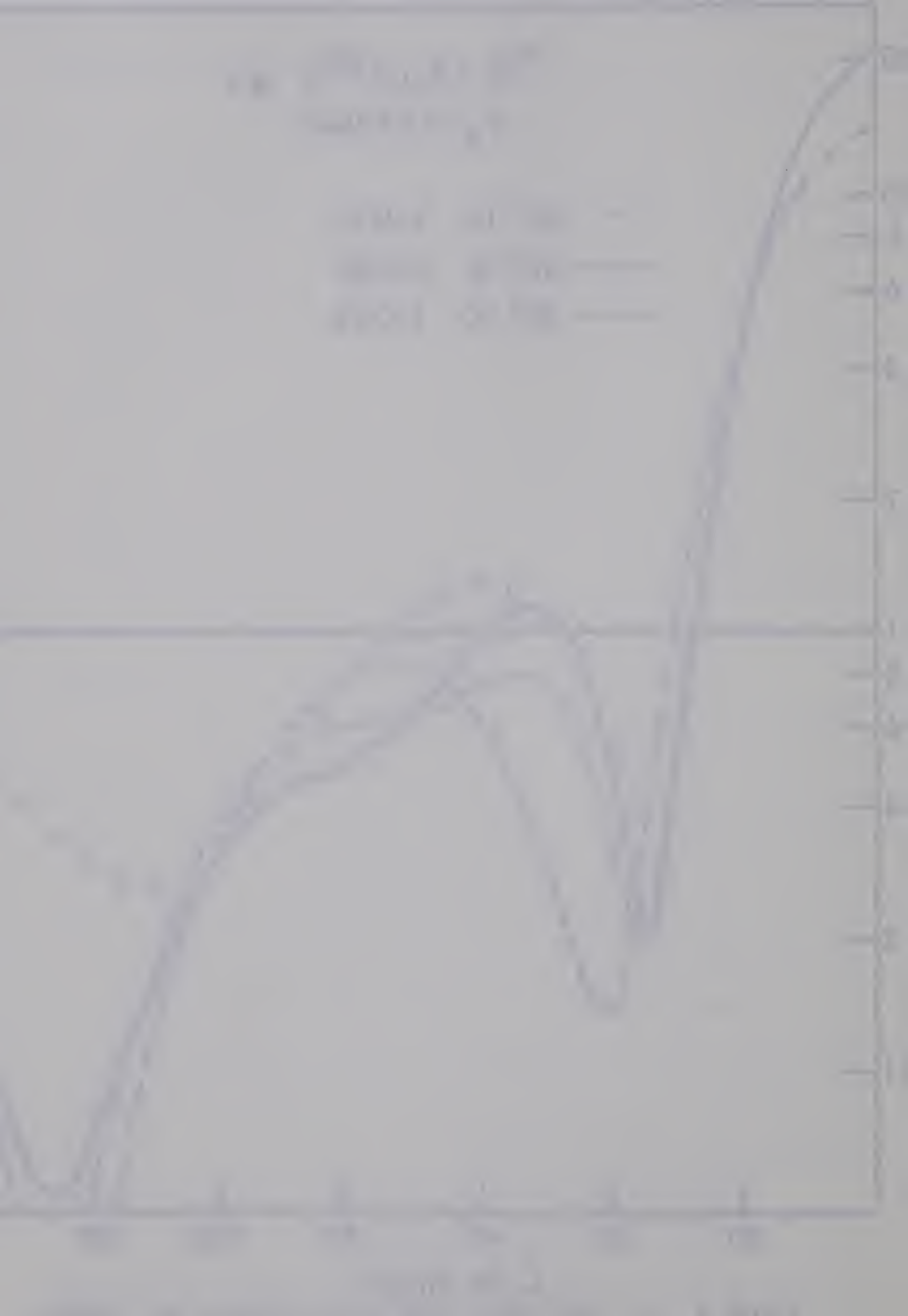

earlier, the experimental points are the actual measured cross-sections less the compound nucleus contribution determined from a Hauser-Feshbach calculation. Because these and all the following fits have been normalized to an experimental point, the representative error bars shown in figures 5-7 to 5-13 indicate statistical errors only. There is rather little to choose between sets B(V~100 MeV) and C(V~150 MeV) although B is somewhat better on the basis of the relative height of the 60^{o} maximum. However, as there is little theoretical basis for considering potentials much deeper than 100 MeV we will not generally consider the predictions of set C in what follows. They are always very similar to the set B predictions, and would only serve to complicate the illustrations unnecessarily.

There is, however, a very large difference in the predictions of sets A and B, that of set B being clearly preferred. It must be acknowledged, however, that if the 5.0 MeV distribution were being used for comparison, this preference would no longer be so obvious.

To illustrate the quality of the fits to the excited levels obtained with these parameter sets, figure 5-10 shows the predictions of sets 1A and 1B to the first excited (1.28 MeV) level in this reaction, again normalized to the stripping peak. Here there appears to be a very slight preference for the 50 MeV set.

Table 5-3 shows the absolute and relative spectroscopic factors obtained using all eight deuteron optical potentials. Considering at present set 1 only, and recalling from chapter 2 the theoretical relative spectroscopic factors calculated by Davies (Davies 66) on the basis of the strong coupling model, namely:

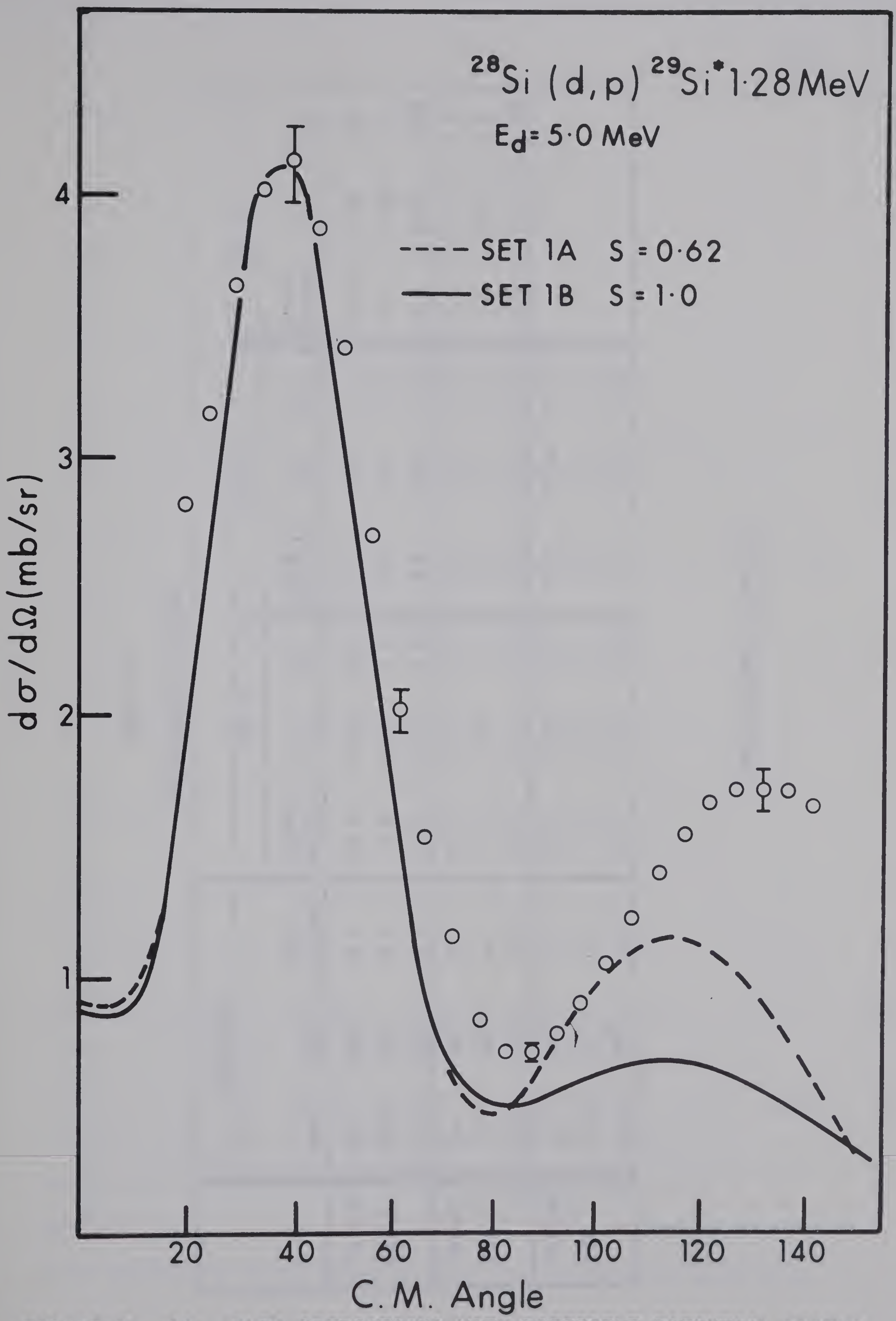

FIGURE 5 - 10: DWBA PREDICTIONS WITH DIFFERENT POTENTIAL DEPTHS

TABLE 5-3

SPECTROSCOPIC FACTORS

	EXPERIMENT			D W B A								
				SET A			SET B			SET C		
	Level	Angle	Cross Section	Cross Section	S_{abs}	S_{rel}	Cross Section	S_{abs}	S_{rel}	Cross Section	S_{abs}	S_{rel}
"5 MeV	gs	20^{o}	5.4	29.4	0.18	1.0	11.1	0.49	1.0	12.4	0.44	1.0
SET 1	1.28	40^{o}	4.1	6.6	0.62	3.4	4.1	1.0	2.0	4.2	0.98	2.1
	2.03	40^{o}	2.0	13.8	0.15	0.83	9.4	0.22	0.45	9.4	0.22	0.50
"MEAN"	gs	20^{o}	5.4	25.1	0.22	1.0	9.0	0.60	1.0	7.6	0.71	1.0
SET 2	1.28	40^{o}	4.1	5.3	0.78	3.5	3.5	1.2	2.0	3.1	1.3	1.8
	2.03	40^{o}	2.0	11.7	0.17	0.77	8.1	0.25	0.42	6.9	0.29	0.41
"TREND"	gs	20^{o}	5.4	26.8	0.20	1.0	7.8	0.69	1.0			
SET 3	1.28	40^{o}	4.1	5.3	0.78	3.9	3.2	1.30	1.9			
	2.03	40^{o}	2.0	11.7	0.17	0.85	7.7	0.26	0.38			

Cross sections in mb./sr.

$$S_{rel\ gs} = 1.0$$

$$S_{rel\ 1.28} = 2.1$$

$$S_{rel\ 2.03} = 0.45$$

then a clear preference is displayed for set B.

Extreme caution must be exercised, however, in the extraction of spectroscopic factors - even relative spectroscopic factors - in a region such as this where the excitation function is known to be resonant. If in Table 5-3 the 20^{o} cross-section 5.0 MeV were used, namely 9.2 mb/sr, then the absolute spectroscopic factor for the ground state using set A would be 0.31, and for set B would be 0.83. The corresponding relative spectroscopic factors would then become:

	Theory	Set A	Set B
$S_{rel\ gs}$	1.0	1.0	1.0
$S_{rel\ 1.28}$	2.1	2.0	1.2
$S_{rel\ 2.03}$	0.45	0.48	0.27

and the preference would then be equally strong for set A.

Consequently the preference for set B based on relative spectroscopic factors is no stronger than the preference (which is not entirely arbitrary) for the 4.84 MeV distribution as being more representative of the direct amplitude in this reaction. The spectroscopic factor, it must be emphasized, can only be related to model predictions to the extent to which the reaction from which it is

extracted is direct.

The results of these comparisons then, is a weak preference for the 100 MeV well depth, supporting current beliefs. One very positive and important conclusion may be drawn, however. For this reaction there is a large difference in the relative as well as in the absolute spectroscopic factors predicted on the basis of assumed deuteron optical potentials with well depths of ~50 and ~100 MeV: quite enough to distinguish between them if reliable direct amplitude measurements are available. This appears to be in contradiction to a widely held philosophy that if only relative spectroscopic factors are of interest, then virtually any parameters or approximations may be used in the DWBA calculation.

(f) Shape ambiguity: The conclusions of the previous section appear to hold as well for the "TREND" and "MEAN" deuteron parameters as for the "5 MeV" parameters used in the illustration. It is now of interest to see which of these groups gives predictions which most closely resemble the experimental distributions.

Figure 5-11 shows the predictions from sets 1B, 2B and 3B to the ground state distribution, normalized as before to the experimental cross-section at 20^{o}. Both the "TREND" and "MEAN" groups predict a second maximum in the diffraction pattern which is not observed experimentally. The "5 MeV" group predicts a shape much more closely resembling the experiment, with only a suggestion of a second maximum. Non-local calculations reduce the relative size of the second maximum appearing in the "MEAN" and "TREND" predictions somewhat, but the shape predicted by the "5 MeV" parameters remains closest to the experimental distribution. Even this shape, however,

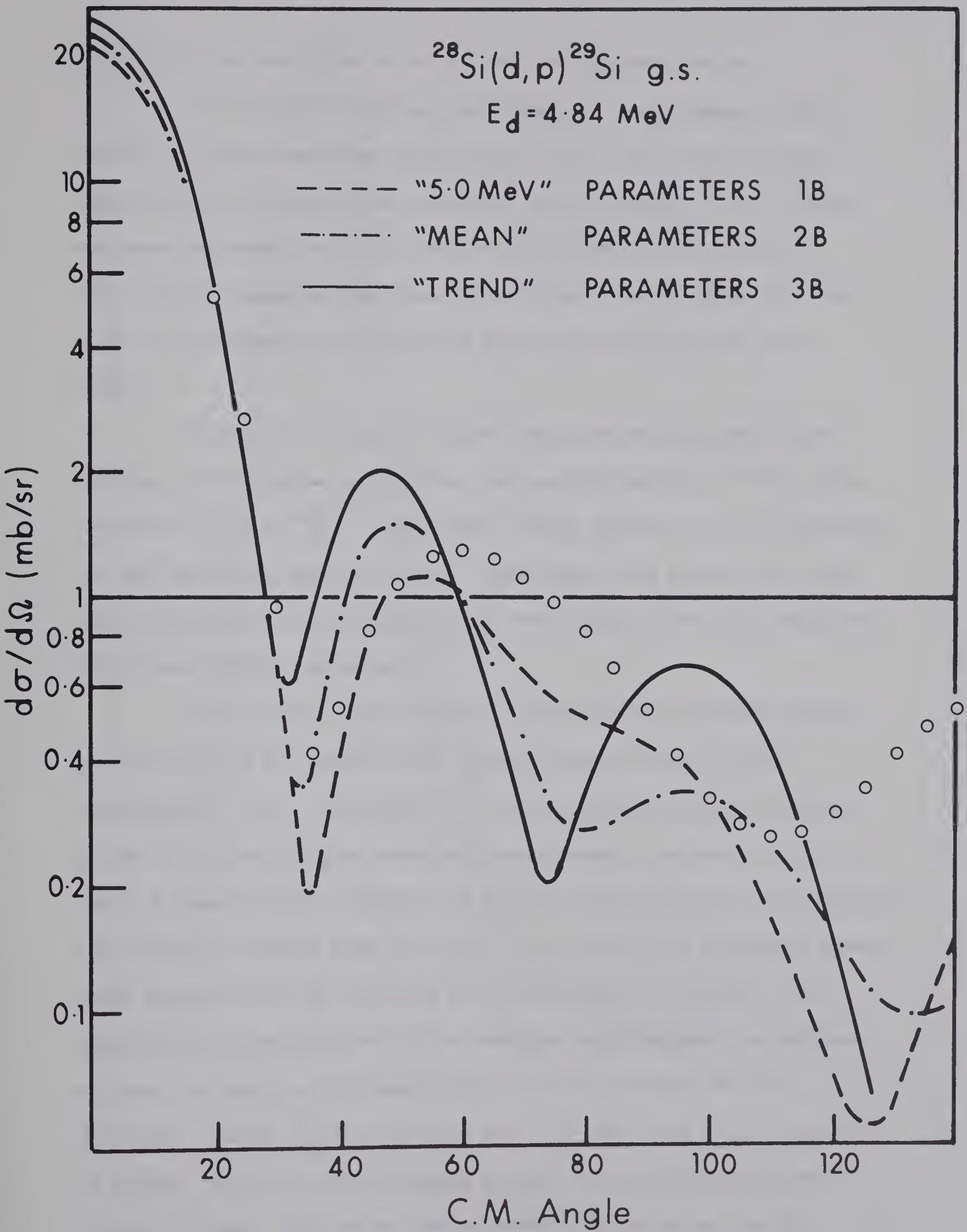

FIGURE 5 - 11: DWBA PREDICTIONS WITH DIFFERENT PARAMETER SETS

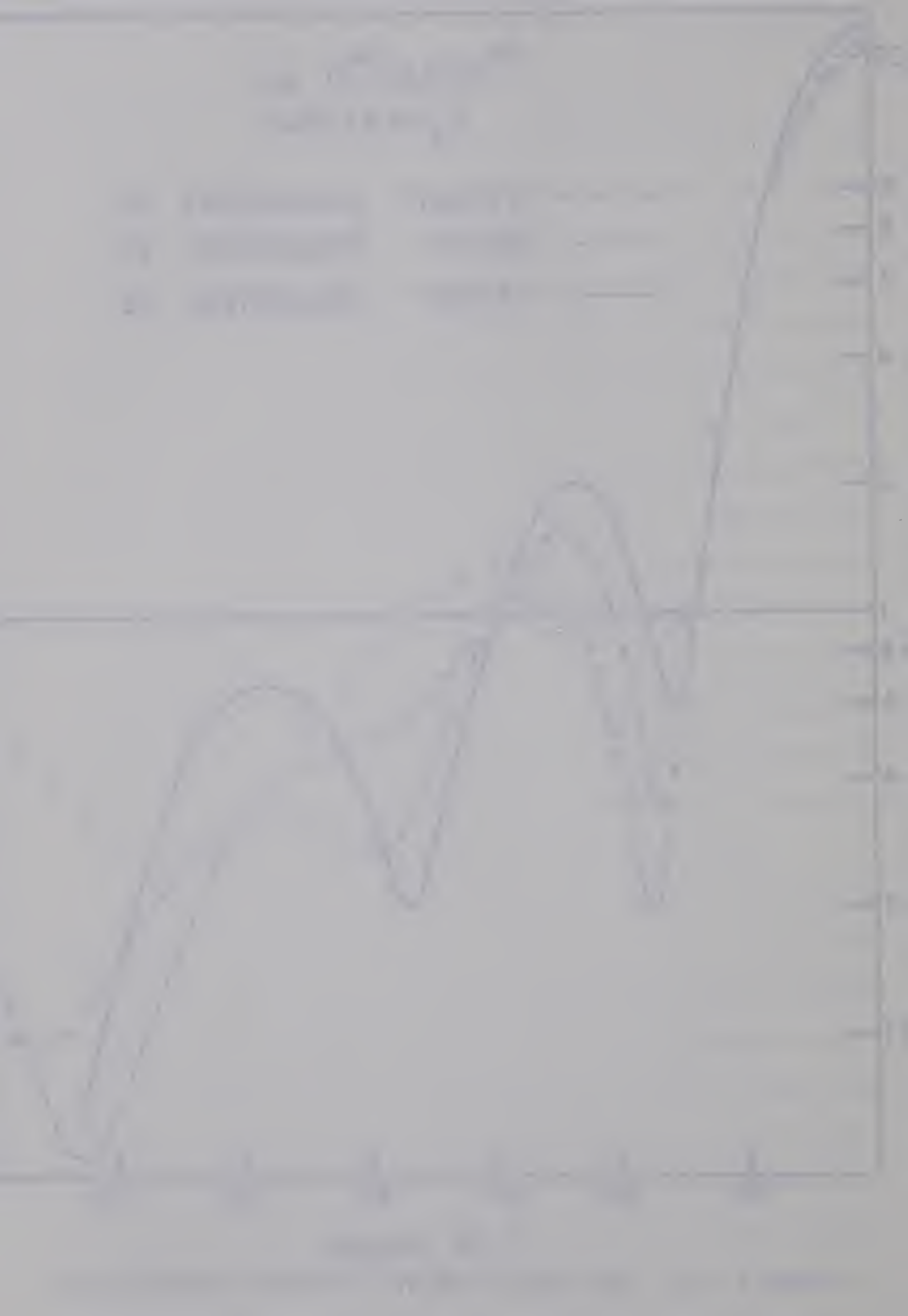

is not quite as satisfactory as in the local approximation.

It should be mentioned here that the experimental distributions at higher energies (Kuehner 60a) show this second maximum very strongly, becoming less prominent as the energy of the incident deuteron decreases until at 6 MeV the experimental distribution very closely resembles the theoretical prediction of group 1B. The 4.84 MeV experimental distribution fits very smoothly into this trend.

Figures 5-12 and 5-13 show the corresponding predictions for the proton groups to the first two excited levels of ^{29}Si in the reaction ^{28}Si(d,p)^{29}Si*. Once again, there appears to be a preference for set 1B on the basis of shape. Once again, the effect of a non-local calculation is to improve only very slightly the fits using the "MEAN" and "TREND" parameters.

The absolute spectroscopic factor for the 1.28 MeV level is expected, on the basis of the strong coupling model, to be approximately 1.0. From Table 5-3, we see that the three parameter groups 1B, 2B and 3B give absolute spectroscopic factors of 1.0, 1.2 and 1.3 respectively. However the large (~30%) decrease in the absolute spectroscopic factors when non local calculations are performed change these numbers to 0.78, 0.94 and 1.0 respectively. Moreover, the experimental uncertainties in the absolute spectroscopic factors are at least as great as the magnitude of the fluctuations in the excitation curves at the stripping peak (15-20%), and so it would not be prudent to draw any conclusions on the basis of these results, except to remark that theory and experiment agree to within 30%.

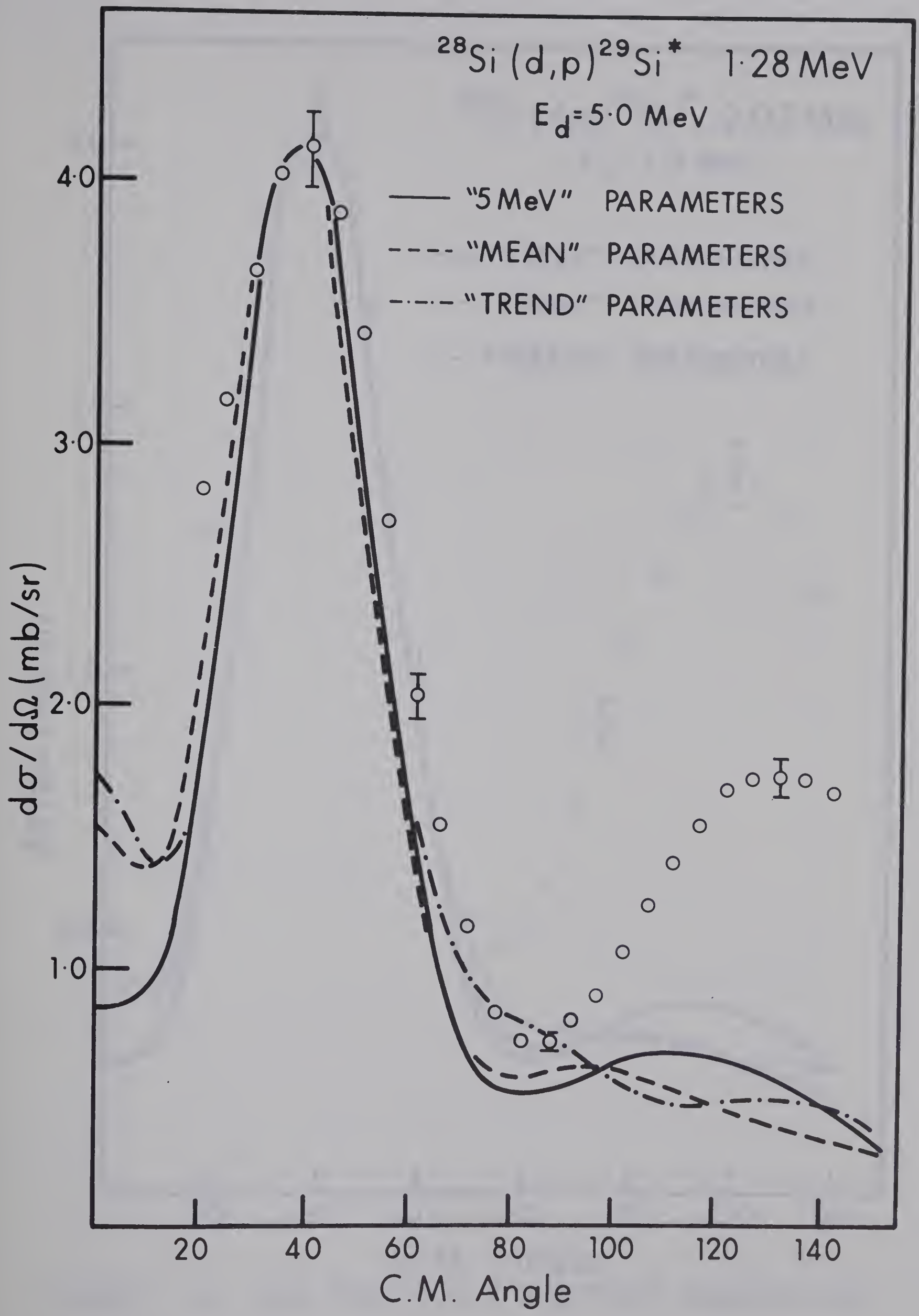

FIGURE 5 - 12: DWBA PREDICTIONS WITH DIFFERENT PARAMETER SETS

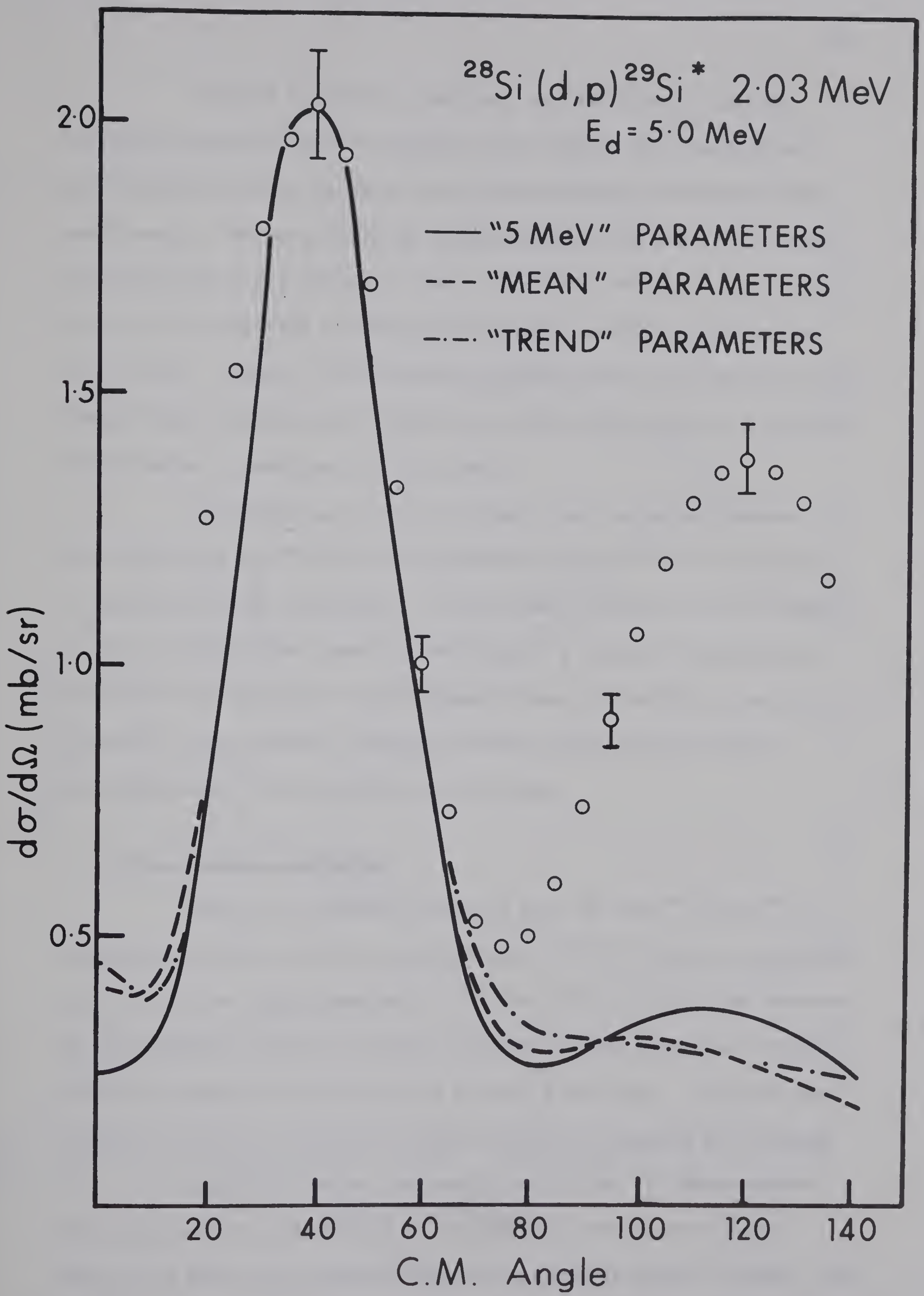

FIGURE 5 - 13: DWBA PREDICTIONS WITH DIFFERENT PARAMETER SETS

It would be nice to conclude, at this point, that the deuteron optical potential obtained from fitting the elastic data at 5.00 MeV provides the best fit to the stripping reaction at the same energy. We have, however, been comparing the predictions with an experimental distribution taken at 4.84 MeV, which we have only assumed will resemble a predominently direct reaction distribution at 5.0 MeV. Indeed, the parameters obtained from the 4.82 MeV elastic data closely resemble the "MEAN" set, and do not predict a stripping distribution resembling the experiment.

It appears as if the relatively good agreement between the experiment and the DWBA calculations using the "5MeV" parameters is probably merely fortuitous. If any real conclusion can be drawn, it is only the rather negative one that in a resonant region such as this it is certainly not an adequate test of the DWBA theory to attempt to fit a single stripping angular distribution without some knowledge of its variation with energy.

5. The $^{28}Si(d,n)^{29}P$ Reaction:

Much of the analysis reported here on the $^{28}Si(d,p)^{29}Si$ reaction has also recently been performed by S. M. Tang for comparison with the mirror (d,n) reaction. This was felt to be of some interest, as the earlier analysis by Davies (Davies 66) was performed without deuteron parameters obtained from elastic scattering. Although the analysis is not yet complete, some preliminary comments may be made.

Figure 5-14 shows the prediction of set 1B compared with the experimental distribution of the ground state neutron group. The fit is seen to be very satisfactory, somewhat better, indeed, than

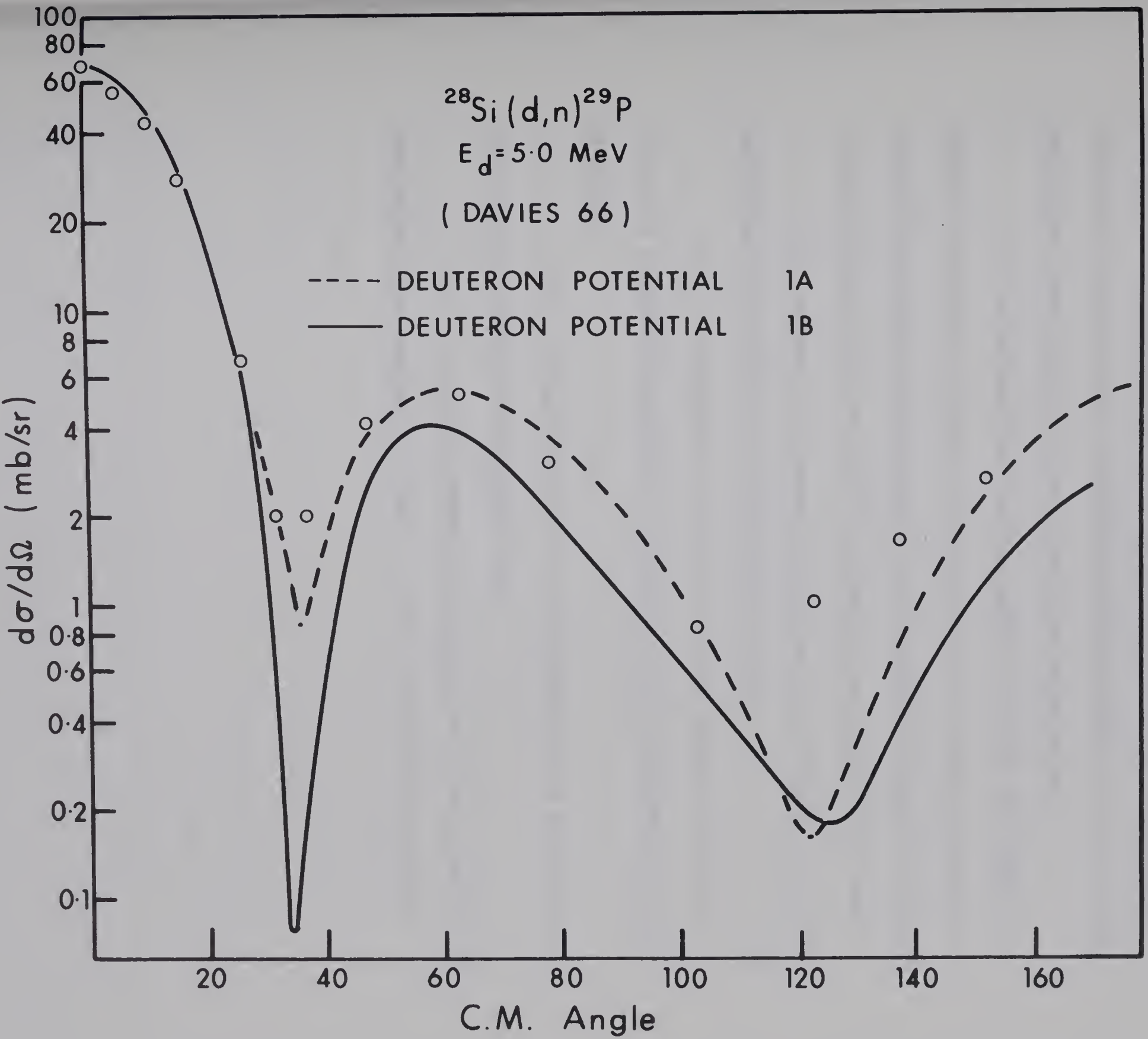
$^{28}Si(d,n)^{29}P$
E_d=5·0 MeV
(DAVIES 66)
---- DEUTERON POTENTIAL 1A
—— DEUTERON POTENTIAL 1B
dσ/dΩ (mb/sr)
100
80
60
40
20
10
8
6
4
2
1
0·8
0·6
0·4
0·2
0·1
20
40
60
80
100
120
140
160
C.M. Angle

FIGURE 5-14

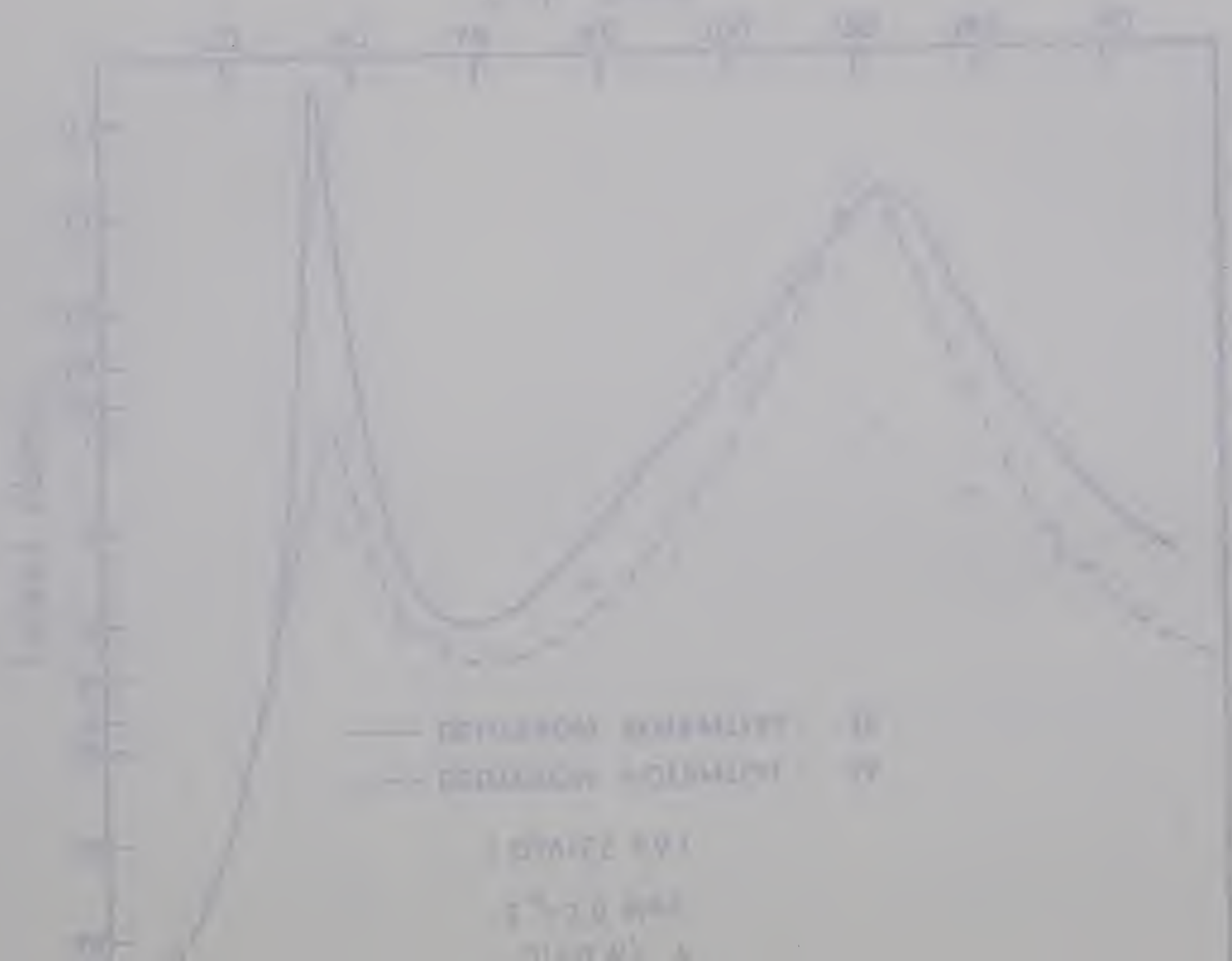

the quality of the predictions to the (d,p) reaction. It should be mentioned here that based on both excitation functions and Hauser-Feshbach calculations, the (d,n) reaction appears to be less influenced by compound and interference effects than the (d,p). The prediction shown resulted from a non-local calculation.

It is interesting that the effect of using the "MEAN" or "TREND" parameters in these calculations is not nearly so severe as in the (d,p) case, and the results can only just be said to indicate a weak preference for the "5MeV" parameters as in the (d,p) case.

At present, it appears that three observations can be made concerning the results of calculations to date.

(i) The quality of the fits to the angular distributions are in general superior to those for the corresponding (d,p) reactions;

(ii) The calculations are considerably less sensitive to the choice of deuteron parameters; and

(iii) The results appear to support, or in any case not to contradict, the conclusions based on the $^{28}Si(d,p)^{29}Si$ reaction.

CHAPTER 6: THE $^{28}Si(d,p)^{29}Si$ g.s. POLARIZATION REACTION

1. Previous Work

The polarization of the ground state group of protons for the reaction $^{28}Si(d,p)^{29}Si$ has been measured at higher energies by several groups. For example, at Ed = 10 MeV by Bercaw and Schull (Bercaw 64); at 13.8 MeV by Pasechnik (Pasechnik 63) and at 15 MeV by Isoya and Marrone (Isoya 62). Moreover, Reber and Saladin (Reber 64) have measured the polarization of the $\ell_n = 2$ proton group from the $^{28}Si(d,p)^{29}Si^*$ 1.28 MeV reaction at Ed = 15 MeV. The results of this higher energy data were all rather similar, the polarization changing sign in the vicinity of the minima of the stripping pattern.

These experiments were motivated by the belief mentioned in Chapter 2 that polarization measurements constitute the most rigourous test of the DWBA Theory. It is particularly hoped that in the case of an $\ell_n = 0$ transfer reaction such as this, where the polarization is due to spin-orbit forces acting on the incoming and outgoing waves directly, that the polarization of the outgoing protons might help to establish the deuteron optical potential more convincingly, and in particular its spin-orbit component.

S. T. Lam (Lam 67) had achieved some success in fitting the $^{28}Si(d,n)^{29}P$ gs polarization data taken at 5.0 MeV using the deuteron parameters obtained by Perey (Perey 66) from fitting elastic scattering data at 11.8 MeV. It was felt that it would be of interest to compare the polarization distribution for the mirror reaction, and to use the optical potentials obtained from the present work in an attempt to predict both of these polarization distributions

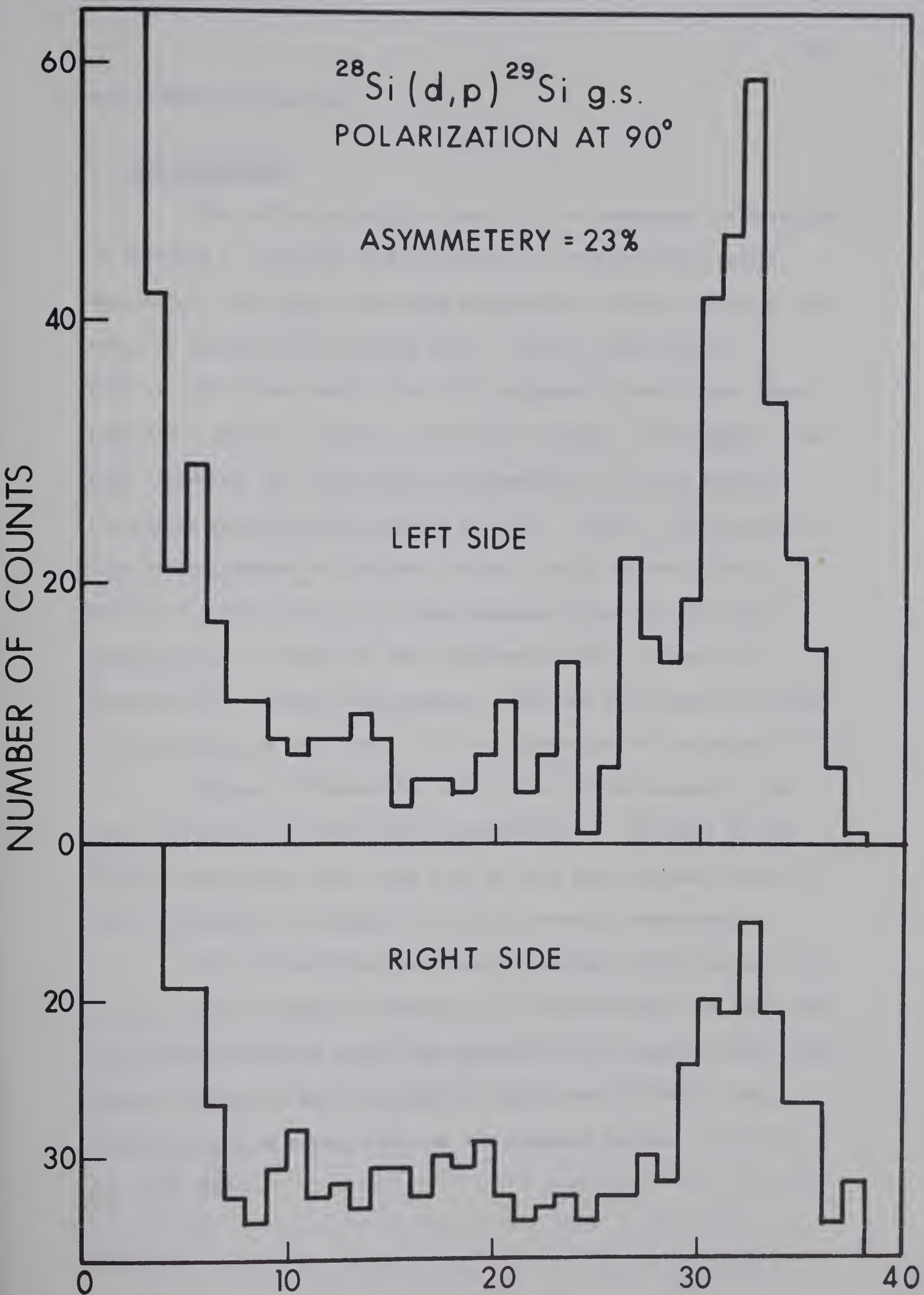

FIGURE 6 - 1: TYPICAL ASYMMETRY RUN

from a DWBA calculation.

2. The Experiment:

The carbon polarimeter used in this experiment is described in Appendix A. Because of the very small cross-sections always associated with double scattering experiments, several measures were taken to increase the counting rate. Firstly, wider slits (1/8" x 3/16") were used in the slit telescope allowing more beam to strike the target. Secondly, very thick targets (~5.5 mgs/cm^2) were used, oriented, for each angle of measurement, so as to minimize the energy spread in the outgoing protons. Thirdly, the quadrupole lens was introduced to increase the solid angle as described in Chapter 3. The first two of these measures also had the effect of spreading out the image at the polarimeter which, although it decreases the counting rate somewhat, also has the beneficial effect of decreasing the sensitivity of the polarimeter to the magnetic field.

Figure 6-1 shows the result of a typical asymmetry run. Only 720 total counts have been accumulated, yet in spite of the measures mentioned above, runs such as this took between 10 and 16 hours, depending, of course, on the differential cross-section.

The average effective target thickness, which varied, of course, with the target orientation, was approximately 500 keV, and the incident deuteron energy was adjusted at each angle so that the deuteron energy at the center of the target was 5.0 MeV. Thus interactions were taking place at all energies between ~4.75 MeV and ~5.25 MeV.

3. Results

The asymmetry, ε, is calculated according to the usual relationship:

$$\varepsilon = \frac{r-1}{r+1} \qquad 6\text{-}1$$

where: $r = \sqrt{r_1 r_2}$

and: $r_1 = L_1/R_1 \; ; \; r_2 = L_2/R_2$

where L_1 and R_1 are the number of counts scattered to left and right respectively with the polarimeter in one orientation, and L_2 and R_2 are the corresponding numbers with the polarimeter rotated by 180^o.

The proton polarization is then calculated from the relationship:

$$P_1 = \varepsilon/P_2$$

where P_2 is the analysing power of the polarimeter.

The absolute statistical error in the asymmetry measurement is

$$\Delta\varepsilon = 2\Delta r/(r+1)^2$$

obtained by differentiating 6-1 with respect to r.

The experimental results are listed in Table 6-1, and shown graphically in figure 6-2. Eight points were obtained in 10^o steps between 30^o and 100^o with absolute statistical errors of $\sim \pm 7\%$.

All measured polarizations were negative, with a decreasing trend from -7% at 30^o to -35% at 100^o. Two typical DWBA predictions are also shown in figure 6-2. The deuteron potential

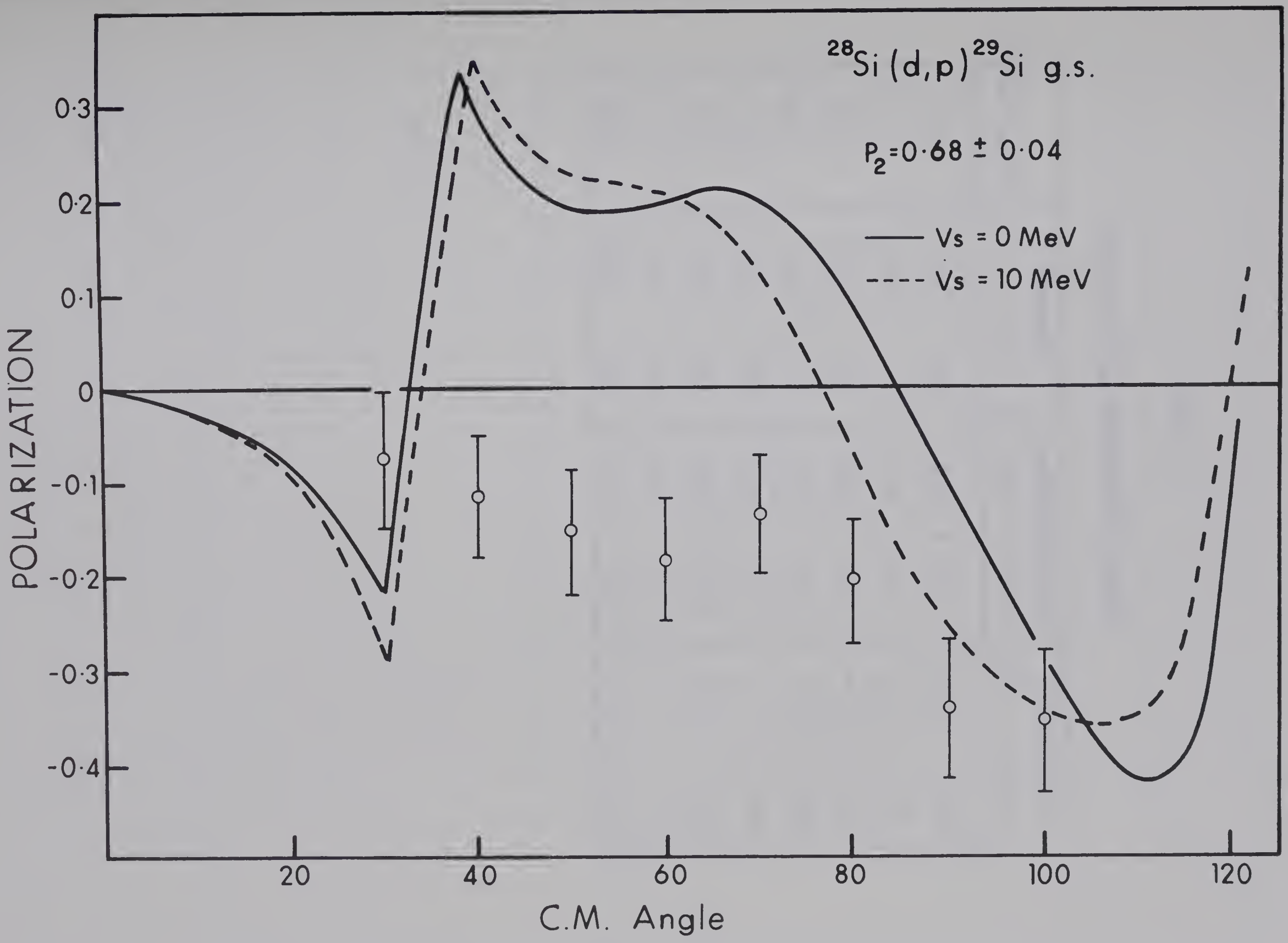

FIGURE 6 - 2: DWBA POLARIZATION PREDICTIONS

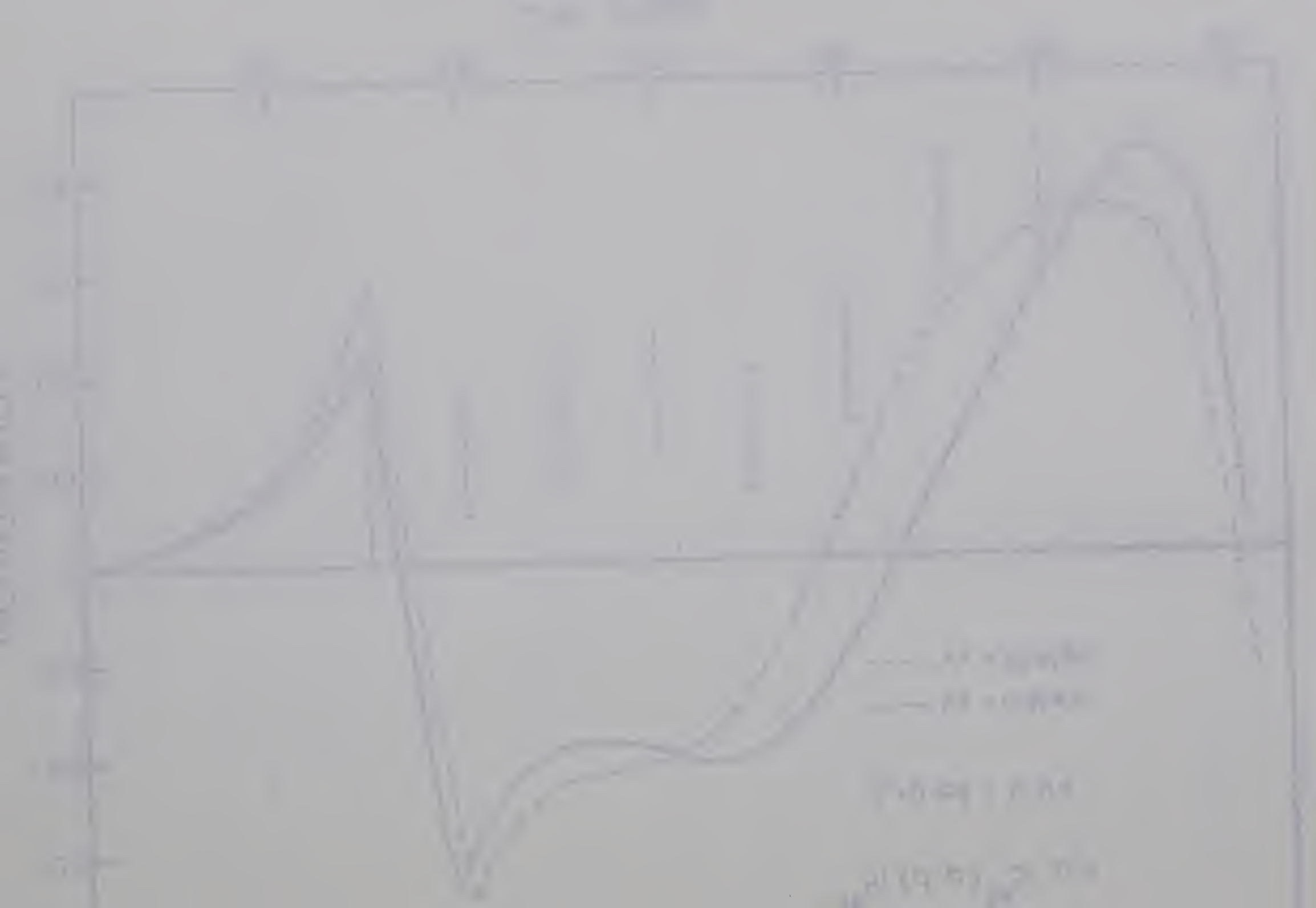

TABLE 6-1

$^{28}Si(d,p)^{29}Si_{gs}$ POLARIZATION RESULTS

cm. Angle	Asymmetry $\varepsilon \pm \Delta\varepsilon$	Analysing Power $P_2 \pm \Delta P_2$	Polarization $P_1 \pm \Delta P_1$
30.9	0.050 ± .040	-0.68 ± 0.04	-0.07 ± 0.06
41.2	0.078 ± .037	-0.68 ± 0.04	-0.11 ± 0.06
51.4	0.103 ± .039	-0.68 ± 0.04	-0.15 ± 0.07
61.6	0.123 ± .037	-0.68 ± 0.04	-0.18 ± 0.06
71.8	0.091 ± .038	-0.68 ± 0.04	-0.13 ± 0.06
81.8	0.138 ± .037	-0.68 ± 0.04	-0.20 ± 0.07
91.9	0.233 ± .037	-0.68 ± 0.04	-0.34 ± 0.07
101.8	0.241 ± .036	-0.68 ± 0.04	-0.35 ± 0.07

used is set 1B with spin-orbit terms of 0 and 10 MeV. These predictions are quite typical of those obtained with all sets of deuteron potentials used - they are quite insensitive to both the shape and strength of the spin-orbit interaction.

It had been intended to take more polarization measurements, both forward of 30^{o}, and farther back than 100^{o}. However it was apparent that the shape which was emerging bore no resemblence to the results at higher energies, or to the polarization of the neutrons from the $^{28}Si(d,n)^{29}P$ gs reaction, or as has already been mentioned, to any DWBA prediction using any deuteron optical model parameters whatever. It was clear that regardless of the results of further measurements, no conclusions concerning the deuteron optical potential could be reached on the basis of the polarization results. In view of the large amount of accelerator time which would be required to obtain further data from which very little information might be extracted, the polarization experiment was terminated at this stage.

4. Comments

The polarization of the ground state neutron group from the $^{28}Si(d,n)^{29}P$ gs reaction is shown in figure 6-3, along with a DWBA prediction using deuteron parameter set 1B and spin-orbit interactions of strengths 0 and 10 MeV. The fit is seen to be remarkably good in all cases, although the calculation is too insensitive to the deuteron parameters to allow the elimination of any set on the basis of this data.

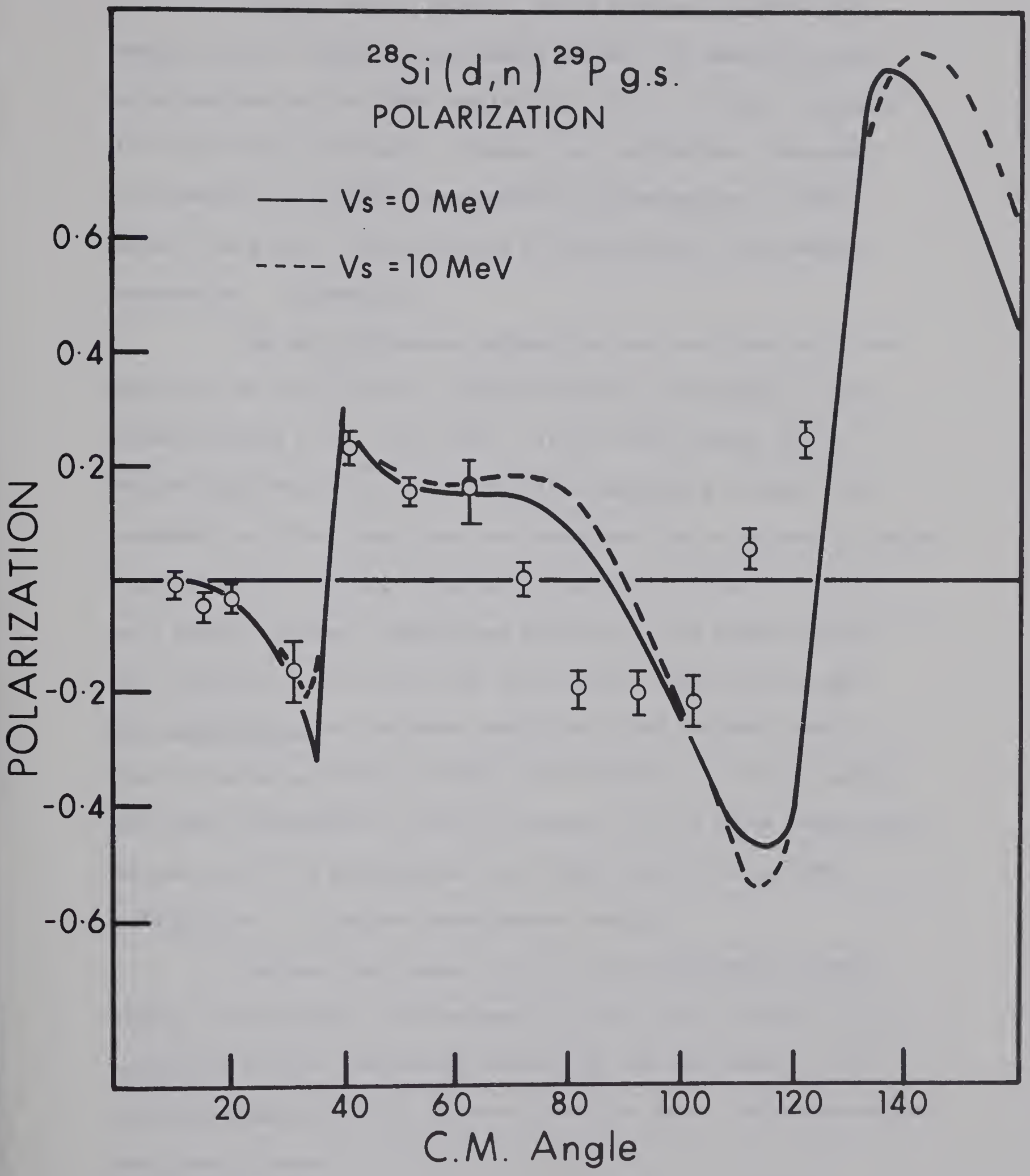

FIGURE 6 - 3: DWBA POLARIZATION PREDICTIONS

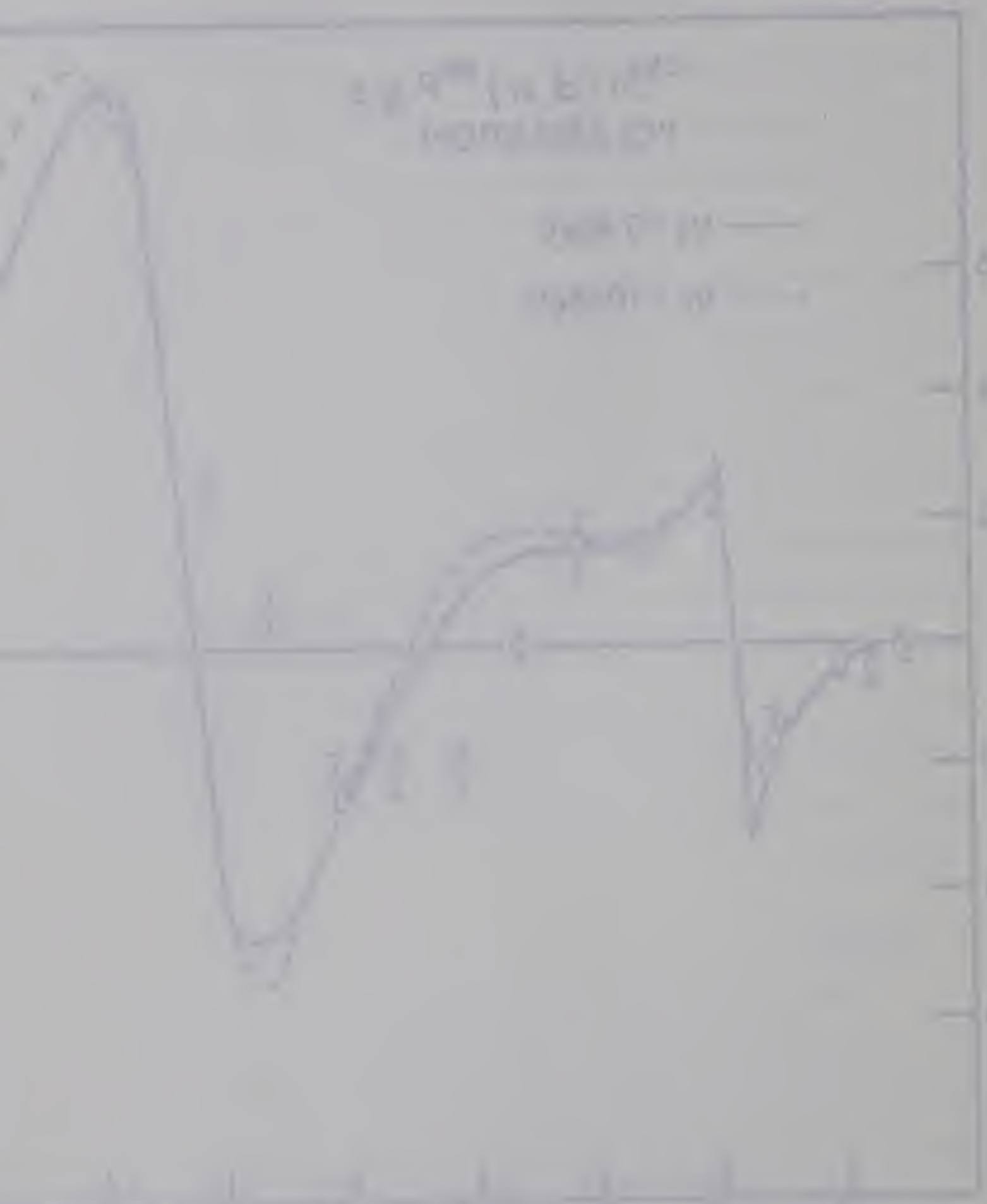

This agreement, however, makes even more obscure the reason for the complete disagreement between the measured proton polarizations and the DWBA predictions. One is, indeed, inclined to suspect the polarimeter. However its calibration, discussed in Appendix A, included measurements of polarizations of +89% as well as giving strong evidence of insignificant instrumental asymmetries. (Appendix A)

The only difference between the two reactions is in the magnitude of the predicted compound nucleus contribution - five times as great in the (d,p) case. It has been pointed out by Bercaw and Schull (Bercaw 64) that if interference between the compound and direct amplitudes are important (as we believe to be the case) then the compound contribution cannot be thought of merely as a nearly isotropic unpolarized addition to the cross-section, but instead will cause both the differential cross-section and the polarization to fluctuate rapidly with the incident energy. Due to the large number of levels participating at any one energy, the energy dependence of the polarization will be quite complicated. Bercaw goes on to warn against the "overly naive" use of DWBA calculations to interpret experimental results.

Whatever the reason for the large disagreement between theory and experiment, and between (d,n) and (d,p) results, it is clear that no firm conclusions concerning the DWBA theory or the parameters used in it can be drawn from this data. Our expectations were overly naive.

CONCLUSIONS:

It cannot be said that the objectives set out in the introduction to this thesis have been satisfactorily achieved, however some positive observations on the results can be made.

(i) In support of current beliefs, a preference has been found for the deuteron optical potential with a strength of ~ 100 MeV, or somewhat less than the sum of the well depths for the individual nucleons.

(ii) There is a large difference in the relative spectroscopic factors obtained using well depths of 50 and 100 MeV. Although this may not always be the case, it would appear advisable, in view of (i), always to use the deeper well.

(iii) It has been demonstrated for this particular case that deuteron potentials may be found which give equally satisfactory predictions to both (d,p) and (d,n) stripping reactions at the same energy.

The majority of comments which may be made, however, are negative rather than positive.

(iv) It is certainly not acceptable, in a resonant region, to attempt to fit any stripping distribution with optical parameters obtained from elastic scattering data at a single energy, nor to present any such fit without a demonstration, including Hauser-Feshbach calculations and excitation functions, that the scattering amplitude is primarily direct.

(v) In a resonant region such as this, uncertain deuteron parameters and fluctuating stripping distributions combine to give uncertainties of at least ±30% in experimentally

determined absolute spectroscopic factors, and dictate against drawing any conclusions on the basis of such measurements.

(vi) Fluctuations in the excitation functions can effect the relative spectroscopic factors as well insofar as they are uncorrelated between the proton groups leading to different residual states. The results of Kuehner et al (Kuehner 60a) indicate that these fluctuations are in the range 10-20% at the stripping peaks of the first two excited levels, and consequently the relative spectroscopic factors are uncertain to this extent.

(vii) The fact that the "5MeV" parameters gave the best fit to the stripping reactions is merely fortuitous, and not in contradiction with (iv). Indeed, the "5MeV" parameters have been shown not to fit the 5.0 MeV distribution, and the parameters obtained from elastic scattering at 4.82 MeV do not fit the stripping reaction at 4.84 MeV.

(viii)When elastic scattering distributions are distorted by contributions from amplitudes other than direct, the parameters of the optical potential are probably no longer constrained to have values consistent with their supposed physical meaning, and the use of such terms as "radius" or "diffuseness" should not be understood too literally.

(ix) Finally, the observation must be made that the polarization measurement did not contribute largely to the above conclusions, but was only of interest insofar as it deviated so greatly and so unexpectedly from the corresponding (d,n) measurement. With the advent of successful polarized ion sources, double scattering experiments should be very carefully screened as

regards both cross-section and the possible theoretical importance of the measurement to justify the expenditure of valuable accelerator time.

The experiments described in this thesis have served to emphasize what is perhaps the most important problem in the study of reaction mechanisms in the low energy or light mass regions - that of intelligently separating the direct, compound and interference amplitudes. It seems improbable that this can be accomplished experimentally, although attempts have been made to do so using the large time differential between the reaction modes and the channelling properties of Silicon crystals. (Gemmel 67).

A more promising approach is that used by M. Bobyr et al on the $^{25}Mg(d,p)^{26}Mg$ reaction. (Bobyr 66). A large number of excitation functions at many angles were taken over an energy range of from 1.5 MeV to 3.0 MeV. Smooth curves were then fit through the large fluctuations using a careful averaging process, and the compound nucleus contribution derived from a Hauser-Feshbach calculation subtracted from these. The remaining smooth curve was assumed to be the energy dependence of the direct amplitude at each angle. From this data, "Direct" angular distributions were constructed, and compared quite successfully with DWBA calculations. The same approach, of course, could be applied to elastic scattering.

This method requires the accumulation of a very large amount of experimental data, and would have been far too time consuming to do with the magnetic spectrometer. The installation of a new charged particle scattering chamber with proposed facilities for mounting up to eight solid state detectors simultaneously,

would make such an experiment on ^{28}Si quite feasible and possibly very interesting.

APPENDIX A

The following appendix is a preprint of a paper to be published shortly in Nuclear Instruments and Methods, with the addition of one paragraph concerning the calculation of the polarimeter analysing power.

A CHARGED PARTICLE POLARIMETER FOR USE WITH A MAGNETIC SPECTROMETER

D. Gurd, G. Roy, and H. Leighton

Nuclear Research Center
Department of Physics
University of Alberta
Edmonton, Alberta, Canada

September, 1967

A CHARGED PARTICLE POLARIMETER FOR USE WITH A MAGNETIC SPECTROMETER†

D. Gurd, G. Roy, and H. Leighton

Nuclear Research Center
Department of Physics
University of Alberta
Edmonton, Alberta, Canada

A charged-particle polarimeter is described which uses proton elastic scattering from a 17 mg/cm^2 Carbon foil as an analyser. Charged-particle groups are selected by a 50 cm magnetic spectrometer, and doubly scattered particles are detected in 10 mm Silicon surface barrier detectors. An analysing power of 68% is achieved for protons entering the polarimeter in the energy range from 5.4 to 6.0 MeV.

1. Introduction

The present paper describes the design and testing of a charged particle polarimeter which is currently being used to measure the polarizations of the outgoing protons in (d,p) reactions.

The polarimeter has been designed for use in conjunction with the University of Alberta 50 cm magnetic spectrometer, as indicated in fig. 1. The scattering chamber, (A), is rigidly attached to the spectrometer which, with the use of a sliding seal of 0.010" stainless steel, could be rotated through the angular range from -20° to +140°.

---

†This work was supported in part by the Atomic Energy Control Board of Canada.

The single quadrupole lens (B) between the chamber and the spectromagnet allows focussing in both planes to be achieved, significantly improving the solid angle of the system[1]. The depolarizing effect of the lens is estimated to be less than 1%[2], while the solid angle is increased by a factor of about 5 to ~ 2×10^{-3} steradians. Several groups[2,3,4,5] have pointed out the advantages of using magnetic analysis before the second scattering in polarization measurements, the most important being the reduction of background problems, due to neutrons originating at the target and beam stop, by the large distance between the target chamber and the polarimeter; and the elimination of unwanted particle groups, even those from nearby proton levels, by the high resolution of the spectromagnet. The magnet, however, also introduces some difficulties which will be discussed in a later section.

2. Design

Although the advantages of Helium as a polarization analyser are well known, the difficulties of using a high pressure gas cell in a vacuum chamber make a solid analyser, such as Carbon, more convenient. Moreover, many measurements have been reported of the polarization in proton-Carbon scattering below 10 MeV[6,7,8,9,10] and sufficient data is now available to make Carbon a useful analyser for (d, p) reactions. We determined, therefore, to use a thick (17 mg/cm^2) Carbon foil* as an analyser, selecting a

---

*Ultra Carbon Corporation, Bay City, Michigan

second scattering angle to give as large an analysing power as possible.

It was decided, following a technique suggested by several other groups[2,3,5] to calibrate the polarimeter at one energy and subsequently to degrade all proton groups under study down to this calibration energy. It is commonly assumed, following Wolfenstein[11] that this degradation, being electronic, does not affect the polarization of the proton beam. Because the proton groups to be studied were in the energy range 7 - 11 MeV, the calibration energy selected was ~ 6 MeV, limited on the low side by the wish to minimize the amount of energy degrading necessary, and on the high side by the maximum accelerator energy available.

Moss and Haeberli[6] have reported both cross-sections and polarizations for proton-Carbon scattering between 4.6 and 8.7 MeV. Their data at 6.18 MeV was used to select both the median angle and the acceptance angle ($45° \pm 7.5°$) of the side counters in order to maximize the polarimeter efficiency, as obtained by folding in the elastic cross-sections with the proton polarizations. This meant locating the Silicon surface barrier detectors approximately 3/4" from the center of the Carbon scatterer.

Fig. 2 shows the resulting polarimeter design, the dimensions being determined by the considerations already mentioned, and the requirement that the instrument fit in the 2-1/2" gap available in the existing spectromagnet facility. The polarimeter is supported on four rods, three of which extend outside the vacuum chamber through O-ring seals and can be externally rotated.

The first of these, in association with gear A, allows the polarimeter to be rotated through 180° about its central axis in order to observe and compensate for any geometrical asymmetries.

The second rod, B, is threaded, and allows the instrument to be moved parallel to its central axis so that it can be located at the spectromagnet focal plane, which is displaced according to the kinematics of the reaction under study. By means of a sliding O-ring seal the polarimeter can also be moved several centimeters along the focal plane to insure that the focussed proton beam enters parallel to the central axis.

The remaining rods provide support to guide the polarimeter and prevent its binding when being moved.

One can also see, in fig. 2, the monitor or "straight through" detector, which was used in steering the beam into the polarimeter, and insuring that the beam entered the polarimeter close to the calibration energy as described in the next section. In front of the slit telescope is located the totally depleted Silicon dE/dx counter, which was required to reduce background difficulties as described in the next section.

The "slit telescope," including the degrading foils, tantalum collimating slits, and Carbon scatterer, can be removed in one piece and interchanged with telescopes having different collimation.

The main body of the polarimeter was machined out of brass to a tolerance of .002". The side and monitor counters are 10 mm solid state detectors[†]

[†]Nuclear Diodes, P.O. Box 135, Prairie View, Illinois 60009

The dE/dx counter is a totally depleted Silicon detector with a thickness of 490 μ[†].

3. Calibration and Operation

3.1 INITIAL TESTS

The polarimeter was inserted in the vacuum chamber and its alignment checked optically with a transit before the whole was mounted on the spectromagnet. The central axis appeared to be parallel with the 90° ray to within 0.4°, and the polarimeter could be removed and reinserted without affecting this alignment measureably.

A Tantalum analyser was then inserted in the instrument in place of the Carbon second scatterer, in order to measure any residual asymmetries in the polarimeter. The scattering from this high Z material, particularly forward of 60°, is expected to be nearly completely Coulomb, and the resulting analysing power is certainly less than 0.01. When the beam entered the polarimeter so as to give zero left-right asymmetry, as described below, no non-statistical asymmetry was introduced by rotating the polarimeter 180°, indicating that there were no appreciable geometric asymmetries in the instrument.

It was at this point that the earlier mentioned difficulties introduced by the use of the spectromagnet became apparent. It was found that the measured asymmetry was rather sensitive to the magnetic field, that is, to

[†]Nuclear Diodes, P.O. Box 135, Prairie View, Illinois 60009

the direction in which the focussed protons entered the polarimeter. This sensitivity is apparent in fig. 3, where it can be seen that if the magnet is set at just 90% of the peak, the asymmetry is as much as 8%. This problem was not as severe as was at first feared, since the very thick targets (~500 keV to 5 MeV deuterons) used in actual experiments resulted in broad peaks and consequently much less sensitivity to field variations. Moreover, since the angular dependence of the elastic cross section for Carbon in the vicinity of 45° is less than the pure Coulomb dependence, the polarimeter proved to be less sensitive with the Carbon analyser in place than during the test runs with Tantalum. Tests indicate that under experimental conditions the field may be changed by as much as 30 gauss with no statistically significant (i.e. < 5%) change in the measured asymmetry.

The need for a coincidence requirement on the side counters to reduce the relatively large background from gamma rays and neutrons originating at the target and beam stop is demonstrated in fig. 4, which shows a typical spectrum in one side counter taken with and without the totally depleted detector. The long low energy tail in the gated spectrum is made up of real counts, as shown by the corresponding random coincidence spectrum which is superimposed. The left-right ratio proved to be constant, within statistics, regardless of the region of the spectra (above the noise) summed, a further indication that the tail is made up of real counts. In practice, all counts from the arrow up were included in the total number of counts on each side.

3.2 CALIBRATION

The analysing power of the polarimeter was measured by observing proton elastic scattering at 45° with E_p = 6.18 MeV where the polarization P_1 is known to be -0.80 ± 0.02.[6] The asymmetry ε in left-right scattering in the polarimeter is given by the usual relation

$$\varepsilon = \frac{r - 1}{r + 1}$$

where

$$r = \sqrt{r_1 r_2}$$

and

$$r_1 = L_1/R_1 \quad ; \quad r_2 = L_2/R_2$$

where L_1 and R_1 are the number of counts scattered to left and right respectively with the polarimeter in one orientation, and L_2 and R_2 are the corresponding numbers with the polarimeter rotated by 180°. By measuring ε, the analysing power of the polarimeter, P_2, could be inferred from the expression

$$\varepsilon = P_1 P_2 .$$

All signs are in accordance with the Basel convention.

For the calibration the combination of a relatively thin target and no energy degradation resulted in a well-focussed, or very narrow image, and consequently increased sensitivity to the field setting. Great care was, therefore, taken to set up the field so as to give zero asymmetry when the Tantalum second scatterer was in place. The Carbon was then put in place

and the asymmetry measured as described above. The combined results of the runs in both orientations is shown in fig. 5. The asymmetry is +54%, corresponding to an analysing power of -68%. Approximately 0.02% of the particles reaching the analyser are scattered into the side counters.

As a check of the energy range over which the measured analysing power could be assumed to be constant, the calibration was repeated, using the same reaction at angles of 35^{o}, 60^{o}, and 80^{o}. The results are listed in table 1. The analysing power appears to be nearly constant in the energy range 5.4 MeV to 6.0 MeV, and this fortunate feature allowed an entire angular distribution to be performed with only a few changes in the degrading foils. Consequently, it was found to be no great inconvenience to change the foils manually.

As protons enter the analyser with energies in the vicinity of 5.9 MeV, and are degraded by approximately 1.2 MeV in the Carbon, the analysing power is affected by the anomaly at 5.4 MeV in proton-Carbon scattering[8]. This renders calculations of the analysing power somewhat difficult. However, a calculation based on the phase shifts given by Moss and Haeberli[6] and modified in the vicinity of the anomaly by those of Duval and co-workers[8] predicts analysing powers increasing from -60% at 5.5 MeV to -77% at 6.0 MeV. The deviation from the measured values is attributable to the uncertainties in the energy dependence of the phase shifts.

These calculations were performed with a computer program which evaluated from given phase shifts the polarization of the protons elastically scattered from Carbon, and averaged these results over the

Table 1

θ_{lab}	θ_{cm}	E_p(out)	P_1	ε	P_2	P_2 (Predicted)
35	37.8	6.00	$-0.78 \pm .04$	$+0.52 \pm .03$	$-0.66 \pm .05$	-0.77
45	48.4	5.87*	$-0.80 \pm .03$	$+0.54 \pm .02$	$-0.68 \pm .04$	-0.74
45				$+0.54 \pm .02$	$-0.68 \pm .04$	
60	64.2	5.68	$-0.36 \pm .06$	$+0.24 \pm .02$	$-0.67 \pm .08$	-0.67
80	84.7	5.39	$+0.92 \pm .13$	$-0.62 \pm .05$	$-0.61 \pm .11$	-0.60

*Calibration Energy

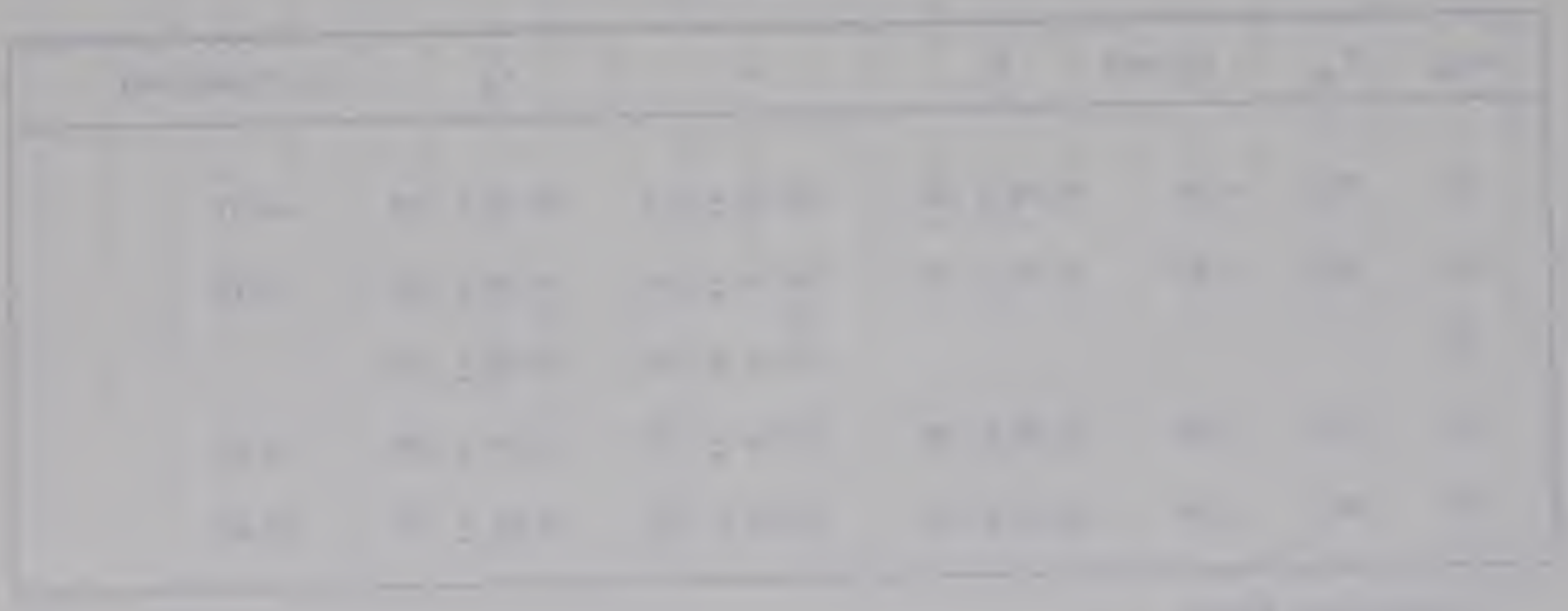

large solid angles subtended by the two side counters. That the anomaly is reasonably well accounted for by the computation is indicated in figure A-7 which shows the calculated variation with energy of the proton polarization compared with the experimental values obtained by Haeberli[6].

With protons from $^{12}C(p,p)^{12}C$ at 45^{o} and E_p = 6.18 MeV entering the polarimeter, a pulse was set to give signals with pulse heights corresponding to the two peaks produced in the monitor counter by the stepped energy degrader located in front of it. In practice, the magnet field was first set to correspond with the proton peak as indicated by the counting rate in the monitor counter, and then the two peaks in this counter were compared with the calibration pulse heights to insure that the protons were entering the polarimeter at the calibration energy.

The region between the lines in fig. 6 indicates, as a function of cross-section, the approximate amount of charge required on the target in order to observe 1000 doubly scattered particles. This is based on our results with a 5 mg/cm^2 Calcium target. Only very approximate results have been suggested, because many parameters, including the orientation of the thick target, the width of the focussed peak, the relative width of the polarimeter collimation, the current in the quadrupole lens, and the target mass must, of course, also be considered. However, the figure should provide some estimate of times required to perform proposed experiments.

The instrument has proved quite successful in measuring polarizations in (d,p) reactions, and it is expected that narrower collimation in the

polarimeter "slit telescope" will decrease its field sensitivity to the point where it could reliably be used in high yield experiments with narrower images; elastic scattering, for example.

The authors are particularly indebted to Mr. N. Riebeek for his careful machining of the polarimeter. One of the authors (D.P.G.) wishes to acknowledge the financial assistance of the National Research Council.

References

1) H. A. Enge, Rev. Sci. Inst. 29 (1958) 885.

2) J. E. Evans, J. A. Kuehner, and E. Almqvist, Phys. Rev. 181 (1963) 1632.

3) E. J. Ludwig and D. W. Miller, Phys. Rev. 138 (1965) B364.

4) A. Isoya and M. J. Marrone, Phys. Rev. 128 (1962) 800.

5) J. C. Hensel and W. C. Parkinson, Phys. Rev. 110 (1958) 128.

6) S. J. Moss and W. Haeberli, Nuc. Phys. 72 (1965) 417.

7) A. C. L. Barnard, J. B. Swint, and T. B. Clegg, Nuc. Phys. 86 (1966) 119.

8) J. S. Duval, Jr., A.C.L. Barnard, and J. B. Swint, Nuc. Phys. 93 (1967) 164.

9) J. E. Evans, Nuc. Phys. 27 (1961) 41.

10) L. Rosen, P. Darriulat, H. Faraggi, and A. Garin, Nuc. Phys. 33 (1962) 458.

11) L. Wolfenstein, Ann. Rev. Nucl. Sci. 6 (1956) 43.

List of Illustrations

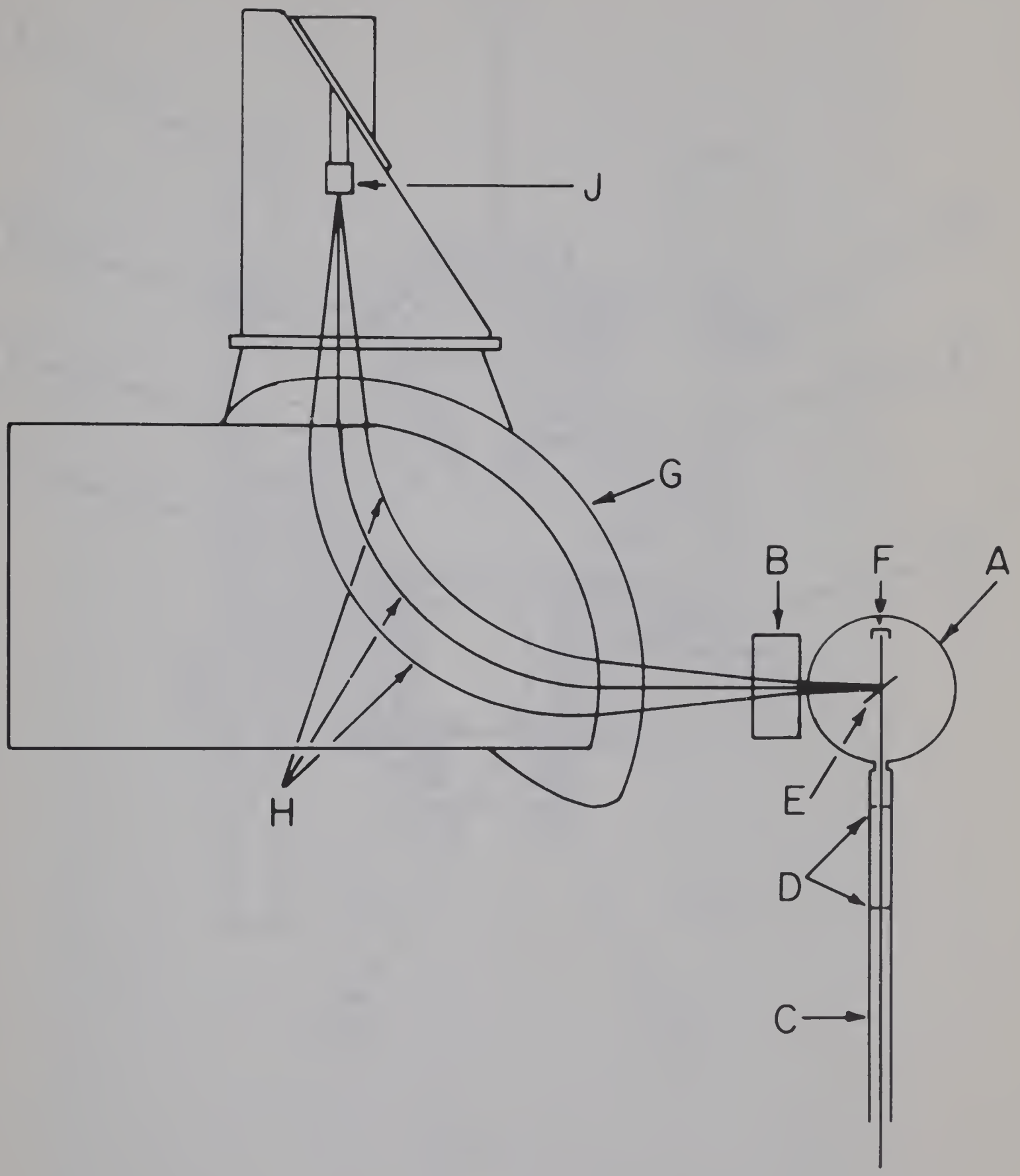

Fig. 1

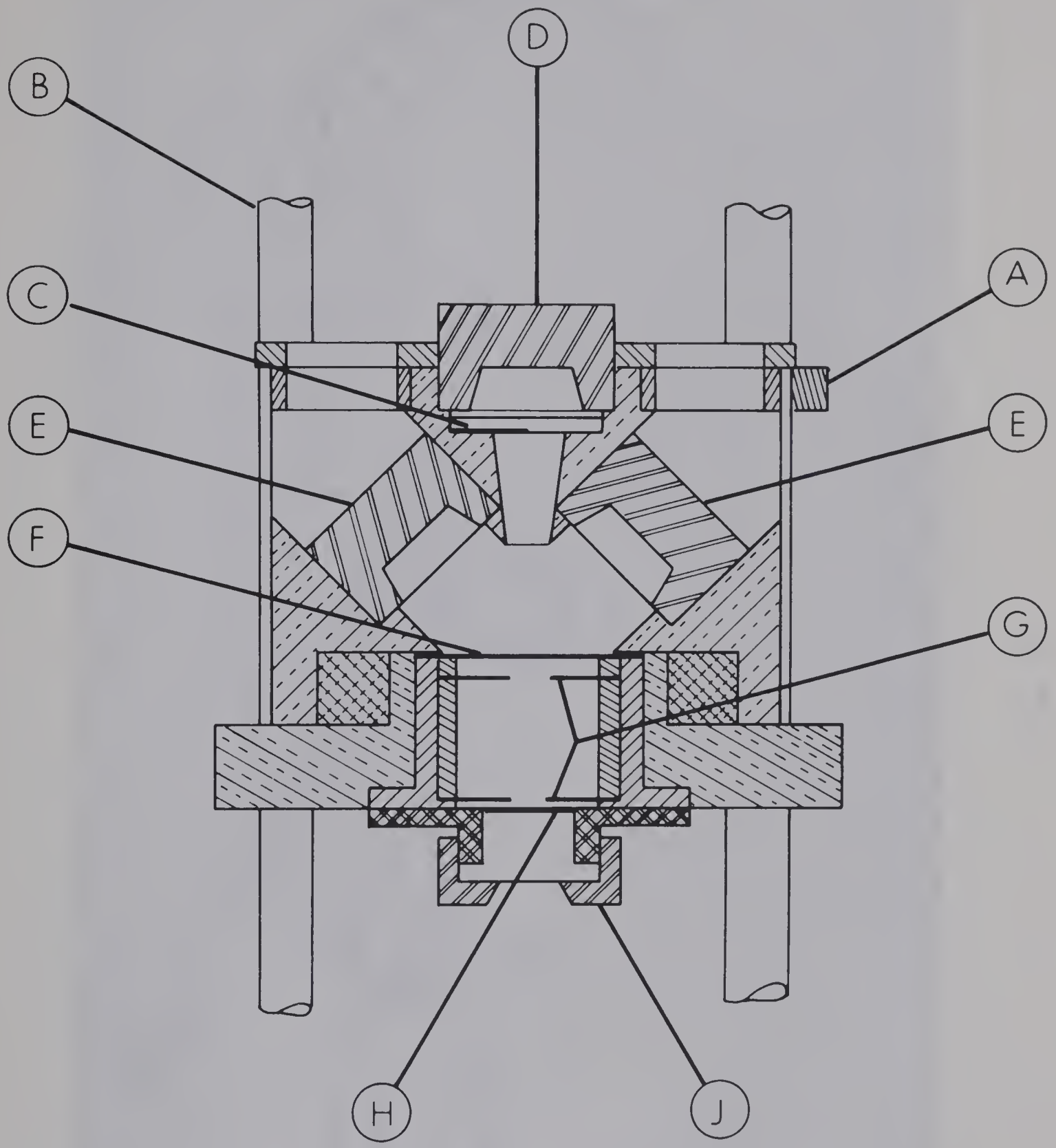

Fig. 2

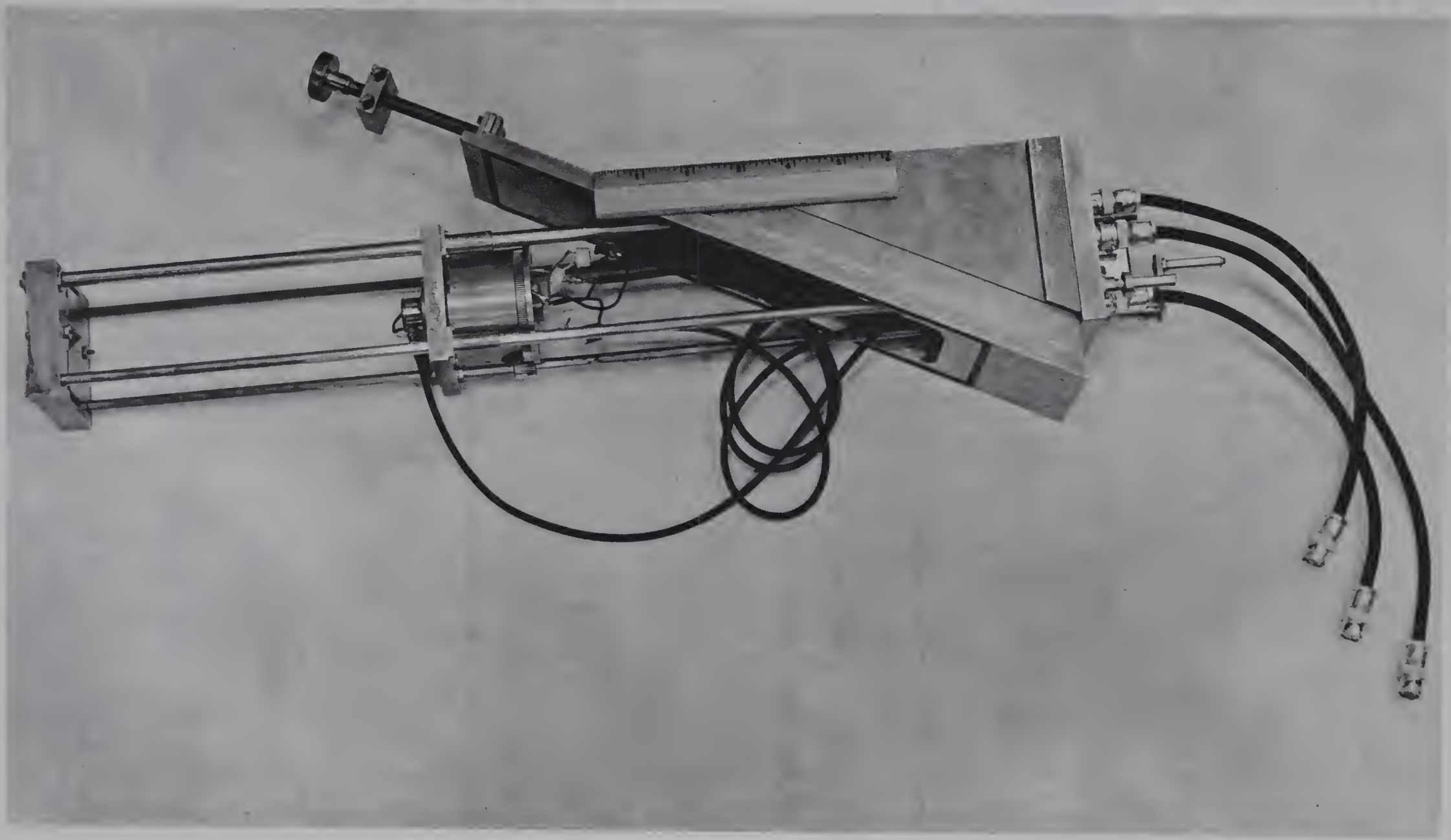

Fig. 2b

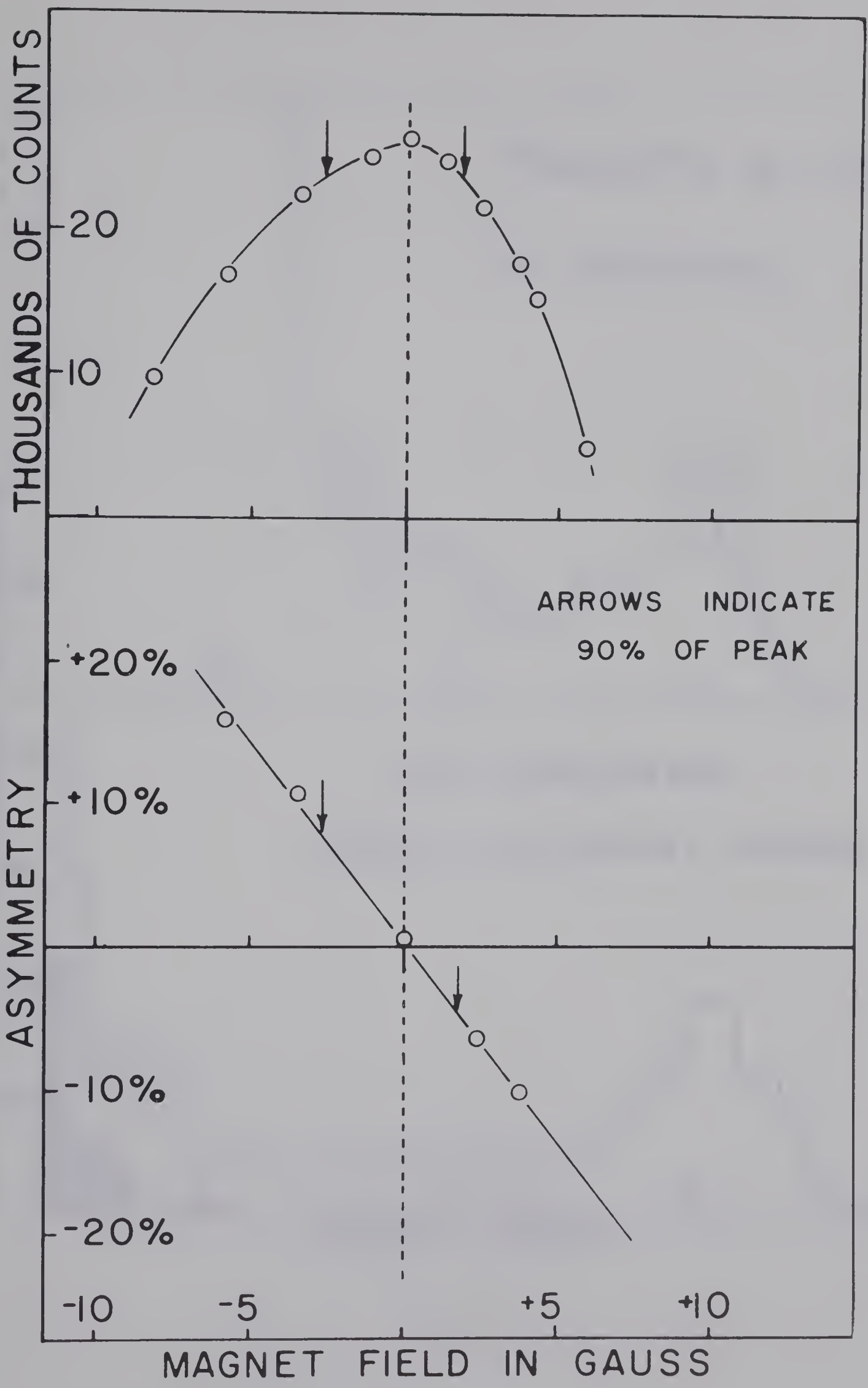
THOUSANDS OF COUNTS
20
10
ARROWS INDICATE
90% OF PEAK
+20%
+10%
ASYMMETRY
-10%
-20%
-10
-5
+5
+10
MAGNET FIELD IN GAUSS

Fig. 3

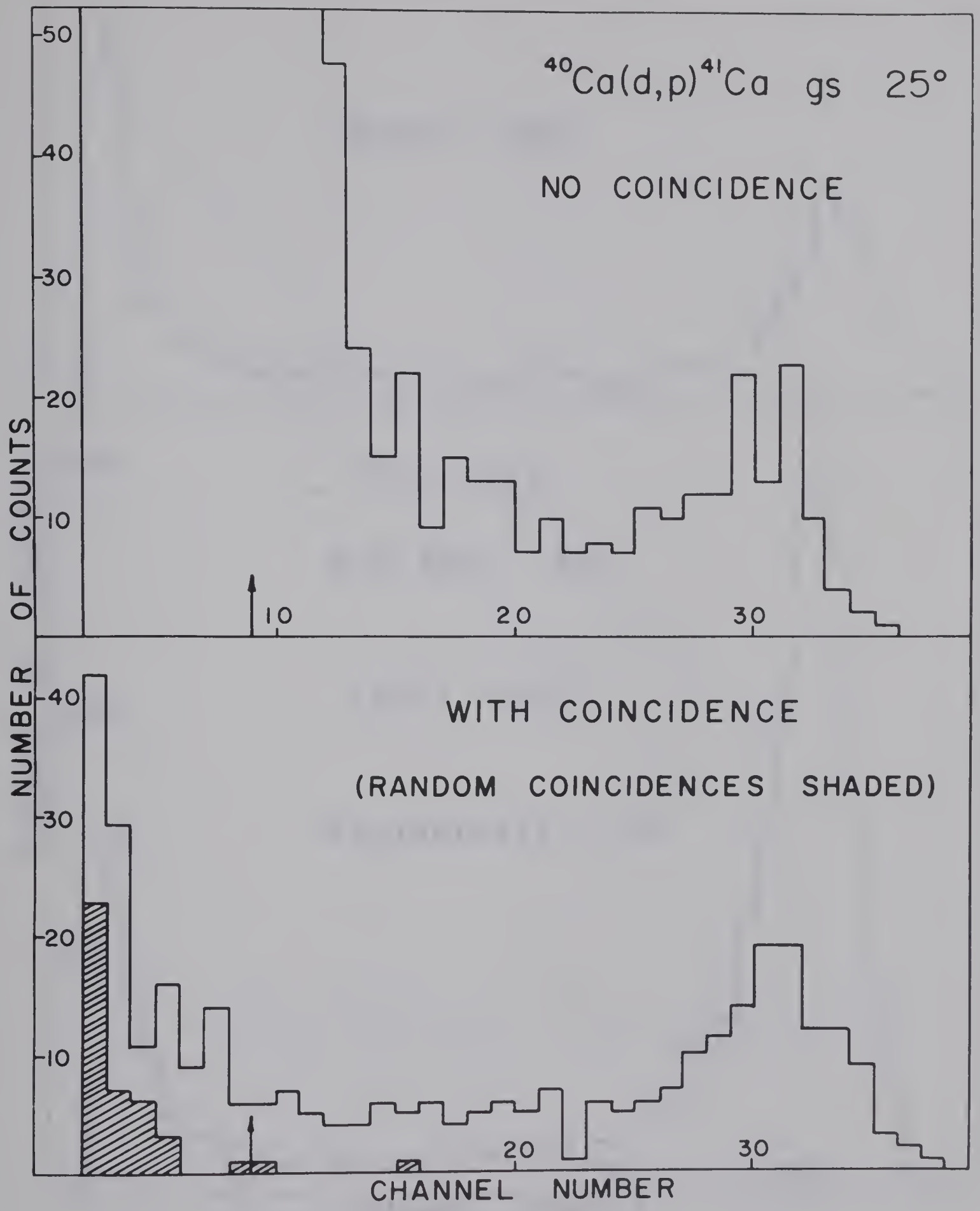
$^{40}Ca(d,p)^{41}Ca$ gs 25°
NO COINCIDENCE
WITH COINCIDENCE
(RANDOM COINCIDENCES SHADED)
NUMBER OF COUNTS
NUMBER
CHANNEL NUMBER
10
20
30
40
50

Fig. 4

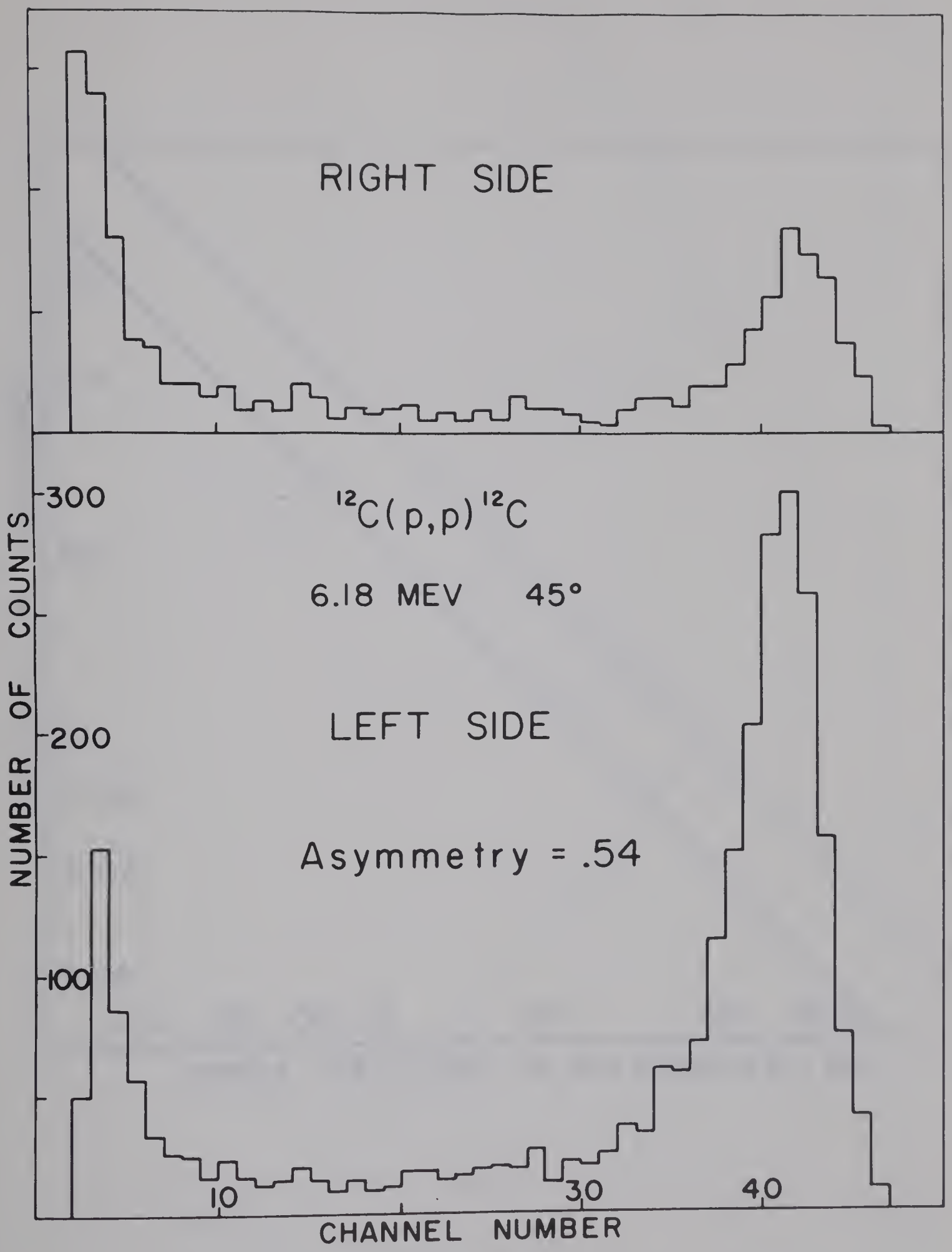
RIGHT SIDE
$^{12}C(p,p)^{12}C$
6.18 MEV 45°
LEFT SIDE
Asymmetry = .54
NUMBER OF COUNTS
300
200
100
10
30
40
CHANNEL NUMBER

Fig. 5

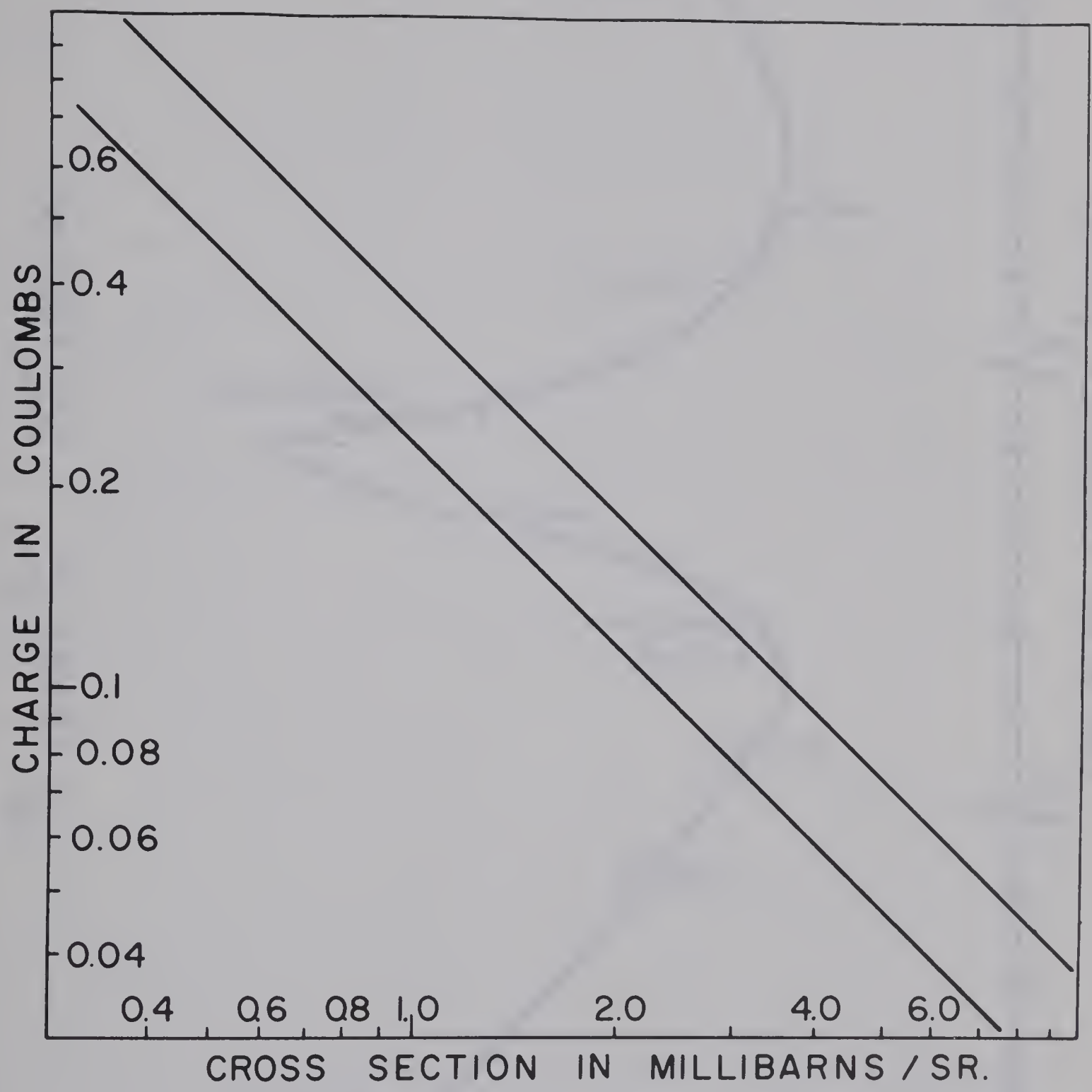
CHARGE IN COULOMBS
0.6
0.4
0.2
0.1
0.08
0.06
0.04
0.4
0.6
0.8
1.0
2.0
4.0
6.0
CROSS SECTION IN MILLIBARNS / SR.

Fig. 6

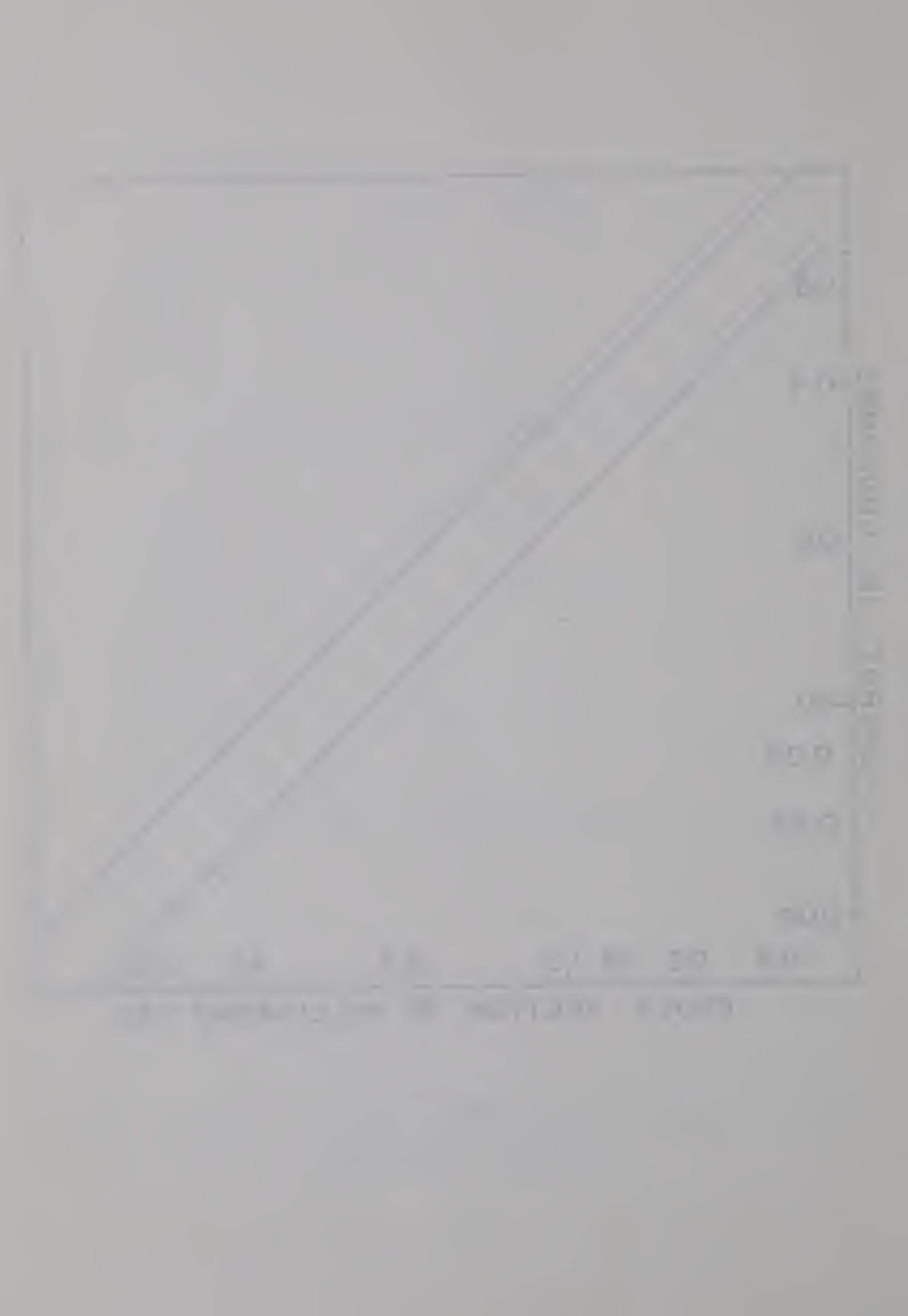

$^{12}C(p,p)^{12}C$ 50° (REF. 6)

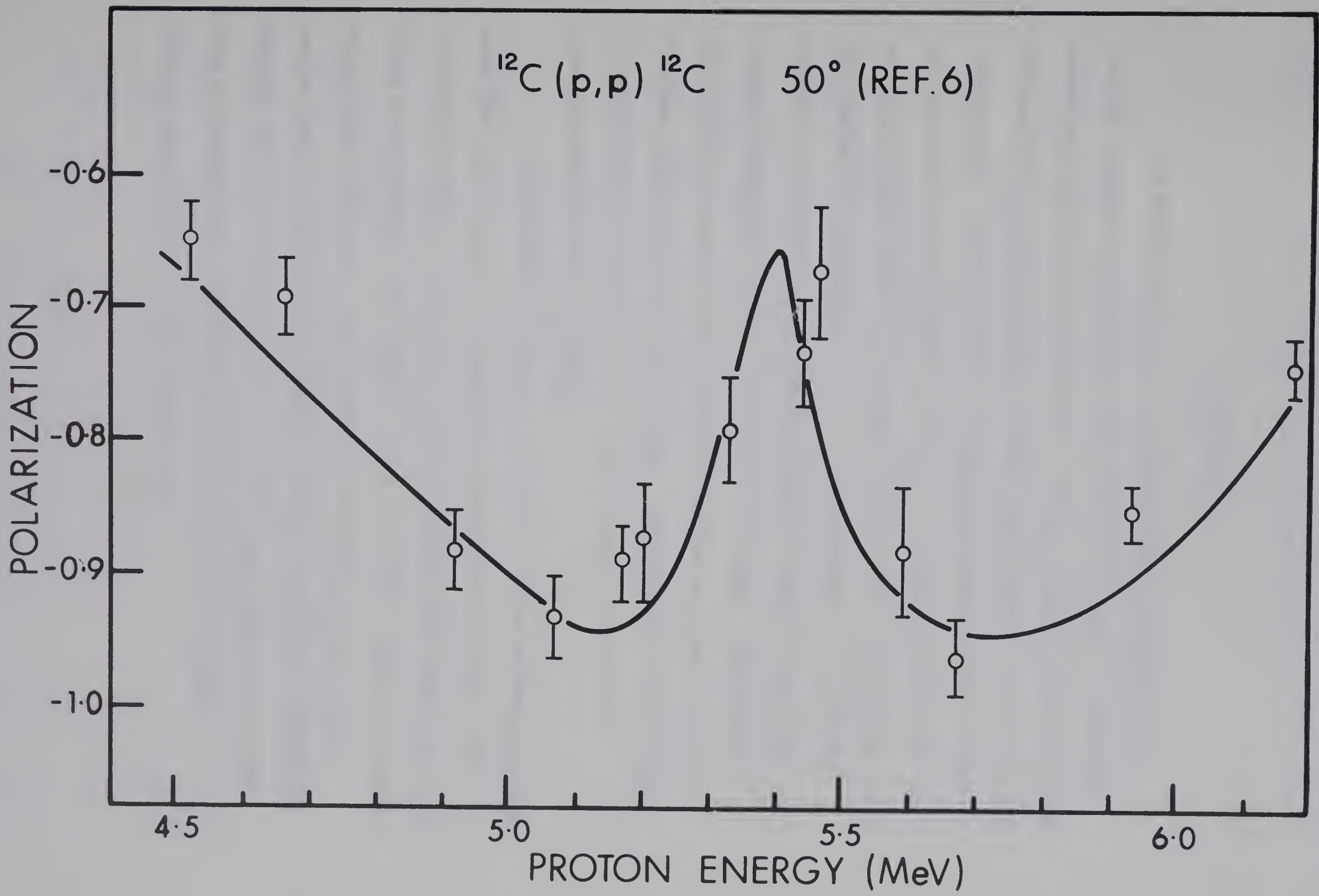

FIGURE A - 7

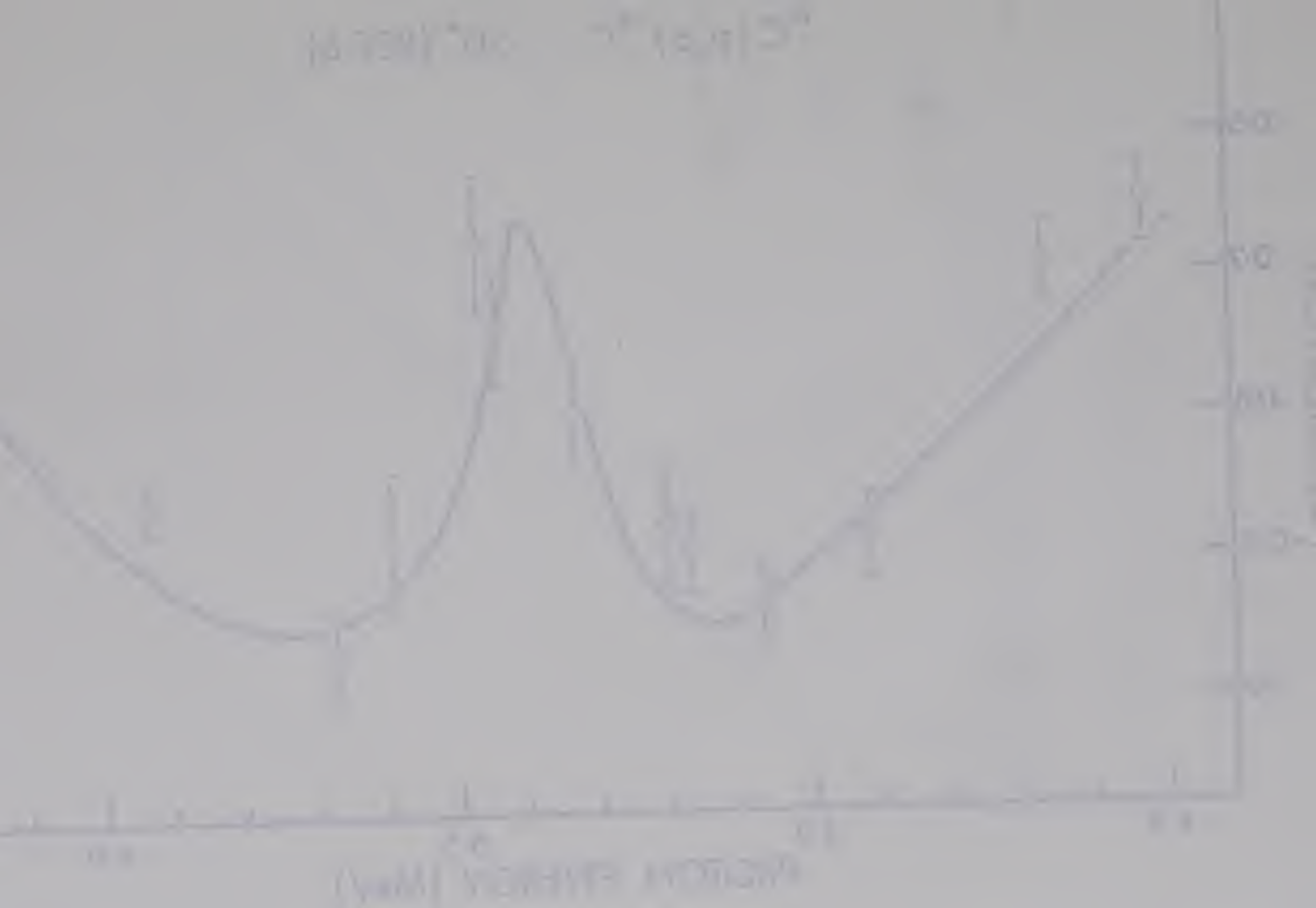

APPENDIX B

In Perey's analysis of deuteron elastic scattering for several isotopes in the energy range 10-26 MeV (Perey 66), deuteron potentials with real well depths of ~ 50 and ~ 100 MeV have been found for nearly all nuclei studied, and have been labelled sets (a) and (b) respectively. In his analysis of the 11.8 MeV data on ^{28}Si, however, set (b) had a real well depth of 179 MeV. It appeared as if the real set (b) had been missed by the search routine, which had instead found the minimum corresponding to "set c" of this thesis. A search was therefore initiated for the missing potential using the same data, and starting parameters close to typical set (b) values. Regardless of the starting parameters used, all six parameter searches arrived at the same final values reported by Perey. Although this had the effect of increasing our confidence in the computer code, it was not otherwise particularly satisfying.

As described in Chapter 4, Section 4, three parameter searches were then used to map out the parameter space more carefully. The results are shown in figure B-1, where it is clear from the χ^2 plot that there is no minimum in the region V = 100 - 120 MeV. There is, however, very little difference in the quality of the fits over the entire region from V = 100 MeV to V = 180 MeV. Figure B-2 shows a comparison between the fit of Perey's set (V = 179 MeV) and a potential obtained from a five parameter search with V held fixed at V = 120 MeV. There is very little to choose between them.

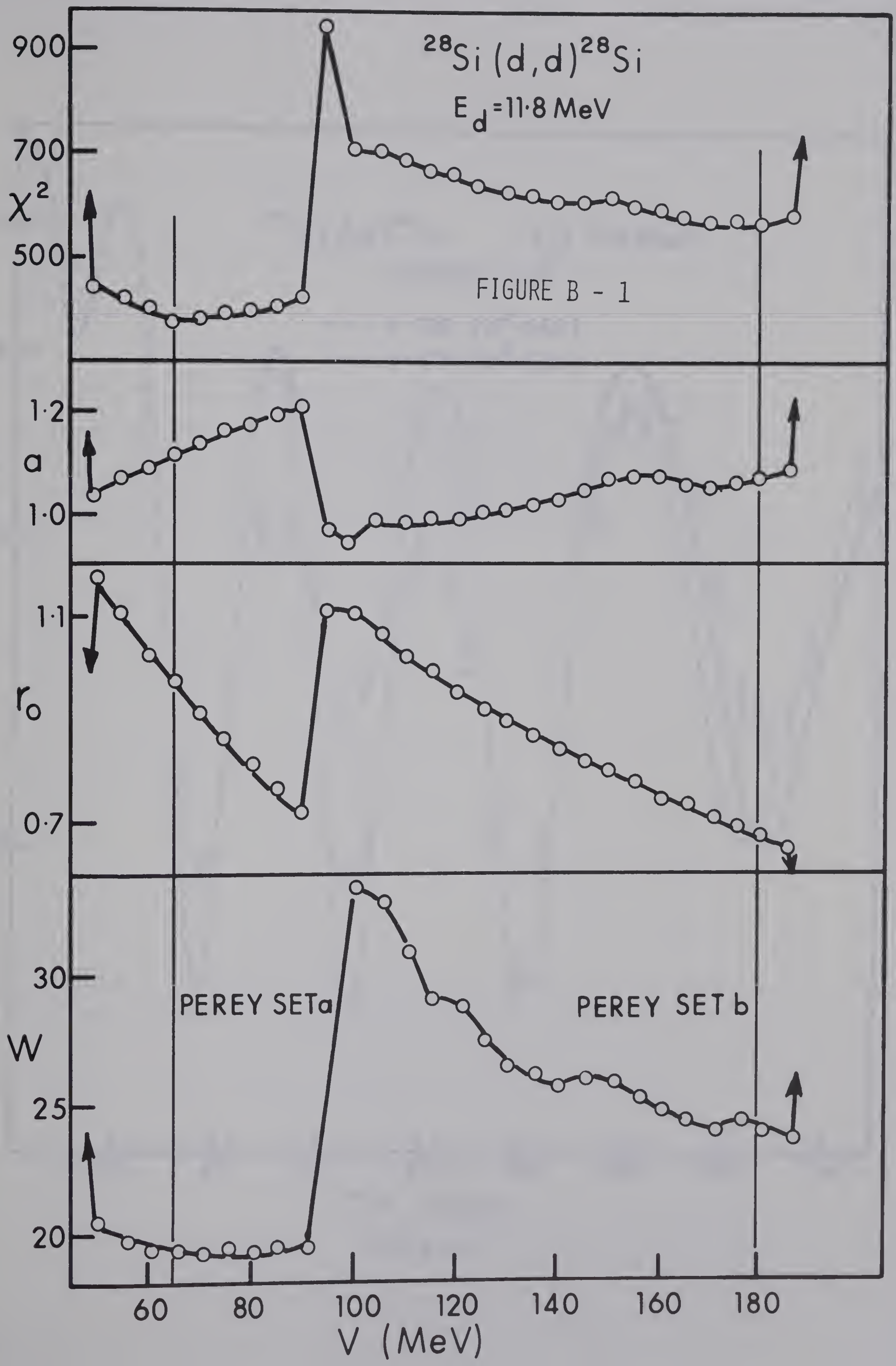
$^{28}Si\,(d,d)^{28}Si$
E_d=11·8 MeV
900
700
χ^2
500
1·2
a
1·0
1·1
r_o
0·7
30
W
25
20
PEREY SETa
PEREY SET b
60
80
100
120
140
160
180
V (MeV)

FIGURE B - 1

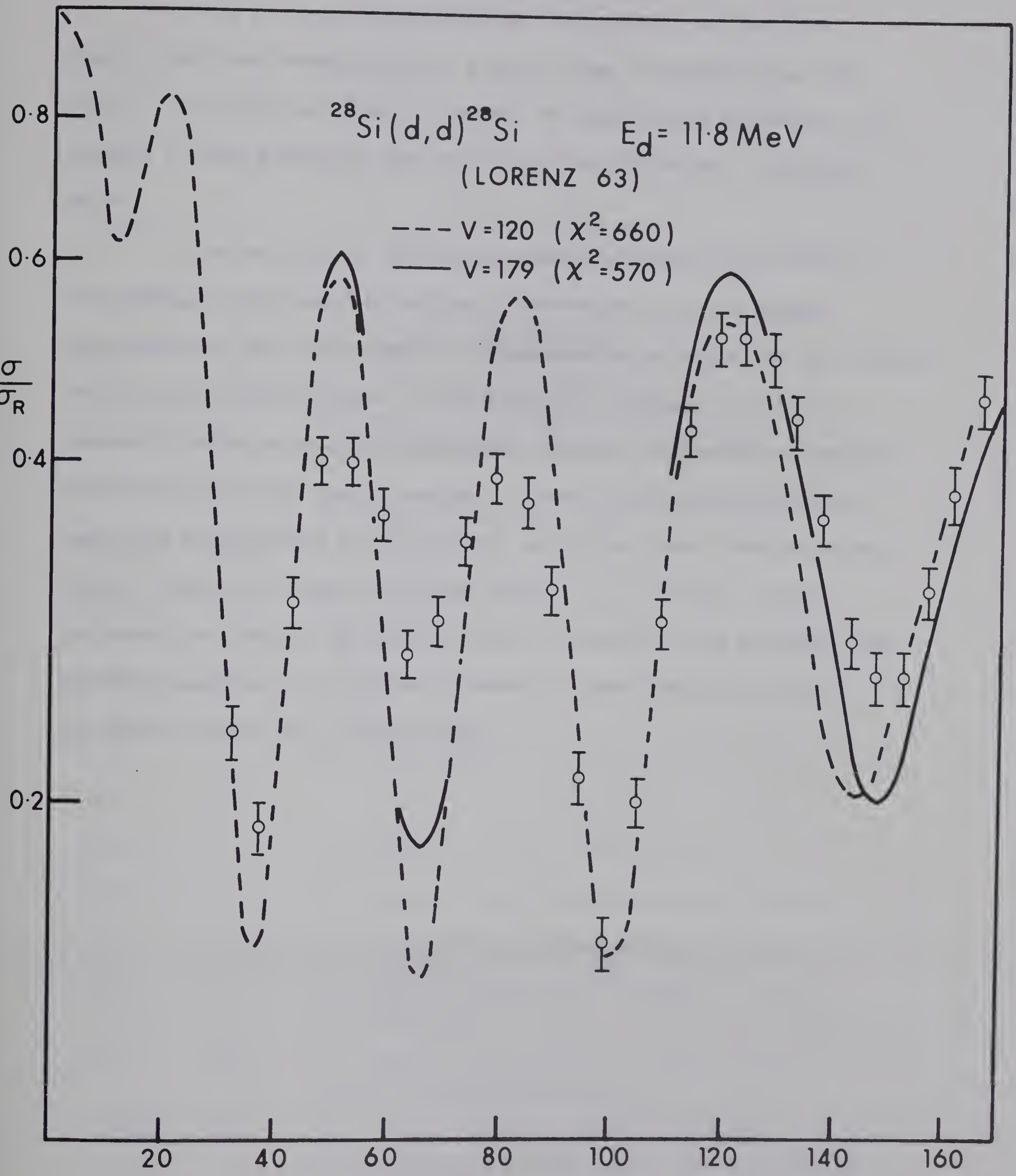
$^{28}Si(d,d)^{28}Si$ $E_d = 11{\cdot}8$ MeV
(LORENZ 63)
--- V = 120 (χ^2 = 660)
—— V = 179 (χ^2 = 570)
$\frac{\sigma}{\sigma_R}$
0·8
0·6
0·4
0·2
20
40
60
80
100
120
140
160
C.M. Angle

FIG.B-2

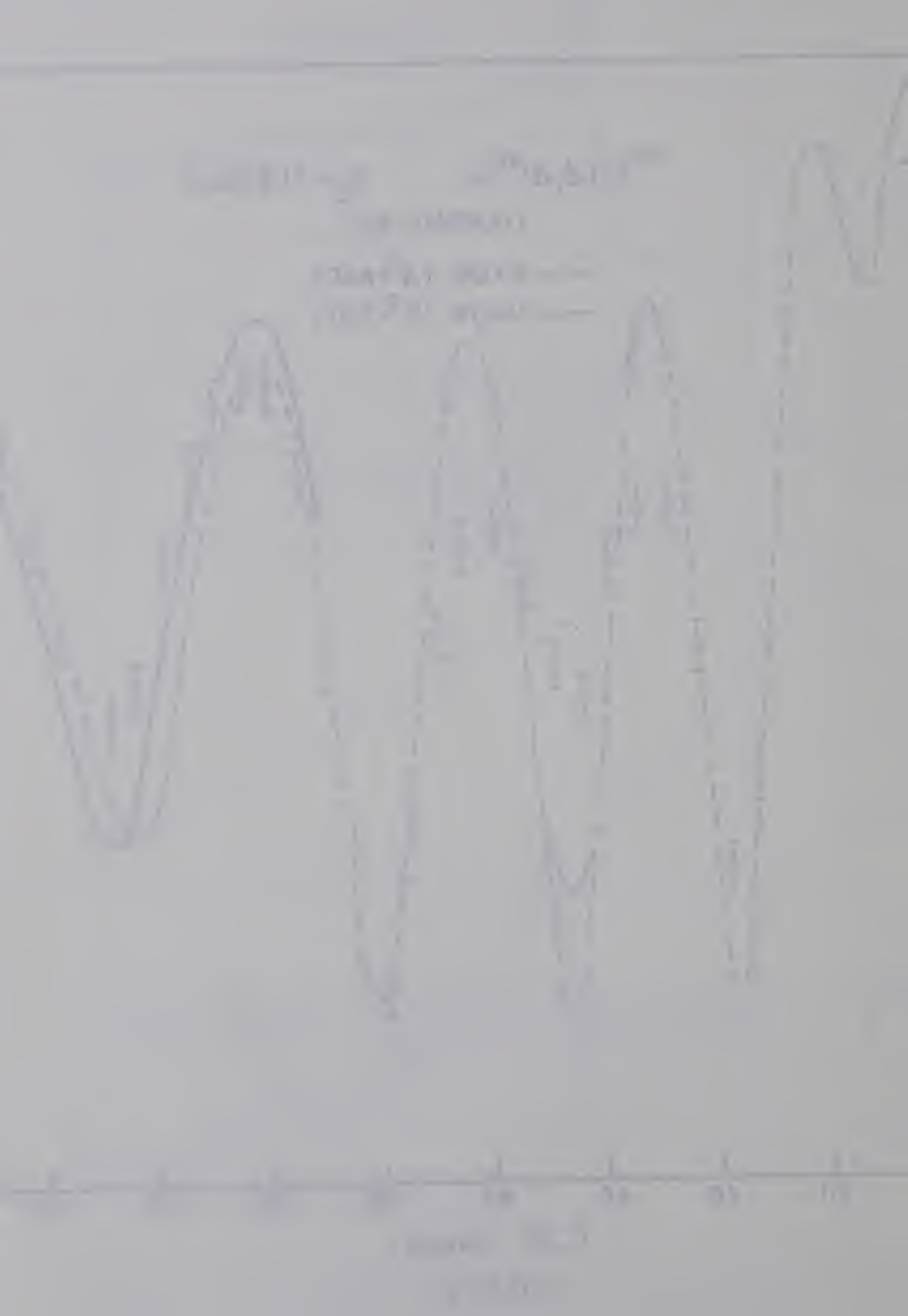

When the same phenomenon was observed for searches over some of the lower energy elastic distributions obtained during this work, it was felt justified to use for the appropriate potentials the results of five parameter searches with V held fixed at a reasonable value.

The topology of the multiparameter χ^2 space is of course very strongly influenced by any small aberration in the angular distributions, due, for example, to experimental accidents or the effects of non-direct contributions. True minima may disappear, or be so reduced in size as not to be detectable without, for example, changing the step size in the search routine. Two well established but often neglected observations should be made concerning these considerations: firstly, that the computer code and details of the search routine influence the results of optical model calculations; and secondly that wherever possible it is always preferable to use average optical potentials rather than isolated sets.

REFERENCES

Bercaw	64	R.W. Bercaw and F.B. Schull, Phys. Rev. 133 (1964) B632
Bobyr	66	V. Bobyr, M. Corti, G.M. Marcazzan, L. Milazzo Colli and M. Milazzo, Energia Nucleare 13 (1966) 421
Bromley	57	D.A. Bromley, H.E. Gove, E.B. Paul, A.E. Litherland and E. Almquist, Can. Jour. Phys. 35 (1957) 1042
Bromley	57a	D.A. Bromley, H.E. Gove and A.E. Litherland, Can. Jour. Phys. 35 (1957) 1057
Buck	63	B. Buck, Phys. Rev. 130 (1963) 712
Butler	67	S.T. Butler, R.G. Hewitt, B.H.J. McKeller and R.M. May, Ann. of Phys. 43 (1967) 282
Davies	66	W.G. Davies, W.K. Dawson, G.C. Neilson and K. Ramavataram, Nuc. Phys. 76 (1966) 65
Davison	68	N.E. Davison,- Private communication
Davydov	58	A.S. Davydov and G.S. Filippov, Nuc. Phys. 8 (1958) 237
Dickens	65	J.K. Dickens and F.G. Perey, Phys. Rev. 138 (1965) 1080
Enge	58	H.A. Enge, Rev. Sci. Inst. 29 (1958) 885
Gedke	67	D.A. Gedke, Univ. of Alberta Ph.D. Thesis
Gemmell	67	D. Gemmell, a private communication
Grandy	67	T.B. Grandy, Univ. of Alberta Ph.D. Thesis
Gurd	66	D.P. Gurd, Univ. of Alberta M.Sc. Thesis
Gurd	67	D.P. Gurd, G. Roy and H.G. Leighton, B.A.P.S. 12 (1967) 664
Gurd	68	D.P. Gurd, G. Roy and H.G. Leighton, Nuc. Inst. and Meth. to be published (1968)
Hausman	66	H.J. Hausman, W.E. Davis, C.V. Phillips, R.P. Sullivan and G.R. Unrine, Phys. Rev. 148 (1966) B1136

Hjorth	65	S.A. Hjorth, J.X. Saladin and G.R. Satchler, Phys. Rev. 138 (1965) B1425
Holt	53	J.R. Holt and T.N. Marsham, Proc. Phys. Soc. A66 (1953) 467
Isoya	62	A. Isoya and M.J. Maronne, Phys. Rev. 128 (1962) 800
Johnson	67	R.C. Johnson and F.D. Santoz, Phys. Rev. Lett. 19 (1967) 364
Kuehner	60	J.A. Kuehner, E. Almquist and D.A. Bromley, Nuc. Phys. 19 (1960) 614
Kuehner	60a	J.A. Kuehner, E. Almquist and D.A. Bromley, Nuc. Phys. 21 (1960) 555
Lam	67	S.T. Lam, Univ. of Alberta Ph.D. Thesis
Lawergren	67	B. Lawergren, A.T.G. Ferguson and G.C. Morrison, Harwell Rept. AERE R-5592 (1967)
Lee	64	L.L. Lee, Jr., Phys. Rev. 136 (1964) B971
Leighton	68	H.G. Leighton, G. Roy, D.P. Gurd and T.B. Grandy, Nuc. Phys. A109 (1968) 218
Leighton	68a	H.G. Leighton, G. Roy and D.P. Gurd, Univ. of Alberta Nuclear Research Center Internal Report
Lorenz	62	W. Lorenz, C. Moyer-Boucke, R. Santo and U. Schmidt-Rohr, Nuc. Phys. 46 (1962) 25
Newton	60	T.D. Newton, Can. Jour. Phys. 38 (1960) 700
Nilsson	55	S.C. Nilsson, K. Danske Vidensk. Selsk. nat.-fys. 29 (1955) 1
Olsen	62	W.C. Olsen, Univ. of Alberta Nuclear Research Center Internal Report
Pasechnik	63	M.V. Pasechnik et al, J.E.T.P. 16 (1963) 1111
Pearson	66	C.A. Pearson and M. Coz, Nuc. Phys. 82 (1966) 533
Pearson	66a	C.A. Pearson and M. Coz, Nuc. Phys. 82 (1966) 545
Pearson	66b	C.A. Pearson and M. Coz, Ann of Phys 39 (1966) 199
Perey	62	F.G. Perey and B. Buck, Nuc. Phys. 32 (1962) 353
Perey	66	C.M. Perey and F.G. Perey, Phys. Rev. 152 (1966) 923

Perey	66a	F.G. Perey, p. 191 in "Proceedings of the 2nd International Symposium on Polarization Phenomena of Nucleons" (Karlsruhe, 1965) P. Huber and H. Schopper, editors.
Perey	67	F.G. Perey and G.R. Satchler, Nuc. Phys. A97 (1967) 515
Preston	62	M.A. Preston, "Physics of the Nucleus" Addison-Wesley (1962)
Reber	64	L.H. Reber and J.X. Saladin, Phys. Rev. 133 (1964) B1155
Rook	65	J.R. Rook, Nuc. Phys. 61 (1965) 219
Rosen	66	L. Rosen, p. 253 in "Proceedings of the 2nd International Symposium on Polarization Phenomena of Nucleons (Karlsruhe, 1965) P. Huber and H. Schopper, editors
Roy	67	R.R. Roy and B.P. Nigam, "Nuclear Physics" John Wiley (1967)
Roy	67a	G. Roy, D. Gedke, H.G. Leighton, T.B. Grandy and D.P. Gurd, B.A.P.S. 12 (1967) 1183
Shey	59	H.M. Shey, Phys. Rev. Lett. 2 (1959) 187
Smith	67	W.R. Smith, private communication
Wildenthal	64	B.H. Wildenthal, R.W. Krone and F.W. Prosser, Phys. Rev. 135 (1964) B680